MONTANA STATE UNIVERSITY

Conjugate natural convection heat transfer in a planar thermosyphon with multiple inlets
by John Joseph Fleming

A thesis submitted in partial fulfillment of the requirements for the degree of Master of Science in Mechanical Engineering
Montana State University
© Copyright by John Joseph Fleming (1994)

Abstract:
The heat transfer results for the numerical investigation of a planar open loop thermosyphon are presented. The thermosyphon flow path is a modified "U" shape. Laminar flow is by natural convection due to heating the left ascending channel of the "U". Air (Pr=O.71) enters at the top and bottom of the right descending channel. The center portion of the "U" is a solid conducting wall and the left channel is bounded by a conducting wall. The left wall is heated isothermalIy along its external surface. All other external surfaces are adiabatic. This configuration is a modification of heat removal systems used in passive reactor cooling, nuclear waste material storage, and various other applications.

The average Nusselt number for this configuration was studied for different values of the governing parameters. These include the Rayleigh number, the ascending channel aspect ratio, the lower inlet width, and the wall thermal conductivity. These results are obtained using the proprietary finite element analysis program COSMOS/M to numerically solve the governing equations.

The average Nusselt number (Nu) is strongly affected by the wall thermal conductivity primarily due to conduction resistance of the heated wall. For restrictive lower inlet widths and low Rayleigh numbers (Ra), Nu decreases. At large Ra however, Nu depends little on the lower inlet width. This is due to compensating inflow at the outlet (recirculation). Recirculation is due to inlet flow restrictions and a developing thermal boundary layer at the heated wall which allows cool reservoir fluid access via the outlet. It is shown that Nu depends on the ascending channel aspect ratio. Another parameter which combines the heated wall geometry and thermal conductivity into one parameter is demonstrated to correlate the heat transfer results well.

The results are compared to published experimental results for a similar problem. The comparison indicates that the present thermosyphon configuration is an efficient heat transfer device for sufficiently large wall , thermal conductivity and lower values of Ra.

CONJUGATE NATURAL CONVECTION HEAT TRANSFER IN A PLANAR THERMOSYPHON WITH MULTIPLE INLETS

by

John Joseph Fleming

A thesis submitted in partial fulfillment of the requirements for the degree

of

Master of Science

in

Mechanical Engineering

MONTANA STATE UNIVERSITY
Bozeman, Montana

April 1994

T1378
F629

APPROVAL

of a thesis submitted by

John Joseph Fleming

This thesis has been read by each member of the thesis committee and has been found to be satisfactory regarding content, English usage, format, citations, bibliographic style, and consistency, and is ready for submission to the College of Graduate Studies.

18 April 1994 — Date

Richard Amen — Chairperson, Graduate Committee

Approved for the Major Department

18 April 1994 — Date

Byron J. Bennett — Head, Major Department

Approved for the College of Graduate Studies

4/26/94 — Date

R. L. Benson — Graduate Dean

STATEMENT OF PERMISSION TO USE

In presenting this thesis in partial fulfillment of the requirements for a Master's degree at Montana State University, I agree that the Library shall make it available to borrowers under the rules of the Library.

If I have indicated my intention to copyright this thesis by including a copyright notice page, copying is allowable only for scholarly purposes, consistent with "fair use" as prescribed in the U. S. Copyright Law. Requests for permission for extended quotation from or reproduction of this thesis in whole or in parts may be granted only by the copyright holder.

Signature John S. Fleming

Date 4/19/94

ACKNOWLEDGEMENTS

I would like to thank Dr. Ruhul Amin for his guidance in the development of this project. I would like to express my appreciation to Dr. Alan George and Dr. Thomas Reihman for their work as committee members.

I would also like to thank Dr. Randy Clarksean at Argonne National Laboratory Idaho Falls for his valuable comments to Dr. Amin during the initial stage of this project.

My deepest appreciation is extended to my wife, Janice, for her understanding and endurance, and to John Gable for his support.

TABLE OF CONTENTS

	Page
LIST OF TABLES	vi
LIST OF FIGURES	vii
NOMENCLATURE	ix
ABSTRACT	xii
INTRODUCTION	1
Motivation for Present Research	4
Problem Description	5
Background	9
PROBLEM FORMULATION	16
Introduction	16
Governing Equations	16
Normalization of Governing Equations	22
NUMERICAL INVESTIGATION	31
Introduction	31
Computational Matrix	31
Computational Mesh	37
RESULTS AND DISCUSSION	42
Introduction	42
Effect of Lower Inlet Width Parameter	46
Effect of Thermal Conductivity Parameter	65
Average Nusselt Number Dependencies	79
Wall Conductivity Parameter	90
Aspect Ratio Parameter	93
CONCLUSIONS AND RECOMMENDATIONS	95
REFERENCES	98
APPENDICES	102
Appendix A-COSMOS/M Finite Element Program	103
Appendix B-FORTRAN Programs	110
Program to Compute Internal Average Nusselt Number	111
Program to Compute External Average Nusselt Number	114
Program for Combining COSMOS/M Output Files	116

LIST OF TABLES

Table		Page
1.	Parameter values and ranges of interest	33
2.	Computational matrix with fixed aspect ratio Ar = 6	35
3.	Computational matrix with fixed aspect ratio Ar = 3	36
4.	Results of mesh independence tests	39
5.	Computed average Nusselt numbers for the benchmark solution vs. the COSMOS/M solution	40
6.	Heated wall conductivity study parameter	90
7.	Overall Nusselt number results for K_r study . .	91
9.	Aspect ratio study parameters	93

LIST OF FIGURES

Figure		Page
1.	General open loop thermosyphon configuration . . .	2
2.	Schematic diagram of problem geometry	6
3.	Schematic diagram of problem showing boundary conditions	21
4.	Basic geometric configurations	34
5.	Element distribution meshes "B" and "A" (W_2=0.75)	41
6.	Isotherm plots with K=5 and Ar=6 for varying W_2 and Ra	48
7.	Stream function plots with K=5 and Ar=6 for varying W_2 and Ra	50
8.	Total mass inflow rate from all sources vs. Ra .	54
9.	Total mass inflow rate from lower and upper inlets vs. Ra	54
10.	Temperature distribution across outlet with parameters W_2 and Ra	57
11.	Vertical velocity distribution across outlet with parameters W_2 and Ra	58
12.	Heat transfer to upper inlet as a percent of total heat transfer ((Q_p/Q_w)100) vs. Ra	60
13.	Ratio of upper inlet to lower inlet mass flow rate (M_u/M_l) vs. Ra	60
14.	Heated wall and fluid interface local Nusselt number distribution with parameters W_2 and Ra	62
15.	Heated wall and fluid interface temperature distribution with parameters W_2 and Ra	63
16.	Isotherm plots with W_2=0.25 and Ar=6 for varying K and Ra	67
17.	Stream function plots with W_2=0.25 and Ar=6 for varying K and Ra	69

LIST OF FIGURES-continued

18. Heated wall and fluid interface temperature distribution with parameters K and Ra 72

19. Vertical velocity distribution across outlet with parameters K and Ra 75

20. Temperature distribution across outlet with parameters K and Ra 76

21. Heat transfer to upper inlet as a percent of total heat transfer ($(Q_p/Q_w)100$) vs. Ra 77

22. Ratio of upper inlet to lower inlet mass flow rate (M_u/M_l) vs. Ra 77

23. Total mass inflow rate from all sources vs. Ra . 78

24. Total mass inflow rate from lower and upper inlets vs. Ra 78

25. Average Nusselt number vs. Rayleigh number with parameters W_2 and K 82

26. Average Nusselt number vs. Rayleigh number with parameters K and W_2 84

27. Published heat transfer results compared with Nu for the present problem 87

28. Published heat transfer results compared with Nu_i for the present problem 89

29. Constant K_r solid/fluid interface temperature distribution comparison cases 1 and 2 92

30. Constant K_r solid/fluid interface local convection coefficient comparison cases 1 and 2 92

31. Correlation of Nu results vs. the modified Rayleigh number with constant K_r 94

32. Program to compute internal average Nusselt number 111

33. Program to compute external average Nusselt number 114

34. Program for combining COSMOS/M output files . . 116

NOMENCLATURE

Symbol	Description
Ar	inner channel aspect ratio, l_1/b
b	inner channel width
B	nondimensional inner channel width b/b
C_p	constant pressure specific heat
g_y	acceleration due to gravity
$\vec{g}$	acceleration vector
Gr	Grashof number $g_y \beta (T_w - T_\infty) b^3/\nu^2$
h_1	left wall thickness
H_1	nondimensional left wall thickness h_1/b
h_2	partition wall thickness
H_2	nondimensional partition wall thickness h_2/b
k	thermal conductivity
K	thermal conductivity ratio k_w/k_a
K_r	wall conductivity parameter $K_r=k_w l_1/k_a h_1=K(L_1/H_1)$
l_1	inner channel height
L_1	nondimensional inner channel height l_1/b
l_2	lower inlet length
L_2	nondimensional lower inlet length l_2/b
M	nondimensional mass flow rate $M = \dot{m}/\mu b$
Nu	average Nusselt number $Nu = \bar{q}\, b/k_a (T_w - T_\infty)$
Nu_1	average Nusselt number (equation 54)
p	pressure

NOMENCLATURE-continued

p_h	hydrostatic pressure
p_m	motion pressure ($p - p_h$)
Pr	Prandtl number ν/α
$\bar{q}$	average local heat flux
Q_p	total heat transfer across partition wall
Q_w	total heat transfer across heated wall
Ra	Rayleigh number $g_y \beta (T_w - T_\infty) b^3/\alpha\nu$
T	temperature
T_o	reference temperature
$\vec{u}$	velocity vector
U_o	characteristic velocity
u	horizontal velocity
v	vertical velocity
w_1	upper inlet width
W_1	nondimensional upper inlet width w_1/b
w_2	lower inlet width
W_2	nondimensional lower inlet width w_2/b
x	cartesian x coordinate
y	cartesian y coordinate

Greek Symbols

α	thermal diffusivity
β	coefficient of volumetric expansion
θ	nondimensional temperature $(T-T_\infty)/(T_w-T_\infty)$

NOMENCLATURE-continued

μ	dynamic viscosity
ν	kinematic viscosity
ρ	density
τ_{xx}, τ_{yy}	normal stresses
ψ	stream function
ψ^*	nondimensional stream function $\psi^*=\psi/\nu$

Subscripts and Superscripts

a	working fluid (air) value
i	solid/fluid interface value
l	lower inlet value
p	partition value
m	maximum
n	direction normal to surface
p	partition value
r	right wall value
u	upper inlet value
w	heated wall value
∞	ambient value
*	nondimensional quantity

ABSTRACT

The heat transfer results for the numerical investigation of a planar open loop thermosyphon are presented. The thermosyphon flow path is a modified "U" shape. Laminar flow is by natural convection due to heating the left ascending channel of the "U". Air (Pr=0.71) enters at the top and bottom of the right descending channel. The center portion of the "U" is a solid conducting wall and the left channel is bounded by a conducting wall. The left wall is heated isothermally along its external surface. All other external surfaces are adiabatic. This configuration is a modification of heat removal systems used in passive reactor cooling, nuclear waste material storage, and various other applications.

The average Nusselt number for this configuration was studied for different values of the governing parameters. These include the Rayleigh number, the ascending channel aspect ratio, the lower inlet width, and the wall thermal conductivity. These results are obtained using the proprietary finite element analysis program COSMOS/M to numerically solve the governing equations.

The average Nusselt number (Nu) is strongly affected by the wall thermal conductivity primarily due to conduction resistance of the heated wall. For restrictive lower inlet widths and low Rayleigh numbers (Ra), Nu decreases. At large Ra however, Nu depends little on the lower inlet width. This is due to compensating inflow at the outlet (recirculation). Recirculation is due to inlet flow restrictions and a developing thermal boundary layer at the heated wall which allows cool reservoir fluid access via the outlet. It is shown that Nu depends on the ascending channel aspect ratio. Another parameter which combines the heated wall geometry and thermal conductivity into one parameter is demonstrated to correlate the heat transfer results well.

The results are compared to published experimental results for a similar problem. The comparison indicates that the present thermosyphon configuration is an efficient heat transfer device for sufficiently large wall thermal conductivity and lower values of Ra.

INTRODUCTION

Natural convection heat transfer has been an area of increasing interest for many years. This interest is prompted by the wide variety of useful engineering applications in which natural convection is an important (or dominant) mode of heat transfer. Natural convection results from buoyancy forces which arise from the interaction of density variations within a fluid and a body force, usually gravity. The density variation is often due to temperature gradients in which case the flow is driven by thermal buoyancy forces. Natural convection is inherently reliable because it is completely self-sustaining; it requires no external pumps as does forced convection to initiate and maintain fluid circulation. This also makes it a relatively low cost heat transfer method, both for initial setup and for operation and maintenance.

Natural convection flows are governed by the conservation laws for mass, momentum, and energy. These laws expressed in mathematical form become a system of coupled, nonlinear partial differential equations. For all non-isothermal buoyancy induced flows the temperature and velocity fields are coupled and must be solved simultaneously.

Analytical solutions for natural convection flows exist for a relatively few situations. Most complex flows of engineering interest are not open to analytical methods, so numerical and experimental methods are relied upon. The

present study is strictly a numerical investigation. It should be noted that numerical results can only be validated by experiment.

The thermosyphon is a natural convection heat transfer device or configuration which makes use of thermal buoyancy forces to drive fluid circulation in systems that may be closed, partially open, or fully open. Of interest here is the open loop thermosyphon in which a circulating fluid is exchanged with a large external (nearly) constant temperature reservoir. The schematic of a typical configuration forming a "U" shaped flow path is shown in Figure 1.

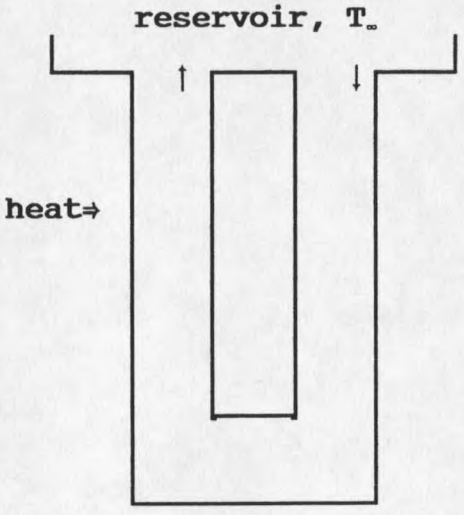


Figure 1. General open loop thermosyphon configuration.

Heat energy is transferred to the fluid in the left ascending leg of the thermosyphon. This causes the fluid to flow upwards due to the thermal buoyancy force. The flow in the ascending leg draws reservoir fluid into the right

descending leg establishing a continuous "open" flow loop.

Open loop thermosyphons have been successfully applied in a number of engineering applications. Cooling of electronic components is an important application [Jaluria (1985)]. Solar energy collection systems utilize natural convection extensively [Kreith and Anderson (1985)]. As shown by Clarksean (1993), passive heat removal from stored nuclear materials is an area of recent interest. Cooling of gas turbine blades is another important application [Japikse (1973)]. On a much larger scale, geothermal processes have been modelled as open loop thermosyphons [Torrance (1979)]. The following provides more detail of an important application of current interest.

The U. S. advanced liquid metal reactor (ALMR) design utilizes an open loop thermosyphon configuration to achieve inherently safe heat removal from a nuclear reactor in the event of the loss of primary coolant [Kwant and Boardman, (1992)]. This passive cooling system known as the reactor vessel auxiliary cooling system (RVAC) can be conceptually described as three vertical concentric cylinders: an inner, an intermediate, and an outer cylinder closed at the bottom. The inner cylinder is the reactor where heat is generated. Air heated by the hot reactor surface flows upward due to thermal buoyancy forces. This flow draws atmospheric air down an outer channel formed by the outer and intermediate cylinders. The resulting steady flow cools the reactor passively and

automatically. The system is designed so that in the event of primary coolant loss, safe reactor temperature levels will not be exceeded. The RVAC system is an important part of the power reactor inherently safe module (PRISM) design strategy.

Motivation for Present Research

Given the inherent reliability and importance of the open loop thermosyphon described above, further understanding is desirable in order to predict performance and optimize design parameters. A literature survey found many studies on natural convection between vertical parallel plates (a form of open loop thermosyphon) with a variety of boundary conditions. Also, some research has been conducted on the general "U" type geometry as in the RVAC system. Few studies however, have explicitly taken into account the thickness and finite thermal conductivity of the bounding wall surfaces. Research of natural convection in enclosures and vertical channels has indicated that the wall material and geometry were often significant parameters.

Previous research investigated open loop thermosyphons with the general "U" type flow configuration (one inlet and outlet) as shown in Figure 1. Modified open loop geometries with more than one inlet have not been explored. Further, no literature was found on the combined effect of wall conductivity and configuration of multiple flow inlets.

Greater understanding of these parameters is required for the optimization of open loop thermosyphons in engineering applications.

Problem Description

The objective of the present study is to conduct a steady state numerical investigation of the heat transfer characteristics of a single phase open loop thermosyphon. The geometry of the problem considered here is shown in Figure 2.

Linear dimensions in Figure 2 are shown in lower case, while the corresponding normalized dimensions are in upper case and enclosed in parentheses. All linear dimensions are normalized with respect to the inner channel width (B=1).

A Newtonian fluid (air, Pr=0.71) flows in the planar thermosyphon and is exchanged with constant temperature (T_∞) surroundings. A partition wall, a left wall, and a right wall of the same material, form the outer and inner channels. Fluid may enter the thermosyphon at two inlets placed at the upper and lower extremities of the outer channel. Fluid exits to the surroundings from the top of the inner left channel.

The flow is driven by a constant temperature boundary condition (T_w) applied at the left wall external surface. All other external surfaces are considered adiabatic. The computational domain is restricted to the thermosyphon to reduce computation time required. Thus, boundary conditions at the flow inlets and outlet are important considerations.

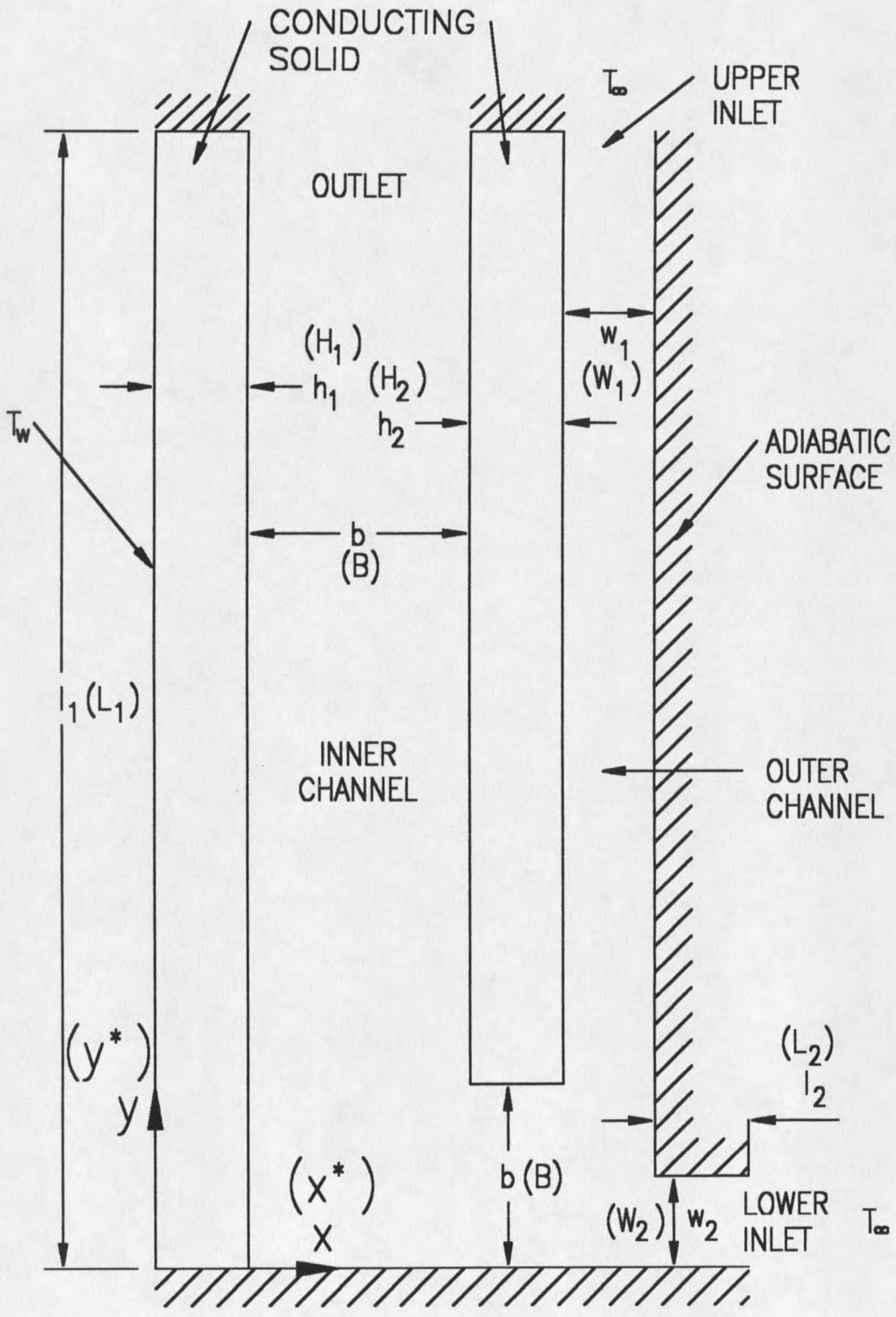


Figure 2. Schematic diagram of problem geometry.

Fluid enters the thermosyphon at the temperature of the surroundings (T_∞). The exiting fluid temperature is part of the solution and is not known a priori. A temperature boundary condition must be applied at the exit, so an approximate condition is specified. Previous work [Abib and Jaluria (1988)] has shown that setting the temperature gradient equal to zero in the vertical direction at the exit adequately approximates the interaction between the surroundings and the thermosyphon. Lateral fluid velocity and normal stress are also set equal to zero to complete the boundary conditions at the inlets and outlet. The Prandtl (no slip) boundary condition holds for all wetted surfaces. Further discussion of boundary conditions is deferred until later sections.

The overall heat transfer for this configuration is characterized by the average Nusselt number computed over the left wall surface. The average Nusselt number is a function of several geometric parameters, including wall widths and lengths, channel widths and length, and inlet widths. The average Nusselt number also depends upon the working fluid Prandtl number (Pr), the Rayleigh number (Ra), and the thermal conductivity of the wall material (k_w) and working fluid (k_a). The present study investigates numerically the average Nusselt number dependencies by varying a number of the parameters discussed above.

The investigation was performed by using a proprietary finite element analysis program known as COSMOS/M, developed by the Structural Research and Analysis Corporation. COSMOS/M was designed for applications ranging from micro-computers to mainframe machines.

The FLOWSTAR module of COSMOS/M was used for solving the equation system noted earlier. FLOWSTAR is a finite element program capable of solving two and three dimensional laminar or turbulent fluid flow and thermal problems including flows coupled with solid region conduction. For non-isothermal flows the fluid is assumed incompressible within the constraints of the Boussinesq approximation. Newtonian and non-Newtonian fluids may be modelled for laminar flow.

The governing equations are discretized using the Galerkin method of weighted residuals. For two dimensional problems, a four node quadrilateral element is used. The interpolation functions are bilinear for both temperature and velocity. The pressure variable is eliminated using the penalty function method. Further information on COSMOS/M and FLOWSTAR is included in Appendix A.

This investigation used a Digital Corporation 486, 66 Mhz computer with 24 MByte of RAM as the primary computing resource. A virtual disk (RAM disk) arrangement was used which significantly reduced computation times, with most cases converging in 30 minutes or less.

Background

The study of natural convection flows in a thermosyphon configuration has been and continues to be an area of considerable interest. Many investigations have been carried out. Much of the earlier work is summarized by Japikse (1973). A more recent review specific to the closed and open loop configurations is given by Mertol and Greif (1985).

Previous studies have looked at a great variety of boundary conditions and geometries. Typically either isothermal or isoflux boundary conditions are applied. This decouples the flow problem from the conduction problem existing in the walls, and implicitly assumes thin walls with large thermal conductivity. Thus, there has been little evaluation of the conduction heat transfer effects of the bounding walls. Some natural convection studies in rather closely related geometries (enclosures and vertical channels) have examined the wall conduction effects. Examples are Burch et al. (1985) and Kaminski and Prakash (1986). These studies lend insight, but do not address the geometry of interest here.

The present work investigates multiple inlets along with wall conduction. The open loop thermosyphon may exchange fluid with one or more large external reservoirs across outlet and inlet openings. A literature review indicates that all the previous works in this area are limited to one inlet and

one outlet. Therefore, the effects of multiple inlets are still unknown. The geometry explored in this research, essentially combines a "L" type channel with a "U" type channel. To the best knowledge of the author no information is available in the open literature which studies this configuration. The following paragraphs summarize some previous works which have the "U" configuration in common.

Lapin (1969) used an approximate analysis and experiment to evaluate the heat transfer capabilities of a "U" type open loop thermosyphon. The author was concerned with cooling of gas turbine blades, which continues to be an important application. Lapin found significant advantages over previous methods. In this case the body force is acceleration due to angular rotation, with coriolis acceleration further complicating the flow.

Torrance (1979) modelled groundwater flow in aquifers as naturally occurring open loop thermosyphons which are heated geothermally from below. Using analytical and numerical techniques the author determined critical Rayleigh numbers for the onset of flow, and exit temperatures. Torrance and Chan (1981) pursued this subject further by numerically considering the open loop thermosyphon embedded in a heat conducting solid, heated from below. A fluid with Prandtl number 2.8, and fluid/solid thermal conductivity ratio of 0.133 was used. Heat transfer rates were determined.

Bau and Torrance (1981) studied experimentally and analytically the dynamic performance of the same configuration, but with symmetric and asymmetric heating of the inlet, outlet, and horizontal legs. They found transient flow oscillations. Under appropriate conditions the oscillations may amplify and eventually cause flow reversal. In all cases steady state flow eventually prevailed. The oscillations are explained by the phase lag between change in heating conditions and generation of the thermal buoyancy force.

Clarksean (1993) studied experimentally the heat transfer characteristics of an open loop thermosyphon used to cool vertical, cylindrical heat sources. The geometry investigated is similar to the three concentric cylinder geometry discussed previously with the outermost surface thermally insulated. The author found that for sufficiently high Rayleigh numbers heat transfer rates became independent of channel width. This is explained by development of boundary layer flows and the limited interaction between boundary layers on adjacent surfaces. Comparison to numerical results [Miyatake et al. (1973)] for a similar geometry showed general agreement. Miyatake et al. considered parallel vertical plates, one with a uniform heat flux and the other adiabatic, but made no allowance for thermal conductivity in the bounding walls.

There is a wealth of information concerning flows in vertical channels or between parallel plates beginning with

Elenbass (1942) who found correlations for the average Nusselt number in terms of the Rayleigh number and channel aspect ratio. Several pertinent studies involving wall conduction in vertical channels and enclosures since Elenbass are discussed below.

Zinnes (1970) studied numerically the wall conduction effects for laminar natural convection from a single vertical plate with arbitrary heating. The results were experimentally verified. He found significant coupling between the natural convection flow and plate conduction. The plate to fluid thermal conductivity ratio (k_w/k_a) greatly affects the degree of coupling.

Kaminski and Prakash (1979) studied the effects of wall conduction in a square enclosure. They restricted the investigation to one conducting wall with three zero thickness walls completing the enclosure. They investigated numerically the overall heat transfer effects as a function of several parameters: Grashof (Gr) and Prandtl (Pr = 0.7) numbers, wall thickness to height ratio (t/L), and wall to fluid thermal conductivity ratio (k_w/k_a). For constant Gr and Pr, they found the overall heat transfer was a function of the independent parameter k_wL/k_at. For a constant value of k_wL/k_at the fluid/solid interface temperature distribution is independent of k_w/k_a and L/t separately. The enclosure fluid "sees" the same thermal driving force, and thus the overall heat transfer is correlated well with this parameter.

Kim and Viskanta (1985) presented numerical and experimental heat transfer results for a planar rectangular enclosure, but with four finite conducting walls. Isothermal boundary conditions were imposed on the external vertical wall surfaces, while the horizontal walls were adiabatic. The authors found that wall conduction reduces the temperature difference across the enclosure fluid, stabilizes the flow, and reduces overall heat transfer. The thermal conductivity ratio, and wall geometry (thickness and length) were important parameters.

Burch et al. (1985) conducted numerical studies of natural convection between two finite conducting vertical plates. The authors report that wall conduction has significant effects on the natural convection heat transfer in comparison to constant temperature walls. The effects are greater at high Grashof numbers, low thermal conductivity ratios, and high wall thickness to channel width ratios. The wall/fluid interface temperature and heat flux distributions are not uniform and are influenced by wall conduction more at higher Grashof numbers.

Mallinson (1987) also investigated numerically natural convection heat transfer in a rectangular enclosure with length (l) and width (w). Walls with finite conductivity and thickness (t) form the lengthwise sides. He used a new approach in modelling the wall-to-fluid interface by deriving a separate equation for the interface temperature. The author

indicates the conditions between the limiting cases of perfectly conducting and adiabatic walls exist when $0.1 \leq (w/t)/K \leq 100$. In this expression K is the wall-to-fluid thermal conductivity ratio, and (w/t) is the enclosure-to-wall width ratio.

Kim et al. (1990) investigated wall conduction effects on laminar natural convection between asymmetrically heated (uniform heat flux) vertical plates. Parameters of interest included: solid to fluid thermal conductivity ratio, wall to channel thickness ratios, and Grashof number. They found significant reduction (22%) in overall Nusselt number due to wall conduction. This occurs at low thermal conductivity ratios, large thickness ratios, and increases with Grashof number.

A recent numerical study investigates mixed convection in a cavity with conducting walls and a localized heat source [Papanicolaou and Jaluria (1993)]. With the assumption of adiabatic walls, the authors reported an error of 5.4% for the average Nusselt number computed over the heat source. This was for the case of relatively low thermal conductivity ratio of 0.8. Error increases as the thermal conductivity ratio increases.

All the above studies which address wall conduction used the thermal conductivity ratio ($K = k_w/k_a$) as an independent parameter to correlate heat transfer results. This parameter arises from the nondimensional form of the continuous heat

flux condition at the wall-to-fluid interface. Geometric parameters related to wall conduction are more problem specific, but clearly geometry plays an important role.

None of the works cited above addressed the questions raised here: effect of wall conduction and multiple inlets in an open loop thermosyphon configuration. Therefore, investigation of these questions may lead to more efficient thermal design of heat transfer equipment.

Other references in addition to those cited previously were invaluable in the progress of the present problem. The fundamentals of buoyancy induced flows are presented thoroughly in a text by Gebhart et al. (1988). Other natural convection references consulted include texts by Kays and Crawford (1980), and Bejan (1984). The textbook by Patankar (1980) is based on finite difference methods but offers insight in the methodology of numerical investigations.

On the subject of finite element analysis several textbooks were found useful. Huebner and Thornton (1982), Chung (1978), and Burnette (1988) were important in understanding FEM so that the method was properly applied to the present problem.

PROBLEM FORMULATION

Introduction

For the present study the natural convection flow of interest is assumed to be a steady state, two dimensional, laminar, and viscous flow of a constant property fluid. The fluid is Newtonian and incompressible. No heat generation exists in either the fluid or solid regions. The surroundings consist of an extensive, quiescent, isothermal reservoir at constant temperature T_∞. Thermal radiative heat transport is also neglected.

The Boussinesq approximation is invoked. It consists of two primary simplifying assumptions. The fluid density is assumed constant except in its interaction with the body force (gravity), from which buoyancy forces arise. All other thermophysical properties are assumed constant, and are evaluated at a selected reference temperature and pressure.

With the assumptions above the governing equations and boundary conditions are expressed in terms of the primitive variables velocity, temperature, and pressure. These equations are then nondimensionalized to isolate relevant nondimensional parameters.

Governing Equations

For the present problem, the fluid flow and heat transfer are described by the conservation laws for mass (continuity),

momentum (Navier-Stokes), and energy. These laws are expressed below by equations (1), (2), and (3) respectively. Heat transfer in the solid regions of the problem domain is described by the energy equation (4). The compressibility work and viscous dissipation terms of the energy equation have been neglected. Note the Boussinesq approximation has not yet been included explicitly in the momentum equation (2).

$$\nabla \cdot \vec{u} = 0 \tag{1}$$

$$\rho(\vec{u} \cdot \nabla)\vec{u} = -\nabla p + \mu\nabla^2\vec{u} + \rho\vec{g} \tag{2}$$

$$\rho C_p(\vec{u} \cdot \nabla T) = k_a\nabla^2 T \tag{3}$$

$$k_w\nabla^2 T = 0 \tag{4}$$

As noted earlier, the driving force behind natural convection flow is the variation in density due to temperature gradients. For the thermal buoyancy force term to appear explicitly in the momentum equation (2), the Boussinesq approximation is used. The following paragraphs detail how it is applied to this problem.

First, the pressure term in equation (2) is replaced with a modified pressure known as the motion pressure. Motion pressure is understood simply as the difference between the actual pressure (p) at any point in the fluid, and the hydrostatic pressure (p_h) that would exist at the same point in the absence of fluid flow. Motion pressure ($p_m = p - p_h$) is due to acceleration, viscous forces, and buoyancy forces.

Consider the following equations (5) and (6). The divergence of the hydrostatic pressure (5) is simply the body force per unit volume due to gravity ($-g_y$). The motion pressure (p_m) divergence is given in equation (6).

$$\nabla p_h = -g_y \rho_\infty \tag{5}$$

$$\nabla p_m = \nabla p - \nabla p_h = \nabla (p - p_h) \tag{6}$$

The pressure gradient and body force terms $(-\nabla p + \rho \vec{g})$ of the momentum equation (2) are rewritten using equations (5) and (6). In the present problem note that $\vec{g} = -g_y$.

$$-\nabla p - \rho g_y = -\rho g_y - \nabla p_h - \nabla (p - p_h) \tag{7}$$

$$-\nabla p - \rho g_y = -g_y (\rho - \rho_\infty) - \nabla p_m \tag{8}$$

Equation (8) above, is substituted into the momentum equation (2) with the result shown below.

$$\rho (\vec{u} \cdot \nabla) \vec{u} = -\nabla p_m + \mu \nabla^2 \vec{u} - g_y (\rho - \rho_\infty) \tag{9}$$

The final term in equation (9) is the buoyancy force per unit volume. It is represented by the density difference which next is rewritten in terms of temperature. The definition for β, the coefficient of volumetric expansion (equation 10), is used to make a simple linear approximation for the buoyancy force term. The final form of the buoyancy force term appears as in equation (11).

$$\beta = -\frac{1}{\rho}\left(\frac{\partial \rho}{\partial T}\right)_p \tag{10}$$

$$-g_y(\rho - \rho_\infty) \approx g_y \rho \beta (T - T_\infty) \tag{11}$$

Gebhart et al. (1988) supplies arguments to support the validity of the approximation in equation (11). The final form of the momentum equation is equation (12).

$$\rho(\vec{u} \cdot \nabla)\vec{u} = -\nabla p_m + \mu \nabla^2 \vec{u} + \rho g_y \beta (T - T_\infty) \tag{12}$$

One objective of this development is to show the correct inlet temperature boundary condition. When the local temperature (T) is equal to the temperature of the surroundings (T_∞) the buoyancy force is zero. Fluid enters from the isothermal surroundings at temperature T_∞. Any other temperature specified at the inlet would introduce a false buoyancy. This holds true except for low Rayleigh numbers where conduction effects extend across the inlet boundary.

The buoyancy term in equation (12) accounts for variation in hydrostatic pressure since when integrated it will be a function of vertical position. How well the buoyancy force term and the constant property formulation models the actual physics depends largely on the reference state selected. Further discussion of the reference state will follow.

Boundary conditions specific to the present problem are presented on the following page. Refer to Figure 2 for dimensioning nomenclature. Figure 3 presents a graphical representation of the boundary conditions used.

$$u = v = 0 \text{ for } \begin{bmatrix} x = h_1 \text{ and } 0 \le y \le l_1 \\ h_1 \le x \le (h_1 + b + h_2 + w_1 + l_2) \text{ and } y = 0 \\ (h_1 + b + h_2 + w_1) \le x \le (h_1 + b + h_2 + w_1 + l_2) \text{ and } y = w_2 \\ x = (h_1 + b + h_2 + w_1) \text{ and } w_2 \le y \le l_1 \\ x = (h_1 + b) \text{ and } b \le y \le l_1 \\ x = (h_1 + b + h_2) \text{ and } b \le y \le l_1 \\ (h_1 + b) \le x \le (h_1 + b + h_2) \text{ and } y = b \end{bmatrix} \quad (13)$$

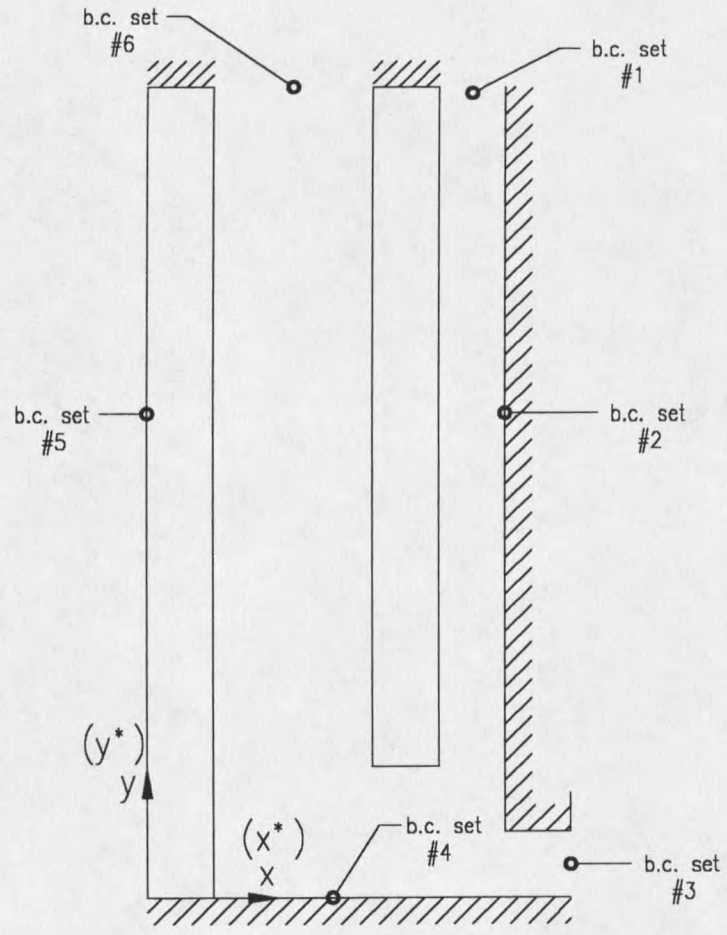
$$T = T_w \text{ for } x = 0 \text{ and } 0 \le y \le l_1 \quad (14)$$

$$\frac{\partial T}{\partial n} = 0 \text{ for } \begin{bmatrix} 0 \le x \le (h_1 + b + h_2 + w_1 + l_2) \text{ and } y = 0 \\ 0 \le x \le h_1 \text{ and } y = l_1 \\ (h_1 + b + h_2 + w_1) \le x \le (h_1 + b + h_2 + w_1 + l_2) \text{ and } y = w_2 \\ x = (h_1 + b + h_2 + w_1) \text{ and } w_2 \le y \le l_1 \\ (h_1 + b) \le x \le (h_1 + b + h_2) \text{ and } y = l_1 \end{bmatrix} \quad (15)$$

$$\begin{bmatrix} u = 0 \\ \tau_{yy} = 0 \\ \frac{\partial T}{\partial y} = 0 \end{bmatrix} \text{ for } h_1 \le x \le (h_1 + b) \text{ and } y = l_1 \quad (16)$$

$$\begin{bmatrix} u = 0 \\ \tau_{yy} = 0 \\ T = T_\infty \end{bmatrix} \text{ for } (h_1 + b + h_2) \le x \le (h_1 + b + h_2 + w_1) \text{ and } y = l_1 \quad (17)$$

$$\begin{bmatrix} v = 0 \\ \tau_{xx} = 0 \\ T = T_\infty \end{bmatrix} \text{ for } x = (h_1 + b + h_2 + w_1 + l_2) \text{ and } 0 \le y = w_2 \quad (18)$$



Boundary conditions:

b.c. set 1 $(T = T_\infty,\ u = 0,\ \tau_{yy} = 0)$ **b.c. set 2** $\left(\frac{\partial T}{\partial x} = 0\right)$

b.c. set 3 $(T = T_\infty,\ v = 0,\ \tau_{xx} = 0)$ **b.c. set 4** $\left(\frac{\partial T}{\partial y} = 0\right)$

b.c. set 5 $(T = T_w)$ **b.c. set 6** $\left(\frac{\partial T}{\partial y} = 0,\ u = 0,\ \tau_{yy} = 0\right)$

b.c. set 7 all wetted surfaces $u = v = 0$

Figure 3. Schematic diagram of problem showing boundary conditions.

The first partial derivative of temperature shown in equation (15) is in the direction normal to the boundary. Also, the normal stress terms in equations (16), (17), and (18) are defined below.

$$\tau_{yy} = - p_m + \mu \frac{\partial v}{\partial y} \quad \text{and} \quad \tau_{xx} = - p_m + \mu \frac{\partial u}{\partial x} \tag{17}$$

One further constraint on the numerical solution is prescribed at the solid-to-fluid interface. Both temperature and heat flux must be continuous across the interface. The continuous heat flux and temperature condition at the solid/fluid interface are given below:

$$\left(k_w \frac{\partial T}{\partial n}\right)_{solid} = \left(k_a \frac{\partial T}{\partial n}\right)_{fluid} \tag{20}$$

$$T_{solid} = T_{fluid} \tag{21}$$

where (n) is the direction normal to the solid surface.

Normalization of Governing Equations

The following dimensionless variables are used to nondimensionalize the governing equations:

$$x^* = \frac{x}{b} \tag{22}$$

$$y^* = \frac{y}{b} \tag{23}$$

$$\vec{u}^* = \frac{\vec{u}}{U_o} \tag{24}$$

$$\theta = \frac{(T - T_\infty)}{(T_w - T_\infty)} \tag{25}$$

$$p_m^* = \frac{p_m}{\rho U_o^2} \tag{26}$$

The characteristic velocity U_o, is defined below in velocity units. The derivation of U_o is discussed in detail later.

$$U_o = \frac{\alpha}{b}\sqrt{Ra\,Pr\,Ar} \tag{27}$$

By substitution of these dimensionless quantities into the governing equations 1,12,3, and 4, the normalized governing equations are obtained. Note the buoyancy term appears only in the vertical (y) component of equation (29). The result is as follows for the fluid region,

$$\nabla \cdot \vec{u}^* = 0 \tag{28}$$

$$(\vec{u}^* \cdot \nabla)\,\vec{u}^* = -\nabla p_m^* + \sqrt{\frac{Pr}{Ra\,Ar}}\,\nabla^2 \vec{u}^* + \frac{\theta}{Ar} \tag{29}$$

$$(\vec{u}^* \cdot \nabla\theta) = \nabla^2\theta \frac{1}{\sqrt{Ra\,Pr\,Ar}} \tag{30}$$

and the solid regions.

$$\nabla^2\theta = 0 \tag{31}$$

The nondimensional parameters appearing in the normalized governing equations are defined as:

$$Ra = \frac{g_y \beta\,(T_w - T_\infty)\,b^3}{\alpha\nu} \qquad Pr = \frac{\nu}{\alpha} \qquad Ar = \frac{l_1}{b}\ . \tag{32}$$

The normalized boundary conditions are also given below. Refer to Figure 2 for dimensioning nomenclature.

$$u^*=v^*=0 \quad \left[\begin{array}{l} x^* = H_1 \text{ and } 0 \le y^* \le L_1 \\ H_1 \le x^* \le (H_1 + B + H_2 + W_1 + L_2) \text{ and } y^* = 0 \\ (H_1+B+H_2+W_1) \le x^* \le (H_1+B+H_2+W_1+L_2) \text{ and } y^*=W_2 \\ x^* = (H_1 + B + H_2 + W_1) \text{ and } W_2 \le y^* \le L_1 \\ x^* = (H_1 + B) \text{ and } B \le y^* \le L_1 \\ x^* = (H_1 + B + H_2) \text{ and } B \le y^* \le L_1 \\ (H_1 + B) \le x^* \le (H_1 + B + H_2) \text{ and } y^* = B \end{array}\right] \tag{33}$$

$$\theta = \theta_w \quad \text{for} \quad x^* = 0 \text{ and } 0 \le y^* \le L_1 \tag{34}$$

$$\frac{\partial\theta}{\partial n^*}=0 \text{ for } \left[\begin{array}{l} 0 \le x^* \le (H_1+B+H_2+W_1+L_2) \text{ and } y^* = 0 \\ 0 \le x^* \le H_1 \text{ and } y^* = L_1 \\ (H_1+B+H_2+W_1) \le x^* \le (H_1+B+H_2+W_1+L_2) \text{ and } y^*=W_2 \\ x^* = (H_1 + B + H_2 + E_1) \text{ and } W_2 \le y^* \le L_1 \\ (H_1 + B) \le x^* \le (H_1 + B + H_2) \text{ and } y^* = L_1 \end{array}\right] \tag{35}$$

$$\left[\begin{array}{l} u^* = 0 \\ \tau^*_{yy} = 0 \\ \dfrac{\partial\theta}{\partial y^*} = 0 \end{array}\right] \quad \text{for} \quad H_1 \le x^* \le (H_1 + B) \quad \text{and} \quad y^* = L_1 \tag{36}$$

$$\left[\begin{array}{l} u^* = 0 \\ \tau^*_{yy} = 0 \\ \theta = 0 \end{array}\right] \text{for } (H_1 + B + H_2) \le x^* \le (H_1 + B + H_2 + W_1) \text{ and } y^* = L_1 \tag{37}$$

$$\begin{bmatrix} v^* = 0 \\ \tau^*_{xx} = 0 \\ \theta = 0 \end{bmatrix} \text{ for } x^* = (H_1 + B + H_2 + W_1 + L_2) \text{ and } 0 \le y^* \le W_2 \qquad (38)$$

where,

$$\tau^*_{yy} = \frac{\tau_{yy}}{\rho U_o^2} = -p_m^* + \sqrt{\frac{Pr}{RaAr}} \frac{\partial v^*}{\partial y^*} \; ; \; \tau^*_{xx} = \frac{\tau_{xx}}{\rho U_o^2} = -p_m^* + \sqrt{\frac{Pr}{RaAr}} \frac{\partial u^*}{\partial x^*} .$$

The fluid-to-solid interface condition is expressed in nondimensional terms where the thermal conductivity ratio, $K = k_w/k_a$, appears as a consequence of the continuous heat flux across the interface.

$$K\left(\frac{\partial \theta}{\partial n^*}\right)_{solid} = \left(\frac{\partial \theta}{\partial n^*}\right)_{fluid} \qquad (39)$$

$$\theta_{solid} = \theta_{fluid} \qquad (40)$$

The function of the preceding nondimensional formulation is primarily to isolate relevant nondimensional parameters. All numerical solutions are performed using the primitive variables as required by COSMOS/M. Thus, the normalized governing equations and boundary conditions are not used for numerical computations.

Relevant nondimensional parameters arise through the normalization of the dependent and independent variables ($\vec{u}$,T,p,x,y) and subsequent normalization of the governing equations and boundary conditions. Thus, the method used to normalize the dependent and independent variables is critical so that important parameters are not overlooked.

The dimensionless variables shown in equations (22) through (26) require some explanation, particularly concerning the characteristic velocity U_o. There is no obvious velocity scale (characteristic velocity) for buoyancy-driven flows, but U_o may be estimated. One estimation method [Gebhart et al. (1988)] equates the kinetic energy per unit volume of the flow, $\rho u^2/2$, to the work done per unit volume by the buoyancy force, $-g_y(\rho - \rho_\infty)$, over some characteristic length (l_1). This is shown below.

$$\rho \frac{u^2}{2} = -g_y (\rho - \rho_\infty) l_1 = \rho\, g_y \beta (T_w - T_\infty) l_1 \qquad (41)$$

Solving equation (41) above for the velocity u, and keeping in mind the definitions for Ra and Ar, the characteristic velocity is found as previously defined in equation (27).

$$u_{max} = U_o = \sqrt{g_y \beta (T_w - T_\infty) l_1} = \frac{\alpha}{b} \sqrt{Ra\, Pr\, Ar} \qquad (42)$$

The characteristic velocity (U_o) defined above was used to normalize the governing equations; however, a more realistic estimation is possible. The development of this estimate is the subject of the following paragraphs. First, it should be made clear that the objective here is to show the existence and theoretical basis for another nondimensional parameter not previously apparent.

The problem with the definition for U_o (equation 42) is the temperature difference $(T_w - T_\infty)$; the actual temperature difference across the fluid is $(T_i - T_\infty)$, where T_i is the

temperature of the fluid-to-solid interface along the heated wall. Due to low wall thermal conductivity T_i may be considerably less than T_w. Thus, U_o depends more realistically on $(T_i - T_\infty)$ rather than $(T_w - T_\infty)$.

A better estimate for U_o is found by estimating the temperature difference $(T_i - T_\infty)$. Assuming one dimensional heat conduction across the heated wall, $(T_i - T_\infty)$ is estimated in equation (43) below. The parameter K_r which appears is the product of the thermal conductivity ratio and the heated wall aspect ratio ($K_r = k_w l_1 / k_a h_1$). This result (equation 43) is substituted into equation (41) with the resulting U_o shown in equation (44).

$$(T_i - T_\infty) \approx \frac{K_r}{K_r + Nu} (T_w - T_\infty) \tag{43}$$

$$U_o = \frac{\alpha}{b} \left(Ra\,Pr\,Ar \left(\frac{K_r}{Nu + K_r}\right)\right)^{\frac{1}{2}} \tag{44}$$

Here the average Nusselt number is computed by averaging the local heat flux over the surface of the heated wall. This is shown in equation (45) using the fluid thermal conductivity (k_a), the solid/fluid interface temperature difference, the heated wall length (l_1), and the average wall heat flux ($\bar{q}$).

$$Nu = \frac{\bar{q}\, l_1}{k_a (T_i - T_\infty)} \tag{45}$$

Note that this definition for Nu is relevant only for this discussion and is not used to present results in this study.

The parameter K_r is the same as that presented by Kaminski and Prakash (1986), and discussed in conjunction with the literature review. Essentially, this shows the dependence of the characteristic velocity U_o on the parameter K_r and illustrates that correct scaling of the governing equations should include this parameter. This has not been shown explicitly in the governing equations (28) through (31), because it results in a messy algebraic expression that does not help clarify the concept. Results of this study are used to verify that K_r is a useful parameter for correlation of overall heat transfer results.

As noted earlier, the formulation assumes constant working fluid properties. These properties however, vary significantly with temperature. To account for variable properties the reference temperature method is used. Selection of a suitable reference temperature (T_o) must answer two questions: what temperature between T_w and T_∞ best approximates the variable property behavior, and what is the maximum temperature range ($T_w - T_\infty$) over which the reference temperature method remains valid.

Sparrow and Gregg (1958), considered natural convection flow from a vertical isothermal surface with perfectly conducting walls, by solving the variable property and constant property formulations. They found the reference

temperature (with $\beta = 1/T_\infty$) at which the constant property results best approximate the variable property results. They found the film temperature, $T_o = (T_w + T_\infty)/2$, serves as an appropriate reference temperature for most engineering applications. They also gave error estimates for use of reference temperatures other than the indicated T_o.

Gray and Giorgini (1976) among other things, provided a method for determining over what temperature range the reference temperature method remains valid for a given Newtonian liquid or gas. Zhong et al. (1985) suggested the maximum difference between the wall and ambient temperatures should be chosen so that $(T_w - T_\infty)/T_\infty \leq 0.1$. For this study the methods above produce essentially identical temperature ranges. These results are based on perfectly conducting walls where $T_i = T_w$.

The temperature difference of interest here $(T_i - T_\infty)$, rather than $(T_w - T_\infty)$, is unknown. Therefore, numerical solutions were obtained by iteration. With the reference temperature (T_o) held constant, the temperature boundary conditions T_w and T_∞ where updated over successive iterations until the relations given below were approximately satisfied.

$$T_o = (T_i + T_\infty)/2 \tag{46}$$

$$(T_i - T_\infty)/T_\infty \leq 0.1 \tag{47}$$

For the present problem and Rayleigh numbers in the range of 10^3 to 2.5×10^5, the iteration procedure is not required.

Sparrow and Gregg (1958) have given data indicating constant property solutions are relatively independent of reference temperature selection for T_w/T_∞ ratios less than approximately 1.15, provided T_o is less than T_w and greater than T_∞. They indicate a maximum deviation (error) of 1%, between the constant and variable property solutions. Thus, iterations are required only for larger Rayleigh numbers.

Another issue that affects the accuracy of the numerical solution is the approximate boundary conditions applied at the inflow and outflow boundaries of the computational domain. Conditions especially at the outflow are essentially unknown. The boundary conditions used here have been investigated and found to result in reliable results for heat transfer and flow fields. Further discussion of inflow and outflow boundary conditions can be found in Abib and Jaluria (1988).

NUMERICAL INVESTIGATION

Introduction

The boundary value problem formulated in the previous chapter is not open to any known analytical solution technique. The governing equations (1,12,3,and 4) form a set of elliptic, nonlinear, coupled, partial differential equations. These equations have been solved numerically using a variety of techniques, including finite differences and finite element methods.

The present work utilizes the finite element method (FEM) primarily because the FEM is applied with relative ease, requiring minimal new computer code for data reduction. Also, the inclusion of solid regions in the problem domain is handled easily by COSMOS/M, simply by constraining all solid region nodes to have zero velocity. The FEM software is relatively user friendly, and is PC compatible which reduces the logistics required to obtain solutions. A brief description of the code is included in Appendix A.

Computational Matrix

The overall heat transfer, represented by the average Nusselt number (Nu), is the objective of interest. The average Nusselt number is computed at the heated wall external surface (equation 48). Note that since Nu is evaluated in a solid region, it cannot be interpreted as representing a convective

heat transfer coefficient. Instead, Nu represents the nondimensional average heat flux normal to the heated wall.

$$Nu = \frac{\bar{q}\, b}{k_a (T_w - T_\infty)} = \frac{k_w}{k_a} \frac{b}{l_1} \frac{1}{(T_w - T_\infty)} \int_0^{l_1} \frac{\partial T}{\partial x} dy \qquad (48)$$

Consideration of the normalized governing equations indicates that a parametric study of the heat transfer characteristics for the present problem involves numerous nondimensional parameters. The average Nusselt number is shown as a function of these parameters below.

$$Nu = Nu(Ra, Pr, Ar, K, \text{other geometric parameters})$$

Other geometric parameters (see Figure 2) which do not appear explicitly in the normalized governing equations but appear in the boundary conditions include: the partition width h_2, the inlet channel widths w_1 and w_2, and the lower inlet channel length l_2. These parameters are normalized with the inner channel width b, and the nondimensional forms are shown below.

$$W_1 = \frac{w_1}{b} \quad W_2 = \frac{w_2}{b} \quad H_2 = \frac{h_2}{b} \quad L_2 = \frac{l_2}{b}$$

Including all parameters, the average Nusselt number functional dependencies are as follows:

$$Nu = Nu(Ra, Pr, Ar, K, W_1, W_2, H_2, L_2)$$

A complete investigation including all of these parameters is beyond the scope of this study.

The project was limited first of all by considering only air as the working fluid (Pr = 0.71). Other constants are the upper inlet channel width ($W_1 = B/2$), the lower inlet channel length ($L_2 = B/2$), and the partition wall thickness ($H_2 = B/2$). With these parameters fixed a total of four parameters remain.

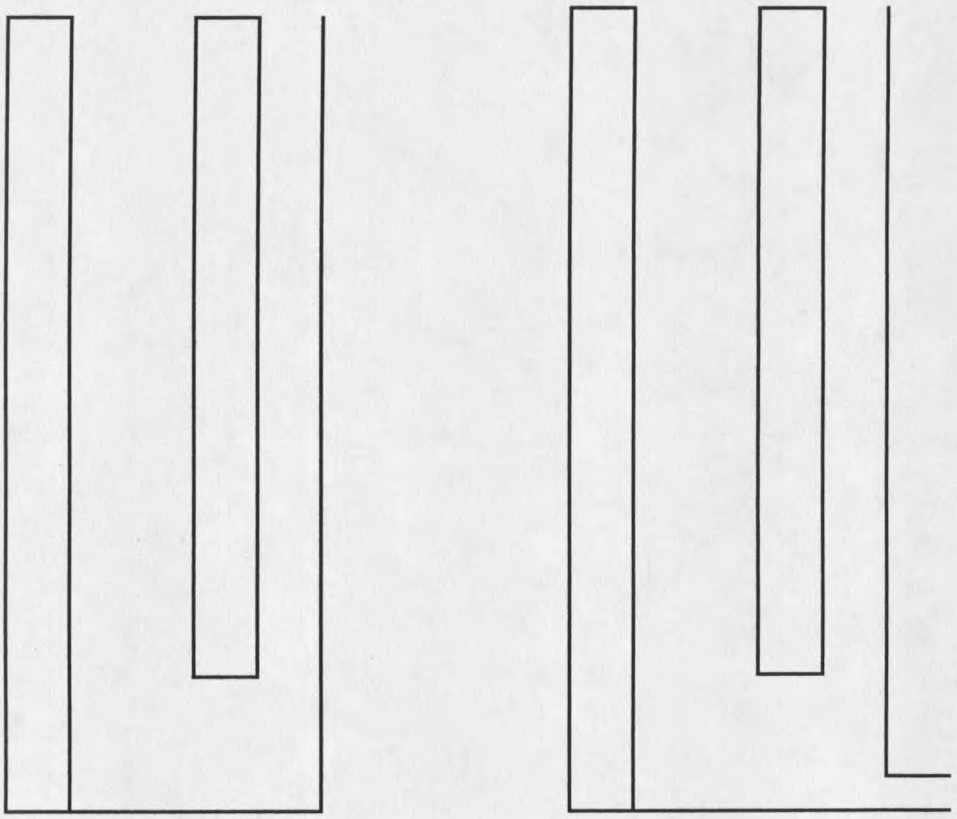
$$Nu = Nu(Ra, Ar, K, W_2)$$

To find the functional dependence given implicitly above, each parameter was varied independently of the others over a range of interest. The discrete values for each parameter in the ranges of interest are given below.

Table 1. Parameter values and ranges of interest.

Rayleigh number (Ra)	10^3, $5x10^3$, 10^4, $5x10^4$, 10^5, 2.5x10, $5x10^5$, 10^6
Thermal conductivity ratio (K)	0.1, 1, 5, 10
Aspect ratio (Ar)	3, 6
Lower inlet width (W_2)	0.0, 0.25, 0.5, 0.75

Figure 4 shown on the following page displays an outline of the basic geometries investigated. The lower inlet width W_2 is the primary geometric parameter. The normalization of the governing equations indicates K_r, the wall conductivity parameter, may also be useful for heat transfer correlations. To evaluate this possibility the thermal conductivity ratio K, the aspect ratio Ar, and the wall aspect ratio l_1/h_1 were varied.



Ar=6 W_2=0.0
$l_1 \backslash h_1$=12

Ar=6 W_2=0.25
l_1/h_1=12

Figure 4. Basic geometric configurations.

The governing equations were solved numerically for a total of 160 cases corresponding to the parameter values and geometries. The solution procedure was organized so that eight solutions spanning the entire range of Rayleigh numbers were obtained for fixed values of K, Ar, and W_2. Next K was varied, and eight more solutions obtained. This pattern continued until all four K values were evaluated. A new value for the lower inlet width W_2 was then assigned, and the procedure was repeated. This pattern continued until all four W_2 values were evaluated. Finally the aspect ratio Ar was varied and a much smaller total number of cases were evaluated. The computational matrix is given below in Tables 2 and 3.

Table 2. Computational matrix with fixed aspect ratio Ar = 6.

Rayleigh number (Ra)	W_2	Thermal conductivity ratio (K)	number of cases evaluated	l_1/h_1
$10^3...10^6$	0.0	0.1, 1, 5, 10	32	12
$10^3...10^6$	0.25	0.1, 1, 5, 10	32	12
$10^3...10^6$	0.50	0.1, 1, 5, 10	32	12
$10^3...10^6$	0.50	1 (K_r = 60)	8	60
$10^3...10^6$	0.50	5 (K_r = 120)	8	24
$10^3...10^6$	0.75	0.1, 1, 5, 10	32	12

Table 3. Computational matrix with fixed aspect ratio Ar = 3.

Rayleigh number (Ra)	W_2	Thermal conductivity ratio (K)	number of cases evaluated	l_1/h_1
$10^3...10^6$	0.50	5 (K_r = 60)	8	12
$10^3...10^6$	0.50	10 (K_r = 60)	8	6

The computational time required to obtain solutions at each Rayleigh number was significantly reduced by using the solution at a lower Rayleigh number as the initial approximation for a successively larger Rayleigh number solution. This is why the computational order described above was used.

Each solution was obtained first using a series of Picard iterations and then switching to Newton-Raphson iterations until the solution converged. Convergence was declared when the norm on the change in each of the dependent variables between successive iterations was less than 0.01%. Note that the analysis was done in terms of the primitive variables, not the nondimensional variables.

Computational Mesh

The computational mesh is chosen so that accurate results are obtained while minimizing computing time. Solution accuracy and computation time increase with the number of elements and nodes. The following is an overview of how the mesh configurations used were chosen.

As discussed earlier, the selection of a working fluid fixes material properties and the maximum temperature difference between the heated wall and the ambient surroundings. Thus, the inner channel width (b) appearing in the Rayleigh number definition depends on the maximum Rayleigh number for which solutions are desired (equation 49). For an order of magnitude increase in the maximum Rayleigh number the physical size of the mesh (b) must increase almost 2.2 times.

$$Ra \propto b^3 \tag{49}$$

It follows for a rectangular geometry the number of nodes must increase more then 4 times, if element size is unchanged. For the computer system used here a doubling of the number of nodes effectively quadruples the computation time. Thus, to increase the maximum Rayleigh number by a factor of 10, the computation time required increases by a factor of 16.

A further limitation on the maximum Rayleigh number attainable is the need to show the solutions obtained are independent of the mesh used. This is done by increasing the

number of elements used, further increasing computation time. Therefore, allowable computation time determines the maximum Rayleigh number attainable. For the present work 28 hours were required for mesh independence tests which means approximately 1.5 hours were required to solve each case.

An independent mesh for each value of the Aspect ratio (Ar), and lower inlet width (W_2) was constructed. The meshes are non-uniform to decrease the number of elements required and still resolve areas of high temperature and velocity gradients. Use of non-uniform meshes is based on the idea that dense packing of small elements in regions of high gradients will yield improved accuracy. This is done provided that regions of larger, less dense elements do not degrade the overall accuracy of the solutions.

To test for mesh independence, two different meshes for a given geometry, mesh "A" and mesh "B", were constructed. Mesh "A" contained approximately twice as many nodes as mesh "B". Solutions for the largest Rayleigh number (10^6) were obtained for both meshes. The computed average Nusselt number was then compared for the two meshes. The results are tabulated in Table 4. In general the results agree well with less than 2% difference in the average Nusselt numbers.

Table 4. Results of mesh independence tests.

number of nodes mesh"A"/mesh"B"	% difference average Nu	Ar/W_2	Rayleigh number
3822/2340	0.7	6/0.0	10^6
3626/2148	1.1	6/0.25	10^6
3998/2347	0.85	6/0.50	10^6
4393/2222	0.8	6/0.75	10^6
2092/1253	1.2	3/0.5	10^6

For a direct comparison , meshes "A" and "B" for the geometric parameters Ar=6 and W_2=0.75 is provided in Figure 5. It is typical of the other meshes used. Numerical results for the cases considered were obtained using the "B" meshes.

As noted previously the numerical solutions for each of the meshes and parameters were obtained using the FLOWSTAR module of the COSMOS/M FEM program. Before any solutions were obtained it was necessary to become familiar with the program and to assess its performance with respect to a benchmark solution.

A benchmark problem put forth by De Vahl Davis and Jones (1983) was used here to validate the FEM program and its correct application. The benchmark problem consists of natural convection flow in a square cavity with differentially heated isothermal vertical sides. The horizontal sides are adiabatic. As can be seen from Table 5 below the computed average Nusselt numbers at various Rayleigh numbers are in excellent agreement.

Table 5. Computed average Nusselt numbers for the benchmark solution vs. the COSMOS/M solution.

	Average Nusselt Number			
Rayleigh number	10^3	10^4	10^5	10^6
benchmark solution	1.118	2.243	4.519	8.800
COSMOS/M solution	1.113	2.238	4.499	8.67
% difference	0.4	0.2	0.45	1.5

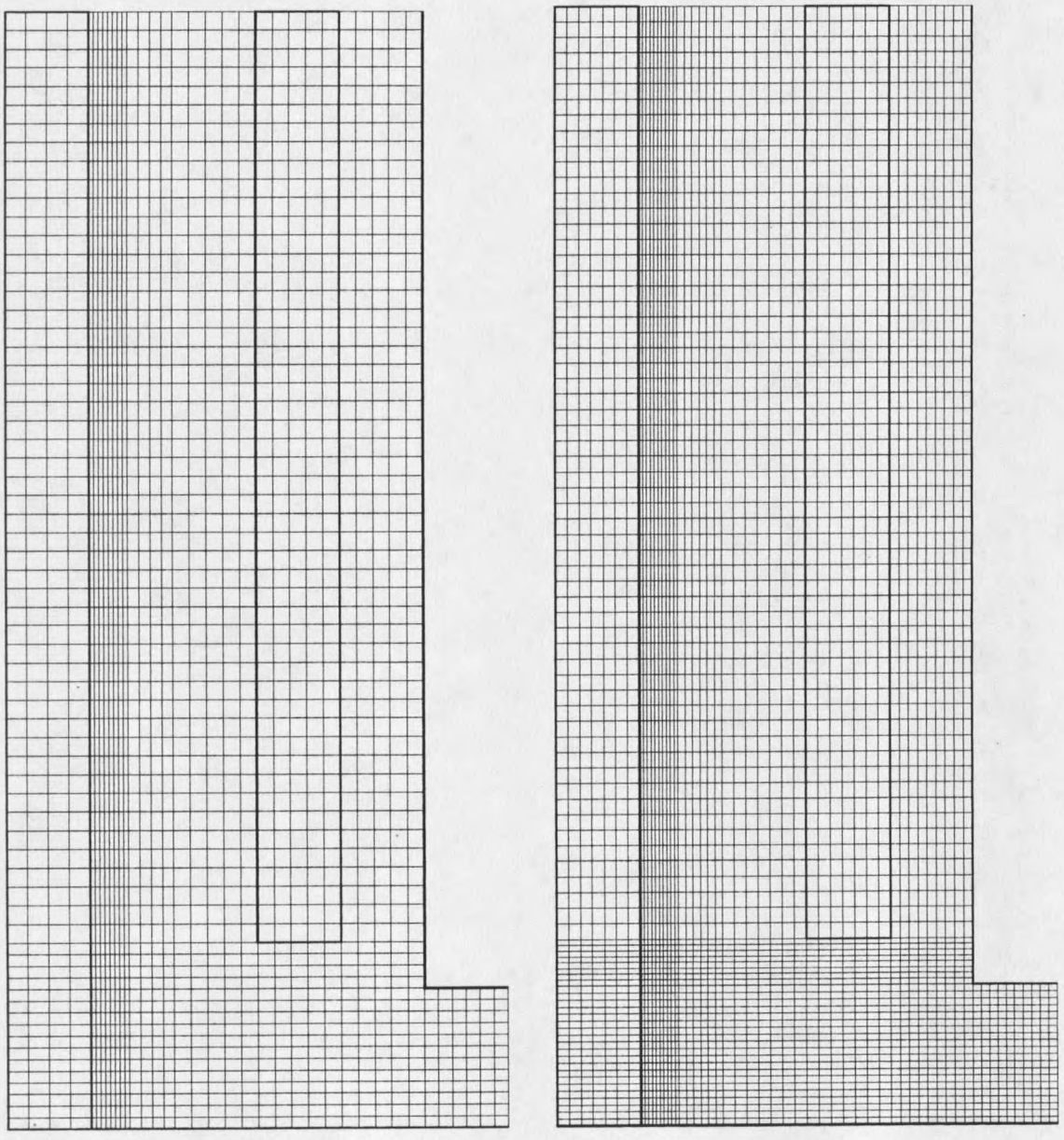


Figure 5. Element distribution meshes "B" and "A" (W_2=0.75).

RESULTS AND DISCUSSION

Introduction

All of the numerical results presented here were obtained using the finite element program COSMOS/M. To ensure accurate results, a preliminary set of analyses and tests were performed. As shown in the previous section, a grid independency test indicates the results are not affected appreciably by the grids chosen for this study. Analysis of the benchmark problem using COSMOS/M demonstrates that the code both functions well and is applied properly. For further evidence of accurate solutions, computations were performed for selected cases to show mass balance over the computational domain. For the cases checked the percent difference between mass flow in and mass flow out was very small and found to be in the range of 5×10^{-5}. These analyses demonstrate that the results obtained in this study are accurate.

As discussed earlier, the objective of this work was to investigate the heat transfer characteristics of the open loop thermosyphon configuration of interest. Of primary interest was the average Nusselt number (Nu) defined by equation (48). In this study, the Rayleigh number (Ra), the thermal conductivity ratio (K), and the lower inlet width (W_2), were varied to understand their effects on Nu. Other parameters examined are the aspect ratio (Ar) and the wall conductivity parameter (K_r).

Solving the discretized governing equations provided values for the primitive variables and their first derivatives at each node. This data was used to compute the following sets of results for each case: (1) the average Nusselt number, (2) stream function and isotherm plots, (3) outlet velocity and temperature profiles, (4) heated wall and fluid interface temperature and heat flux distribution, (5) total mass flow rate through upper and lower inlets, (6) total mass flow rate including inlets and any mass inflow at the outlet, and (7) total heat transfer through the partition wall to the upper inlet flow.

Some data reduction was required to obtain these results. A FORTRAN code was written to compute Nu by Simpson's rule integration of the nodal temperature gradients along the heated wall (equations 48 and 54). Another FORTRAN code was developed to extract data from the COSMOS/M output and format the data for plotting purposes. These program listings are included in Appendix B.

In the following sections parameters Ra, W_2, and K are varied and the effects are studied with respect to results (1) through (7). The inner channel aspect ratio (Ar) is examined to verify it is an independent parameter. Also, the problem formulation indicates the wall conductivity parameter (K_r) may be independent. The results are used to verify this.

Before discussing the results in detail the following points will aid in interpretation. The dimensional stream

function (ψ) is computed at each node and these nodal values are used to produce contour plots. The nodal values are obtained by the line integral shown below.

$$\Delta\psi = \int_a^b \vec{u}\cdot\vec{n}\,d\Gamma = \psi_b - \psi_a \qquad (50)$$

Here $\vec{n}$ is the unit normal to the integration path (Γ) and $\vec{u}$ is the velocity vector along the integration path. Physically, $\Delta\psi$ is the volume flow rate that passes between any two points (a and b) in the flow. This value is path independent.

Computation of the stream function nodal values begins at the coordinate system origin. The stream function value (ψ_o) for node a_o at the origin is arbitrarily set equal to zero. Equation (50) is then used to find ψ for nodes adjacent to a_o. The process continues until all nodal values are evaluated.

For this problem this means that ψ in the heated wall region and its surfaces is zero. Any boundaries that are directly connected to the origin, i.e. do not cross a fluid region, have $\psi = 0$ also. The key point is that in the solid partition wall and its surfaces ψ is constant and non-zero. Thus, the partition wall surface is a streamline with a constant, non-zero value designated here as ψ_p. This is also true of the right adiabatic wall where the stream function is designated ψ_r.

For the nondimensional stream function contour plots 10 levels are shown. Values for ψ^*_1 and ψ^*_{10} are given along with

the maximum (ψ^*_m). The difference between any two adjacent levels is equal to $\psi^*_m/10$. Also listed is the partition stream function value (ψ^*_p), and the right wall value (ψ^*_r) if it is non-zero.

Physically, ψ^*_p represents the total volume flow rate due to inflow from the upper and lower inlets. The total inflow from all sources including any inflow at the outlet is represented by ψ^*_m. Contours of constant ψ^* for incompressible steady state flow are equivalent to streamlines. Thus, the local velocity vectors are tangent to the stream function contours.

The isotherm plots show the nondimensional temperature (θ) field. Ten levels are shown; the contour nearest the heated wall external surface is $\theta = 0.95$. The contour nearest the inlets is $\theta = 0.05$. The difference between any two adjacent levels is 0.10. At the inlets $\theta = 0$, and at the heated wall external surface $\theta = 1$.

The nondimensional temperature (θ) always lies between 0 and 1 for all Rayleigh numbers. However, the relative magnitude of the temperature difference ($T - T_\infty$) varies as follows:

$$(T - T_\infty) = Ra\theta \frac{\alpha \nu}{g\beta b^3} \qquad (51)$$

For constant fluid properties, the temperature difference magnitude is proportional to the product of Ra and θ.

The isotherm plots are useful because they graphically show the variation of temperature gradients throughout the problem domain. In solid regions the temperature gradients, or contour spacing, directly indicate thermal energy transport. For fluid regions more densely spaced isotherms indicate greater convection heat transfer.

Effect of Lower Inlet Width Parameter

The computed isotherms and stream function contours for various values of Ra and W_2 are shown in Figures 6 and 7. The Rayleigh number (Ra) is varied by changing the temperature difference across the thermosyphon ($T_w - T_\infty$). Other parameters are fixed with K = 5 and Ar = 6.

Observation of the isotherm plots (Figure 6) reveals changes in the temperature field due to parameters Ra and W_2. Several trends are evident, and are described in the following sections.

(a) For Ra greater than 2.5×10^5 the temperature field becomes relatively independent of the lower inlet width (W_2). At the largest Rayleigh number (10^6), little change is apparent for changes in W_2. At lower Ra ($< 2.5 \times 10^5$) there are significant changes in the temperature field with changing W_2. For example, at Ra = 10^3 the isotherm $\theta = 0.05$ penetrates much farther from the inlets as W_2 increases. For $W_2 = 0.0$, little penetration is seen, and conduction across the partition wall is very evident.

(b) As Ra increases the isotherms move toward the heated wall. This effect is greater at low Ra ($\leq 5x10^4$) as W_2 is increased up to 0.50. This trend results in the development of a thermal boundary layer at the heated wall.

(c) Along the solid-to-fluid interface of the heated wall there is a non-uniform temperature and heat flux distribution. The non-uniform heat flux is shown by the isotherm spacing near the wall-to-fluid interface.

Consideration of the stream function plots (Figure 7) also shows some definite trends due to changes in Ra and W_2. The most evident trends are described below.

(d) The occurrence of inflow (recirculation) at the outlet is apparent. This is evident due to the streamlines that both begin and end at the outlet. Recirculation clearly tends to increase with Ra and decrease with larger W_2. Increasing W_2 from 0.25 to 0.50 decreases the recirculation in the range of 63 to 99 percent for the cases shown. Further increase (W_2=0.75) has little effect with a maximum of 7 percent additional decrease in recirculation.

(e) A velocity boundary layer develops along the heated wall as the Rayleigh number is increased above $5x10^4$. The boundary layer tends to decrease in thickness with increasing Rayleigh number.

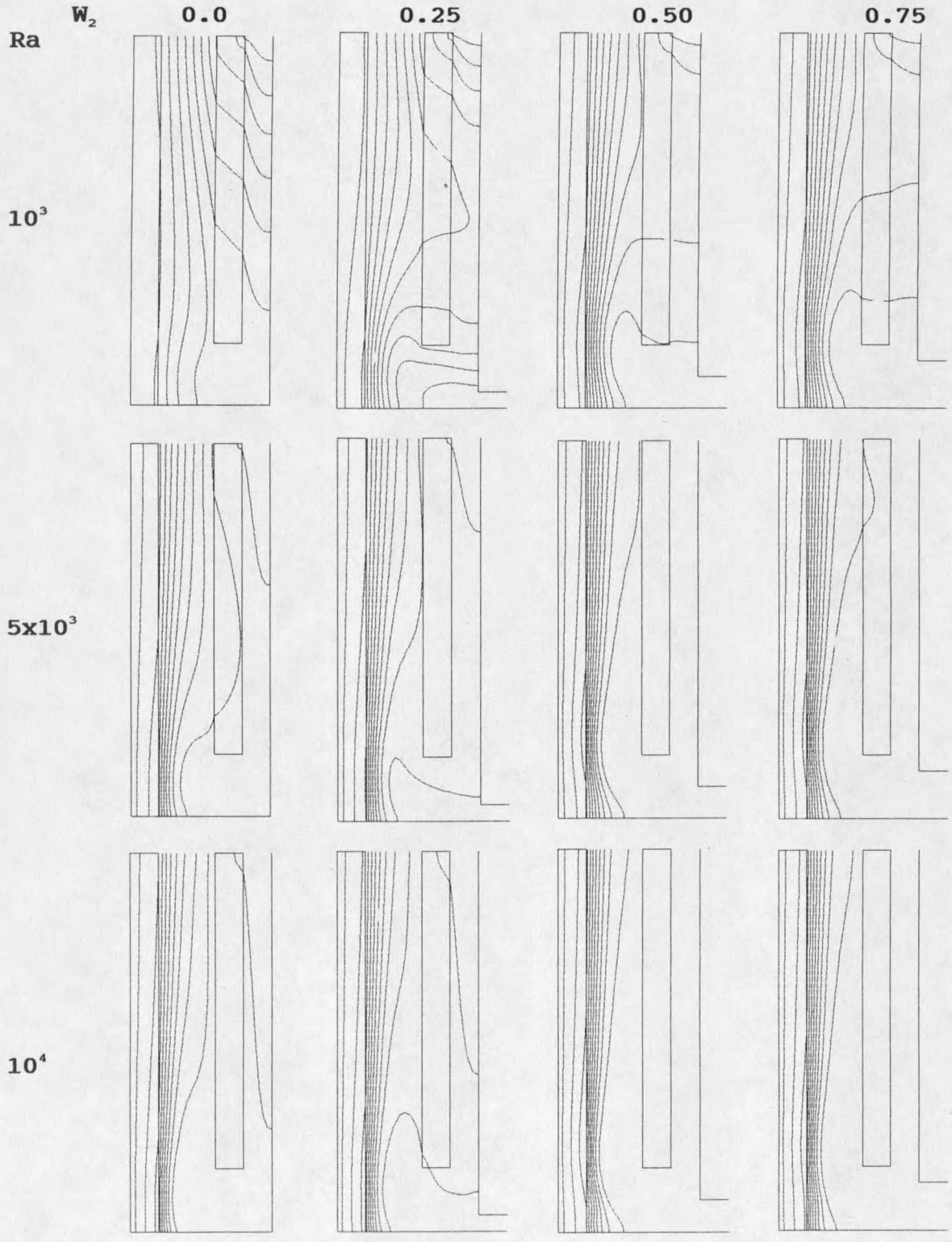


Figure 6. Isotherm plots with K=5 and Ar=6 for varying W_2 and Ra.

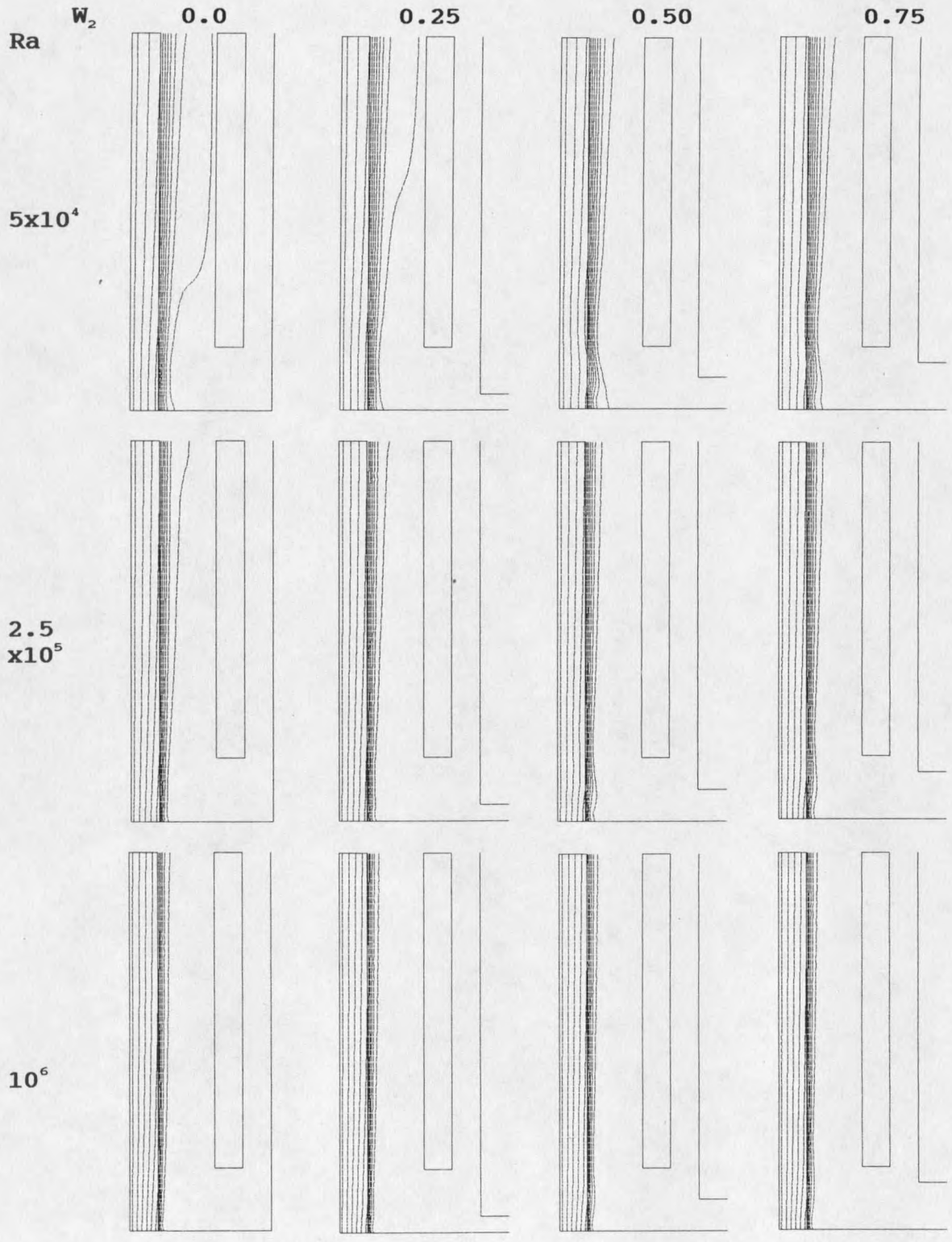


Figure 6.--Continued

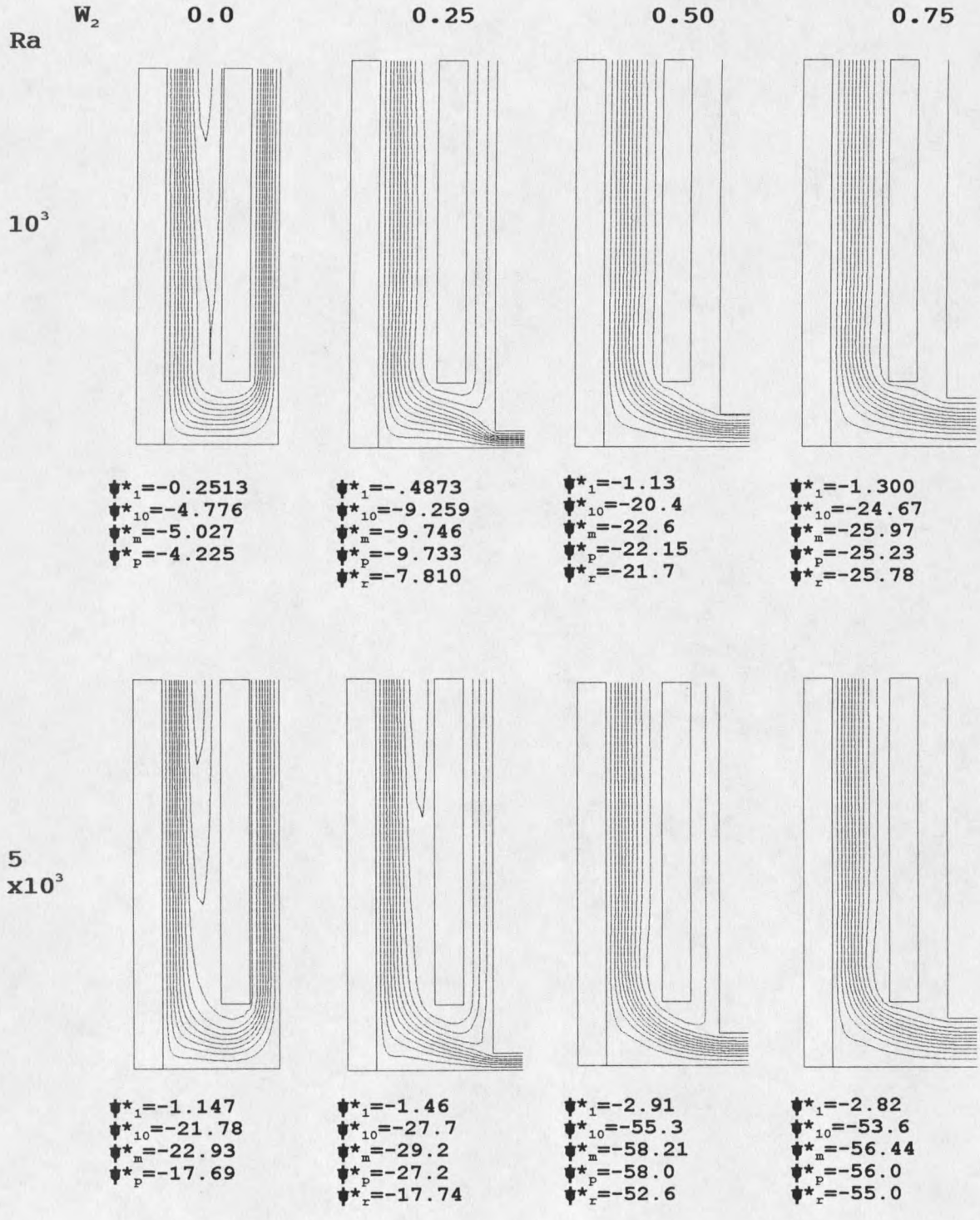


Figure 7. Stream function plots with K=5 and Ar=6 for varying W_2 and Ra.

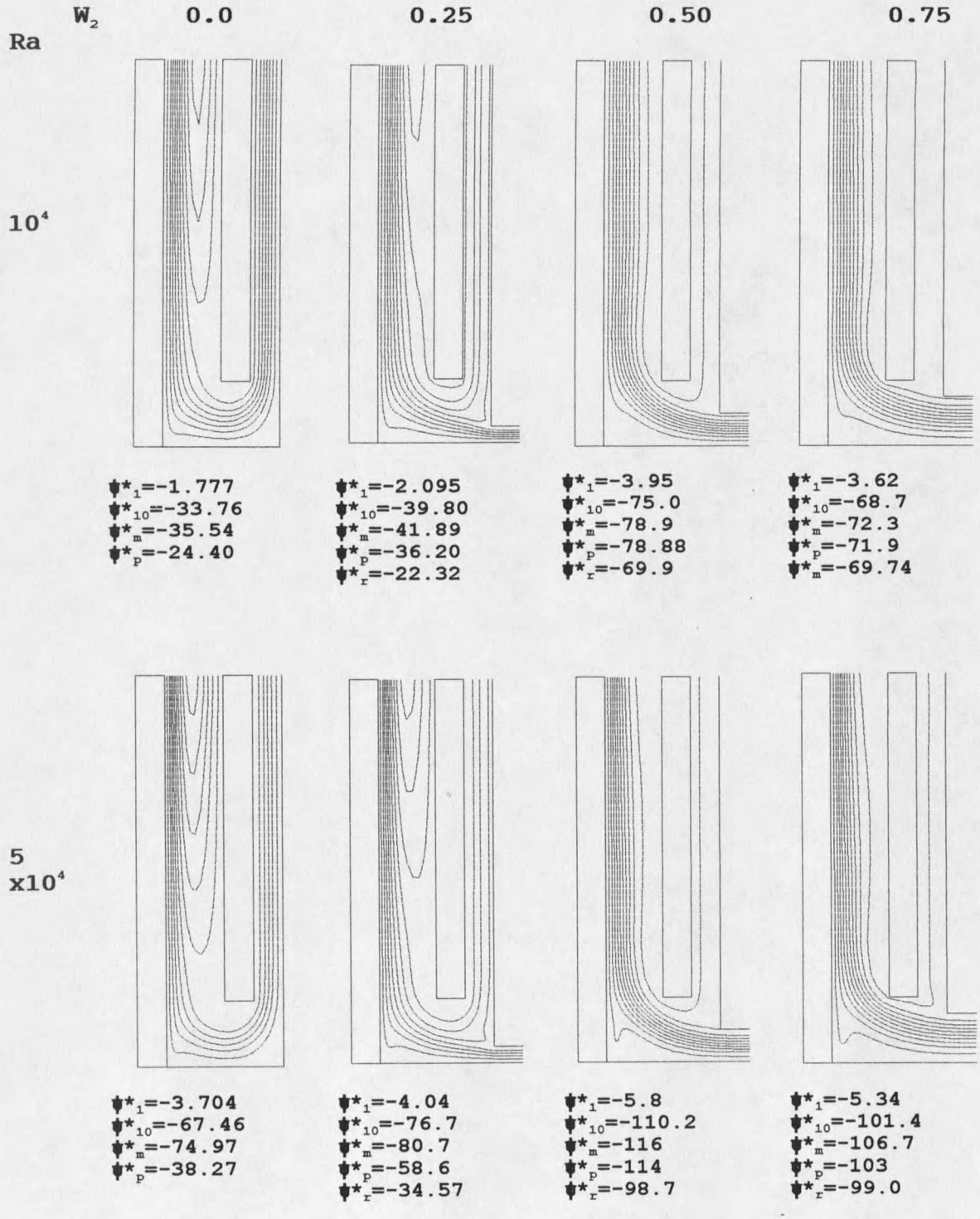


Figure 7.--Continued

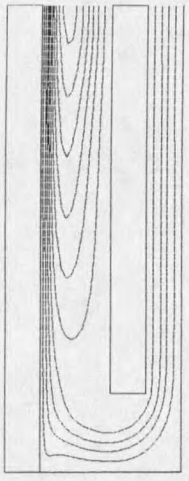
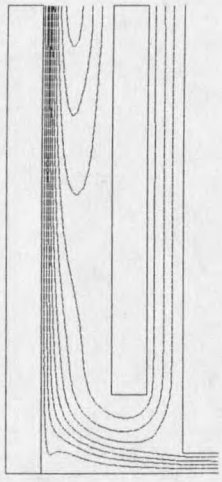
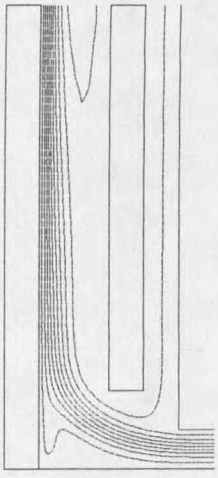
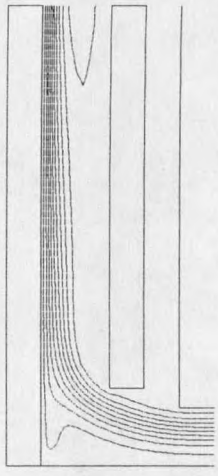
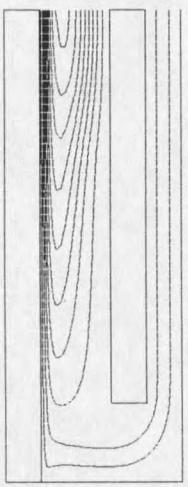
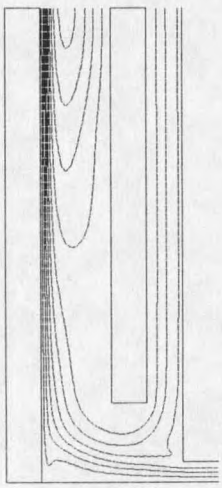
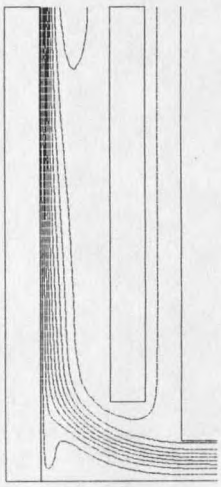
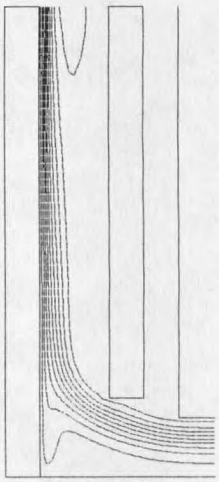
Ra	W_2 = 0.0	0.25	0.50	0.75
2.5×10^5				
	ψ^*_1=-6.262 ψ^*_{10}=-119.0 ψ^*_m=-125.24 ψ^*_p=-48.35	ψ^*_1=-6.592 ψ^*_{10}=-125.2 ψ^*_m=-131.8 ψ^*_p=-89.21 ψ^*_r=-50.55	ψ^*_1=-7.88 ψ^*_{10}=-150 ψ^*_m=-158 ψ^*_p=-143.6 ψ^*_r=-125	ψ^*_1=-7.65 ψ^*_{10}=-145 ψ^*_m=-153 ψ^*_p=-138 ψ^*_r=-135.7
10^6				
	ψ^*_1=-8.930 ψ^*_{10}=-169.7 ψ^*_m=-178.6 ψ^*_p=-33.88	ψ^*_1=-9.31 ψ^*_{10}=-177 ψ^*_m=-186.1 ψ^*_p=-112.7 ψ^*_r=-62.2	ψ^*_1=-10.5 ψ^*_{10}=-199 ψ^*_m=-209 ψ^*_p=-183.5 ψ^*_r=-159.2	ψ^*_1=-10.5 ψ^*_{10}=-200 ψ^*_m=-210.3 ψ^*_p=-185 ψ^*_r=-184.4

Figure 7.--Continued

The observations described in (a) through (e) are next examined to determine the mechanisms that cause these effects. First, consider (d), the recirculation at the outlet. Figure 7 shows that for fixed Ra decreasing W_2 (< 0.50) tends to increase the recirculation. Thus, if insufficient mass flow is available at the inlets due to flow restrictions compensating flow will be drawn in at the outlet. Recirculation also increases with Rayleigh number. Figures 8 and 9 give some indication why this occurs.

Figure 8 shows the normalized total mass inflow rate from all sources including recirculation at the outlet. Figure 9 shows the amount of this flow originating at the upper and lower inlets. These Figures indicate that the total mass flow rate required increases with Ra. However, for restrictive W_2 (< 0.50) inflow at the inlets shows a lower rate of increase. Therefore, at larger Ra the inlets supply an increasingly smaller fraction of the total mass flow and as such recirculation compensates.

Figure 9 shows another interesting characteristic. The curve for W_2=0.0 has an inflection point at approximately Ra=3×10^5. Beyond this point inlet flow actually decreases while the total mass flow requirement (Figure 8) continues to increase. This indicates recirculation is becoming dominant and reduced flow at the inlets does not depend on flow restrictions there. It is not clear how important this effect is for less restrictive W_2 values.

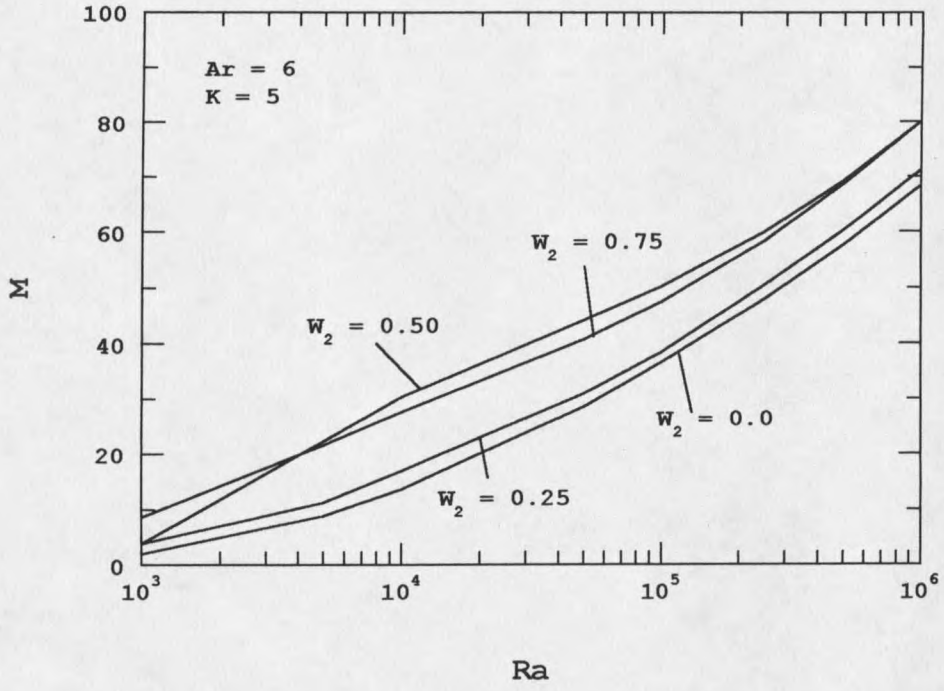


Figure 8. Total mass inflow rate from all sources vs. Ra

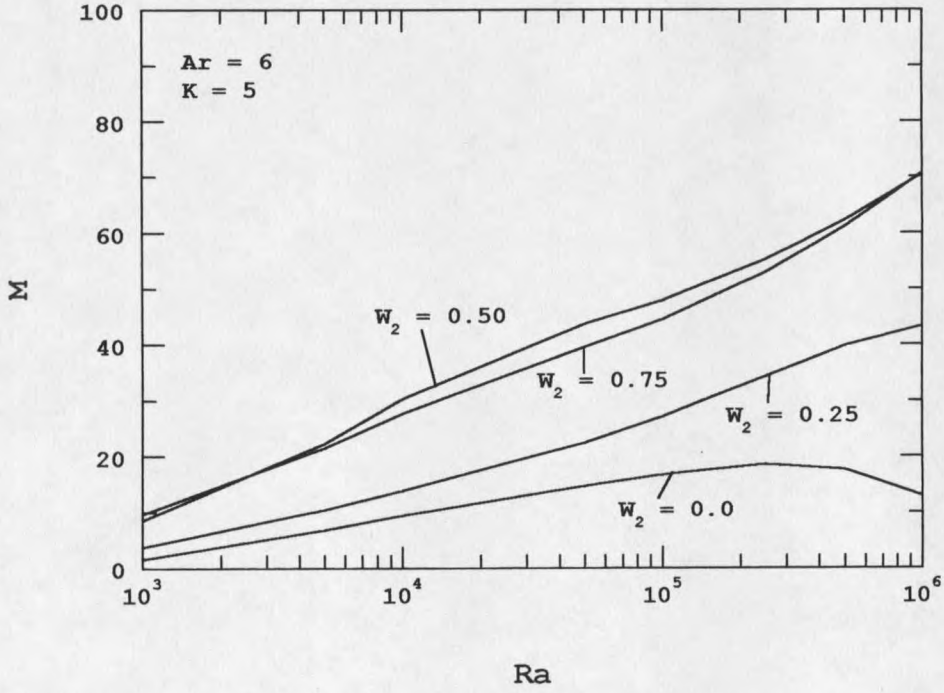


Figure 9. Total mass inflow rate from lower and upper inlets vs. Ra.

The effect discussed above occurs also because the thermal and velocity boundary layer thicknesses along the hot wall decrease with larger Ra. This essentially makes more area of the inner channel (outlet) available for inflow. This trend is discussed further.

Consider (b) the isotherm movement and developing thermal boundary layer. Examination of the normalized energy equation (30) indicates that as Ra increases the conduction terms become less important and the convection terms dominate. Thus, convection effects tend to decrease the penetration due to conduction of elevated temperatures away from the heated wall. This effectively reduces the thermal boundary layer thickness. This effect is evident in the isotherm plots and is further detailed by Figure 10 which plots the normalized temperature profile across the outlet.

Figure 10 indicates decreasing W_2 to 0.50 or less causes increased temperature penetration primarily at low Ra ($<5x10^4$). This is due to the increased flow restriction at the inlets which reduces inflow and therefore reduces convection effects. This increases conduction effects so that temperature penetration is greater.

The thermal boundary layer behavior is important in understanding the outlet recirculation. At low Ra elevated temperatures (θ=0.2 or more) extend well across the outlet and inner channel. As Ra is increased the thermal boundary layer approaches the wall. This creates a growing portion of the

inlet and inner channel where the temperature and therefore the thermal buoyancy forces are small. Fluid in this region is drawn toward the wall just as fluid from the inlets. Thus, the outlet becomes at least partially an inlet. This behavior is detailed in Figure 11 which plots the normalized vertical velocity profile across the outlet.

Figure 11 also shows that the vertical velocity increases with Ra. This is because increasing Ra essentially increases the temperature difference ($T_w - T_\infty$) across the thermosyphon. This increases the solid-to-fluid interface temperature which imparts a larger thermal buoyancy force to the fluid. Thus, a larger vertical velocity results. This is the reason for the observed velocity boundary layer development, as discussed in (e) earlier.

It is useful at this point to discuss the flow restrictions. For the present problem, the partition wall, the inlet channels, and associated boundaries all serve to restrict fluid inflow. Various mechanisms cause the flow restrictions.

Flow restriction at the inlets is in large part due to viscous losses. These depend among other things on the inlet channels lengths and widths. Another obvious result of the partition and inlet configuration is that the reservoir fluid has limited physical access to the heated wall.

The conducting partition wall complicates the flow, by introducing temperature dependent flow conditions at the upper

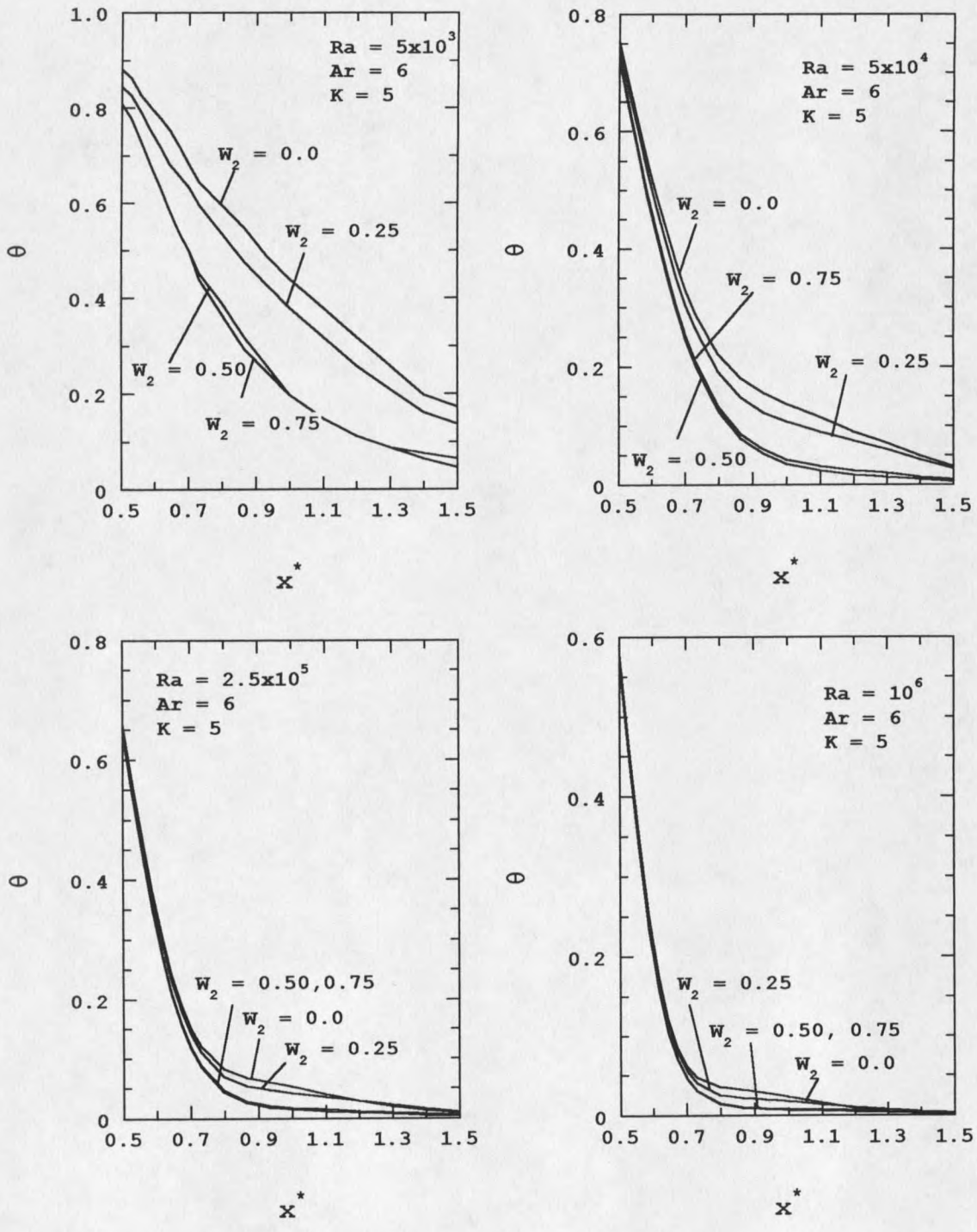


Figure 10. Temperature distribution across outlet with parameters W_2 and Ra.

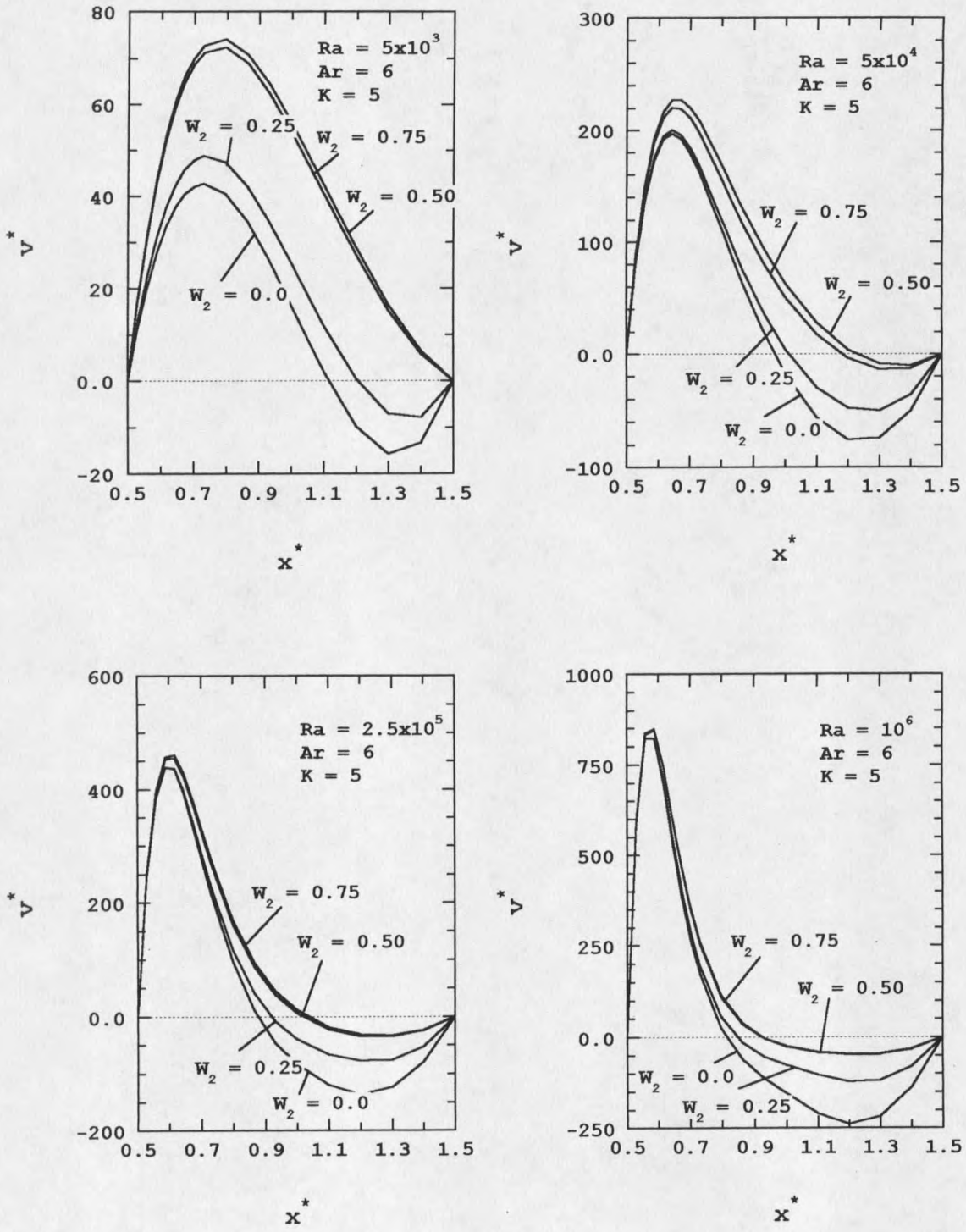


Figure 11. Vertical velocity distribution across outlet with parameters W_2 and Ra.

inlet channel. If the partition wall were adiabatic, flow inside the upper inlet channel would be isothermal flow due to pressure gradients. With a conducting partition however, thermal buoyancy forces oppose the flow.

Buoyancy forces at the upper inlet are due to heat energy transferred across the partition originating at the heated wall. Heat transfer from the heated wall to the partition (across the inner channel) is by conduction in the fluid only as there is no fluid velocity in this direction. Thus, flow restriction due to the partition heat transfer is expected to decrease with increasing Ra (decreased conduction effects).

To study the effect of partition conduction, the total heat transfer through the partition as a percentage of total heat transfer at the heated wall is shown as a function of Ra and W_2 (Figure 12). The total heat transfer through the partition was computed by integration of the computed temperature gradients at the nodes along the right wall of the partition.

Figure 12 shows that the amount of heat transfer to the upper inlet flow decreases markedly with larger W_2 for Ra less than $5x10^4$. This is due to reduced convection heat transfer inside the upper inlet channel. Convection declines because of less mass flow there due to less lower inlet restriction. Figure 13 supports this by plotting the ratio of the upper inlet to the lower inlet mass flow as a function of Ra and W_2. The upper inlet flow decreases with larger W_2.

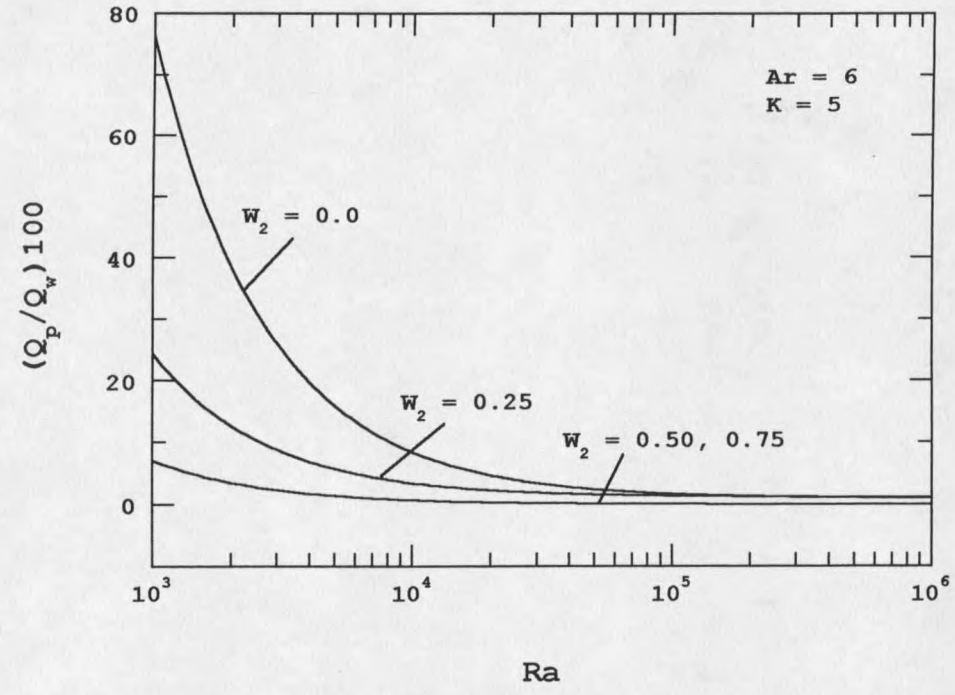


Figure 12. Heat transfer to upper inlet as a percent of total heat transfer ($(Q_p/Q_w)100$) vs. Ra.

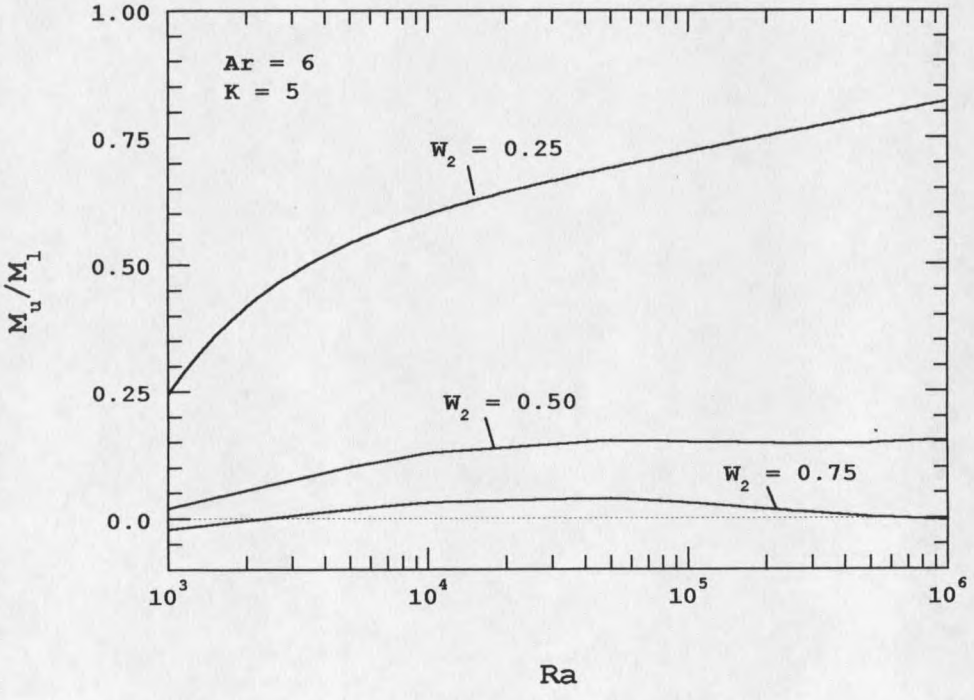


Figure 13. Ratio of upper inlet to lower inlet mass flow rate (M_u/M_1) vs. Ra.

As expected, Figure 12 shows the partition heat transfer decreases very significantly with increasing Ra. Thus, flow restriction due to opposing thermal buoyancy forces becomes negligible for Ra greater than $5x10^4$ and essentially independent of W_2.

Reasons for the observation (a), reported earlier, that the temperature field is independent of W_2 for Ra greater than $2.5x10^5$ are now evident. With increasing Rayleigh number, heat transfer in the fluid is dominated by convection, and a thermal boundary layer develops. This has two primary results: (1) cool reservoir fluid has greater access to the heated wall via the outlet (recirculation), (2) opposing buoyancy effects in the upper inlet decrease and improve access there. Access is improved sufficiently to compensate for any flow restriction due to the inlet configuration and W_2. These results indicate the average Nusselt number will also be independent of W_2 at large Ra (for constant K and Ar).

The non-uniform temperature and heat flux distribution, as reported earlier in (c), is also due to inlet flow restrictions (W_2). Figures 14 and 15 plot the local Nusselt number (Nu_y) and temperature (θ_i) with respect to vertical position along the wall/fluid interface.

Peaks in Nu_y are evident at points where cool lower inlet fluid first comes in contact with the hot wall. These peaks are greater for larger W_2 because the lower inlet flow is increased. A corresponding reduction in θ_i occurs at these

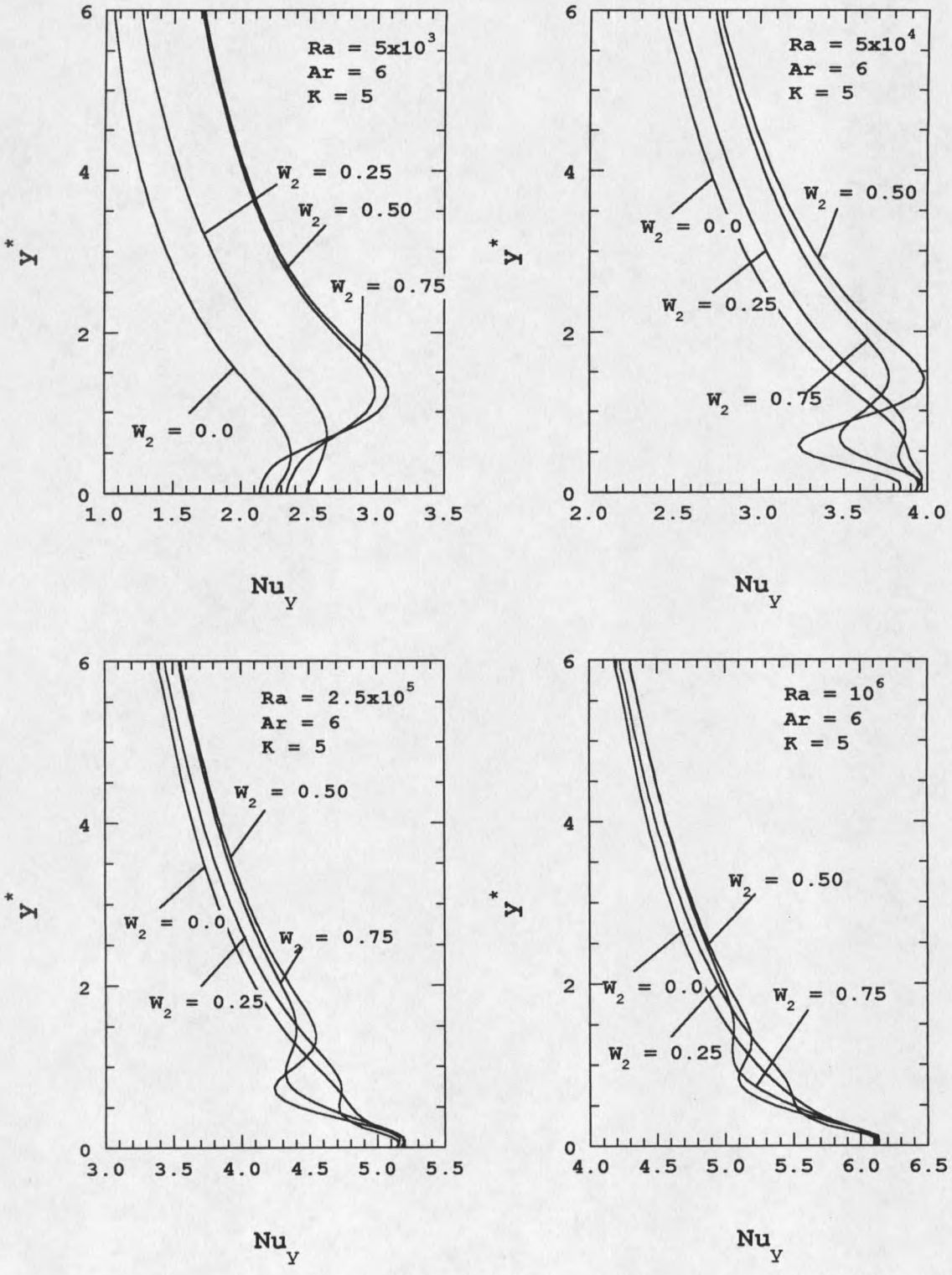


Figure 14. Heated wall and fluid interface local Nusselt number distribution with parameters W_2 and Ra.

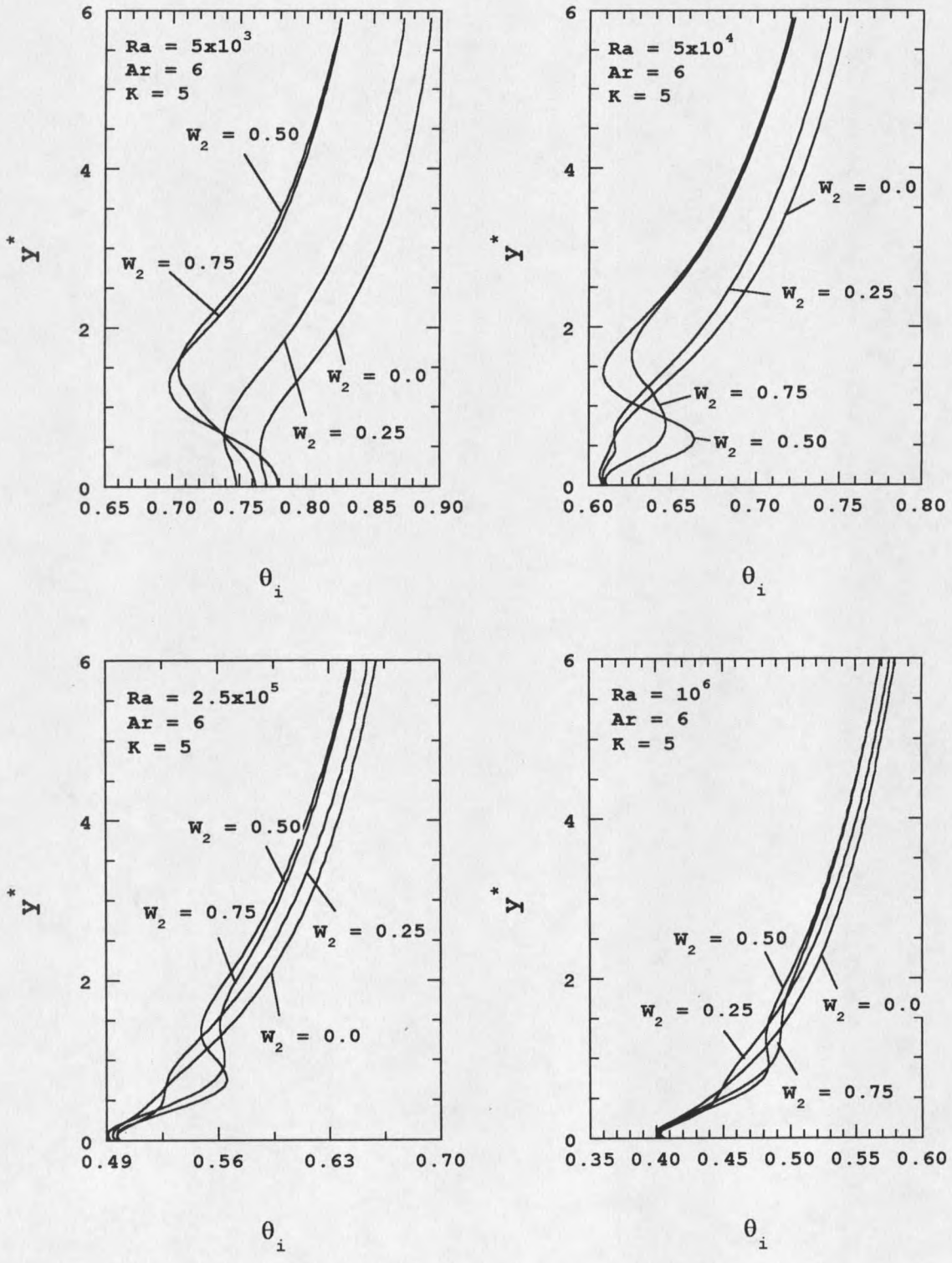


Figure 15. Heated wall and fluid interface temperature distribution with parameters W_2 and Ra.

points. This is expected as increased local heat flux should decrease the local temperature of the solid wall. These effects diminish as Ra is increased. This is not surprising because, as already shown, the temperature field (including θ_i) becomes independent of W_2 at large Ra.

Effect of Thermal Conductivity Parameter

The computed isotherms and stream function contour plots for various Ra and K values are shown in Figures 16 and 17. The other parameters are fixed with $W_2 = 0.25$ and Ar = 6. The isotherm plots (Figure 16) are examined first for characteristic trends. The trends will be described and later examined to determine causes.

(a) The most obvious trend occurs in the heated wall where the temperature gradients across the wall increase with reduced K. This is most evident for K values less than 5.

(b) A surprising trend is that the temperature field does not change dramatically for a given Ra as K increases. This observation is valid in a region extending from approximately the middle of the inner channel outward towards the inlets. This characteristic appears to be true regardless of the Rayleigh number magnitude. The exception to this trend is at K = 0.1 where most of the temperature drop is across the wall.

(c) It is also evident that a thermal boundary layer develops with increasing Ra. It appears that for a given Ra increasing K accelerates this effect.

Observation of Figure 17, the stream function plots, also reveals some clear trends. These are described below.

(d) Recirculation at the outlet tends to increase with both parameters Ra and K. Note that with the restrictive lower inlet width (W_2=0.25) between 20 and 50 percent of the

total mass flow enters at the upper inlet for each case.

(e) It is clear that a velocity boundary layer develops as Ra increases. This boundary layer also develops more readily for larger K values.

The characteristics described above are next examined to determine causes for the observed behavior. First consider observation (a), the heated wall temperature gradients. The temperature gradients across the wall are due to wall thermal conductivity and convection at the wall surface. Both are affected strongly by K. The relative importance of these two effects cannot be discerned from Figure 16. As discussed earlier, convection effects increase with reduced flow restriction and increased Ra.

Next examine observation (d) the recirculation tendency which increases with both Ra and K. As shown previously, it is due to restricted inflow and is increased by thermal and velocity boundary layers forming. As they develop, more area of the outlet is available for fluid inflow. Thus, anything that promotes boundary layer development will promote recirculation.

Increasing K reduces the wall conduction resistance and effectively increases the wall-to-fluid interface temperature (θ_i). Increasing Ra has a similar effect because larger Ra essentially means ($T_w - T_\infty$) is increased. Figure 18 details this effect; recall that θ_i and Ra determine the magnitude of ($T_i - T_\infty$). Increasing θ_i promotes boundary layer development

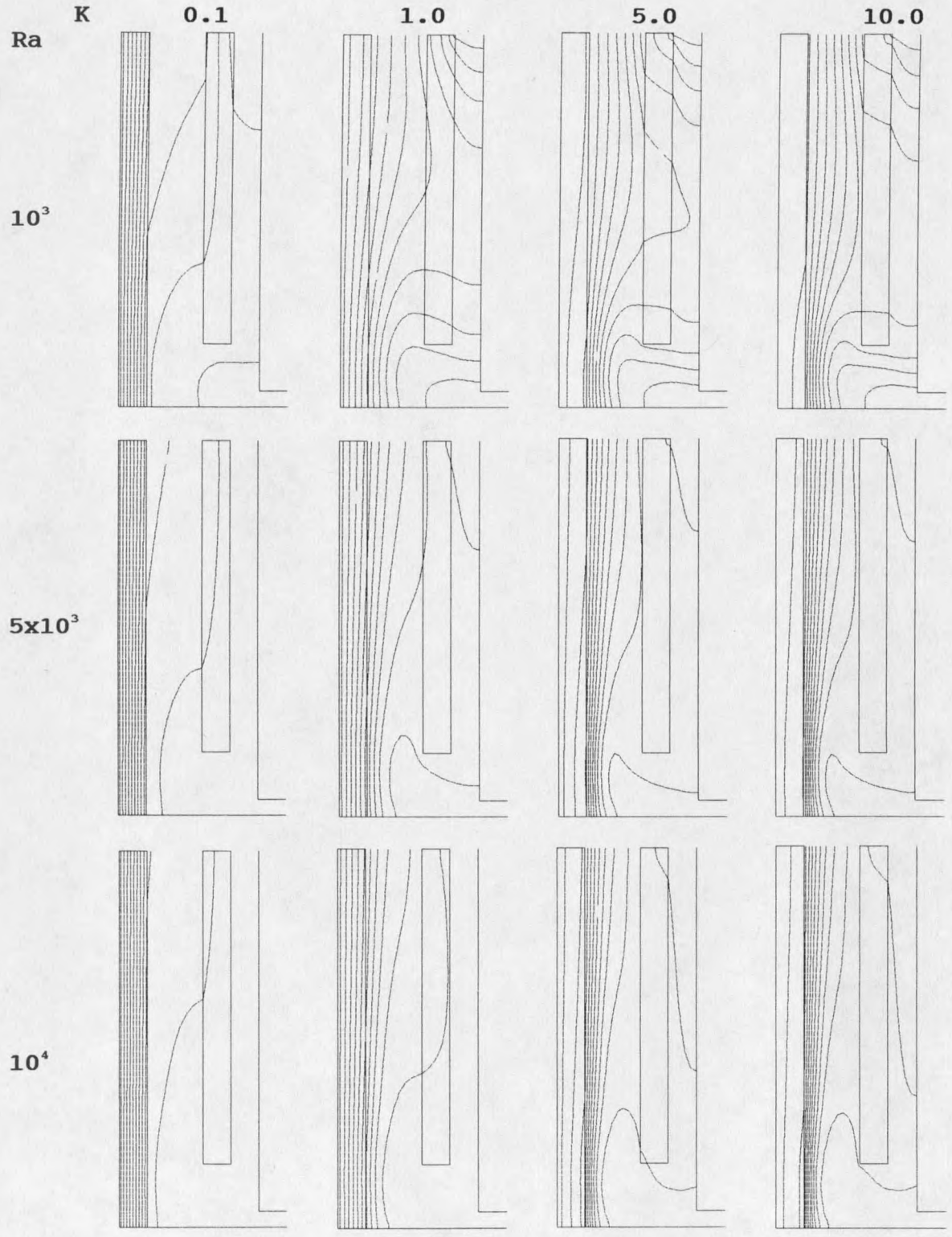


Figure 16. Isotherm plots with W_2=0.25 and Ar=6 for varying K and Ra.

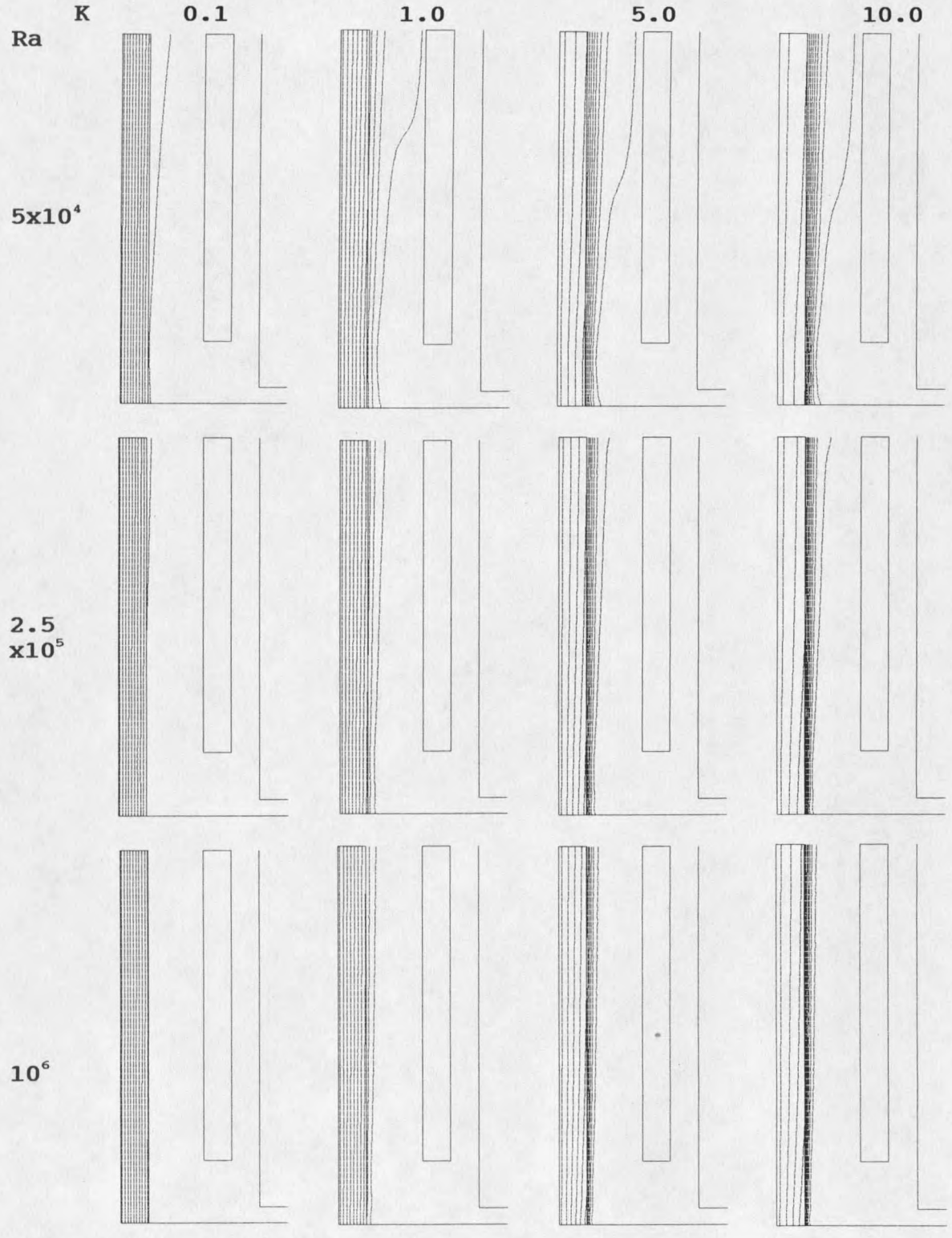


Figure 16.--continued

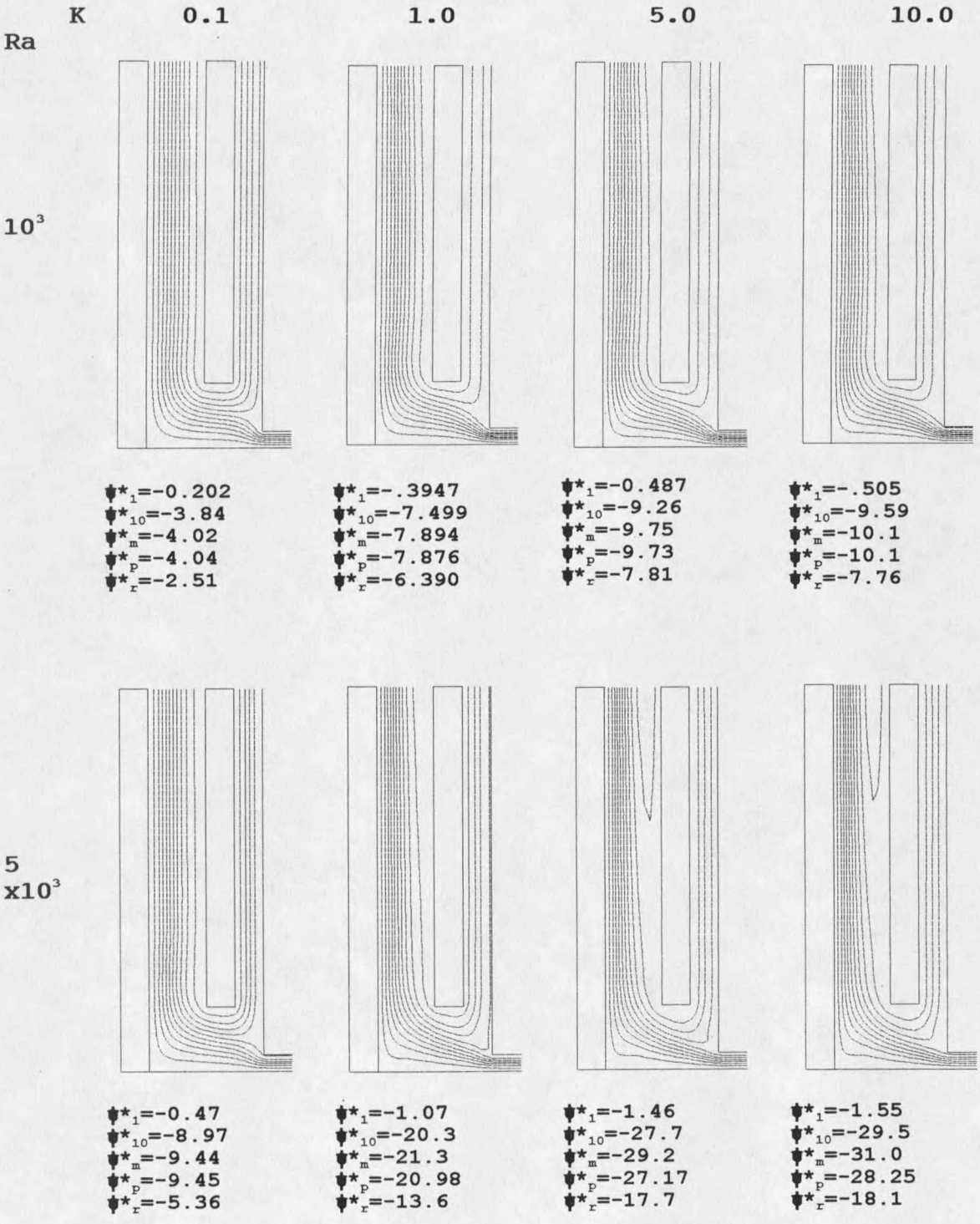


Figure 17. Stream function plots with W_2=0.25 and Ar=6 for varying K and Ra.

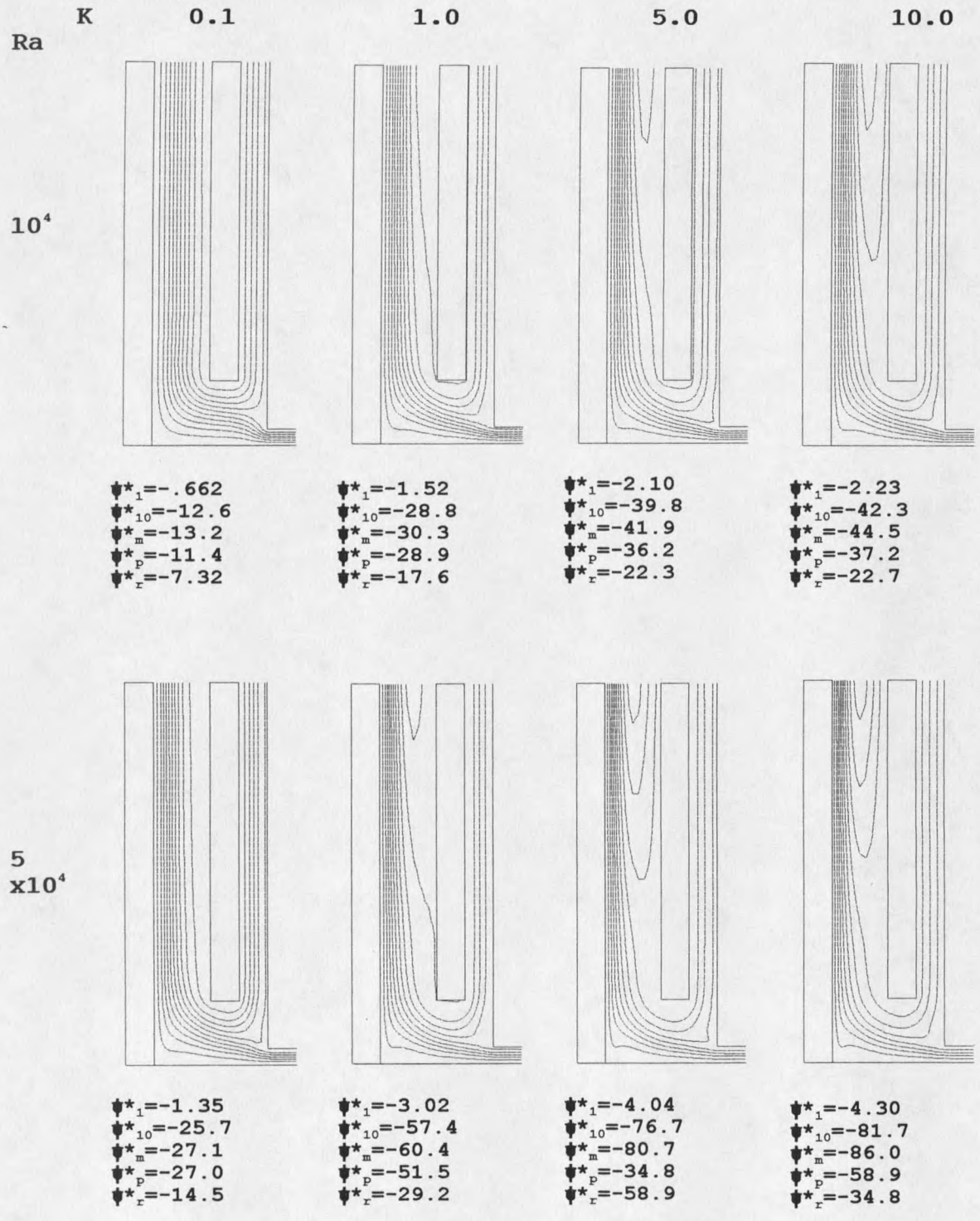


Figure 17.--continued

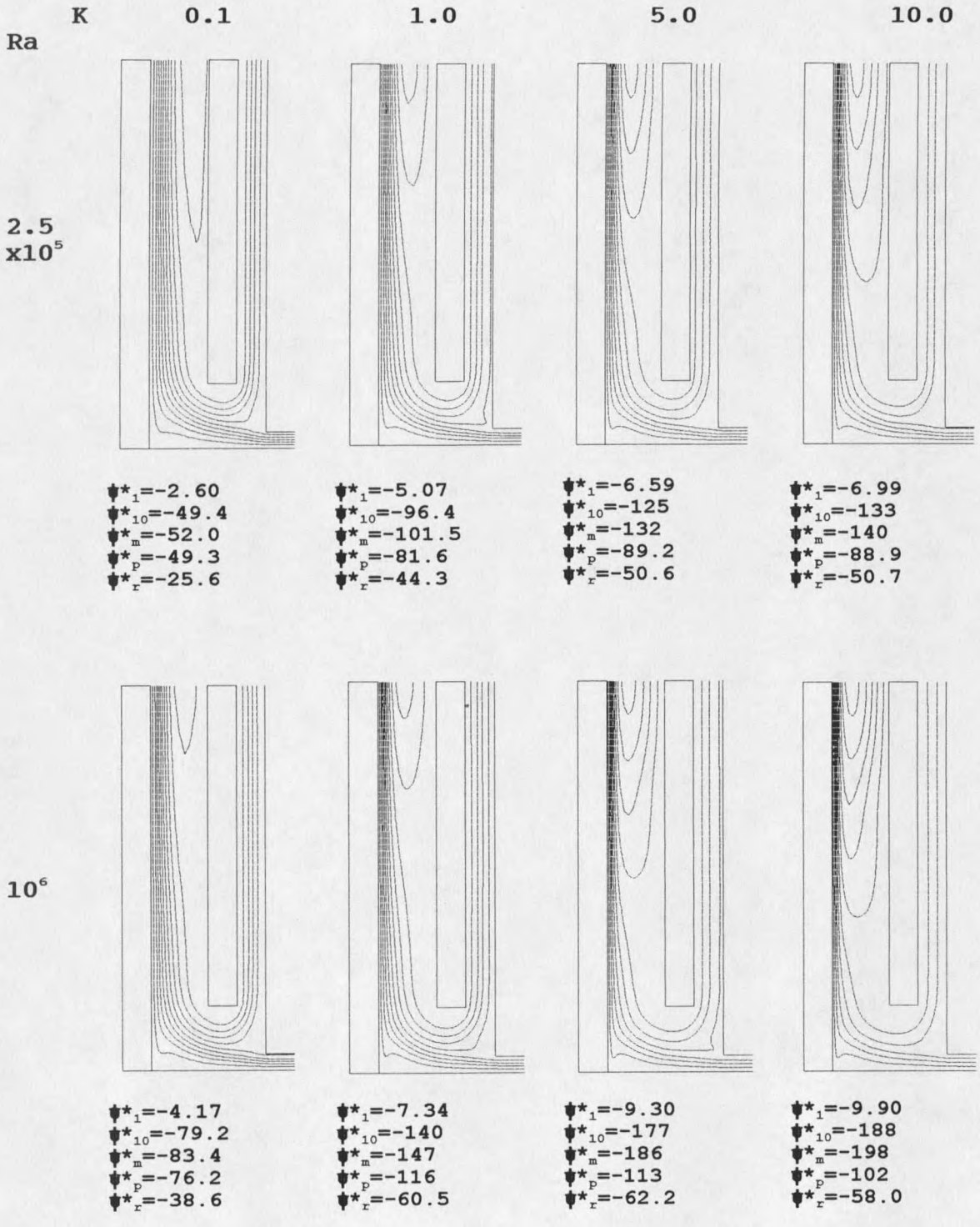


Figure 17.--continued

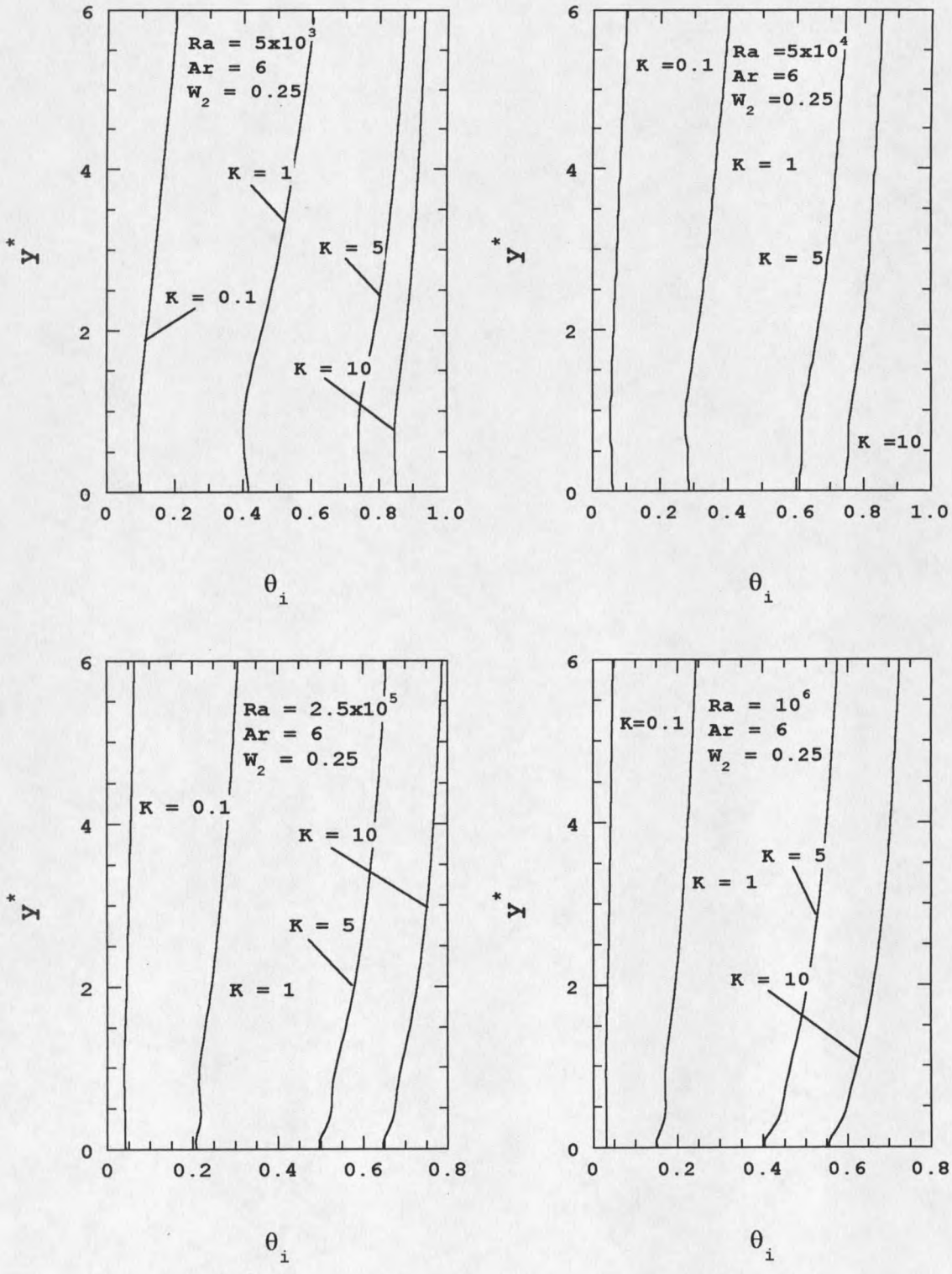


Figure 18. Heated wall and fluid interface temperature distribution with parameters K and Ra.

because it imparts a larger thermal buoyancy force to the fluid. This results in a greater vertical velocity near the wall and a reduction in the thermal and velocity boundary layer thicknesses, as discussed earlier in observations (c) and (e). These effects are evident in Figure 19 and 20 which show vertical velocity and temperature profiles at the outlet.

Near and within the heated wall [observation (b)], K has a large influence on the temperature field. It has much less influence further from the wall. This is explained simply by noting that much of the temperature drop occurs across the wall or across the thermal boundary layer. Increasing K reduces the temperature drop across the wall. This sharply increases the temperature drop across the thermal boundary layer because θ_i is greater. In contrast, decreasing K magnifies the wall temperature drop, and lessens the boundary layer drop. The net effect is that for a constant Rayleigh number the isotherms on the boundary layer edge ($\theta \leq 0.25$) are relatively stationary, depending little on K.

The effect of K on opposing buoyancy effects in the upper inlet channel is also of interest here. One expects increased K at the partition to increase the heat transfer there. Figure 21 shows the heat transfer to the upper inlet flow via the partition as a percentage of total heat transfer at the heated wall. It indicates that increasing K does increase the partition heat transfer as much as 100%, but only at relatively low Rayleigh numbers ($5x10^4$). For larger Ra

conduction across the inner channel is so reduced that the partition thermal conductivity is irrelevant. This indicates flow restriction due to opposing buoyancy forces is only important at low Ra.

Figure 22 shows the ratio of upper inlet to lower inlet mass flow, which decreases with increasing K. Recall that recirculation increases with K, which also reduces the inlet flows. For low Ra ($<5x10^4$) it is not apparent how much of the reduction in upper inlet flow is due to recirculation and how much is due to opposing buoyancy effects. At large Rayleigh numbers the reduced upper inlet flow with increasing K can be attributed to increased recirculation.

Figure 23 shows the normalized total mass inflow rate that is due to recirculation and inflow at the inlets. It also increases markedly with K. This is due to the reduced heated wall conduction resistance and the corresponding greater interface temperature. Increasing θ_i causes greater thermal buoyancy force and more vigorous flow at the wall.

Figure 24 shows the normalized total mass flow originating at the upper and lower inlets. The curves K = 10 and K = 5 show inflection points in the region of Ra = $3x10^5$. These inflections indicate a maximum mass flow rate at the inlets is being approached. Increasing Ra beyond the inflection points may actually decrease inflow at the inlets as noted in Figure 9. This supports the observation that recirculation tends to become dominant at high Ra.

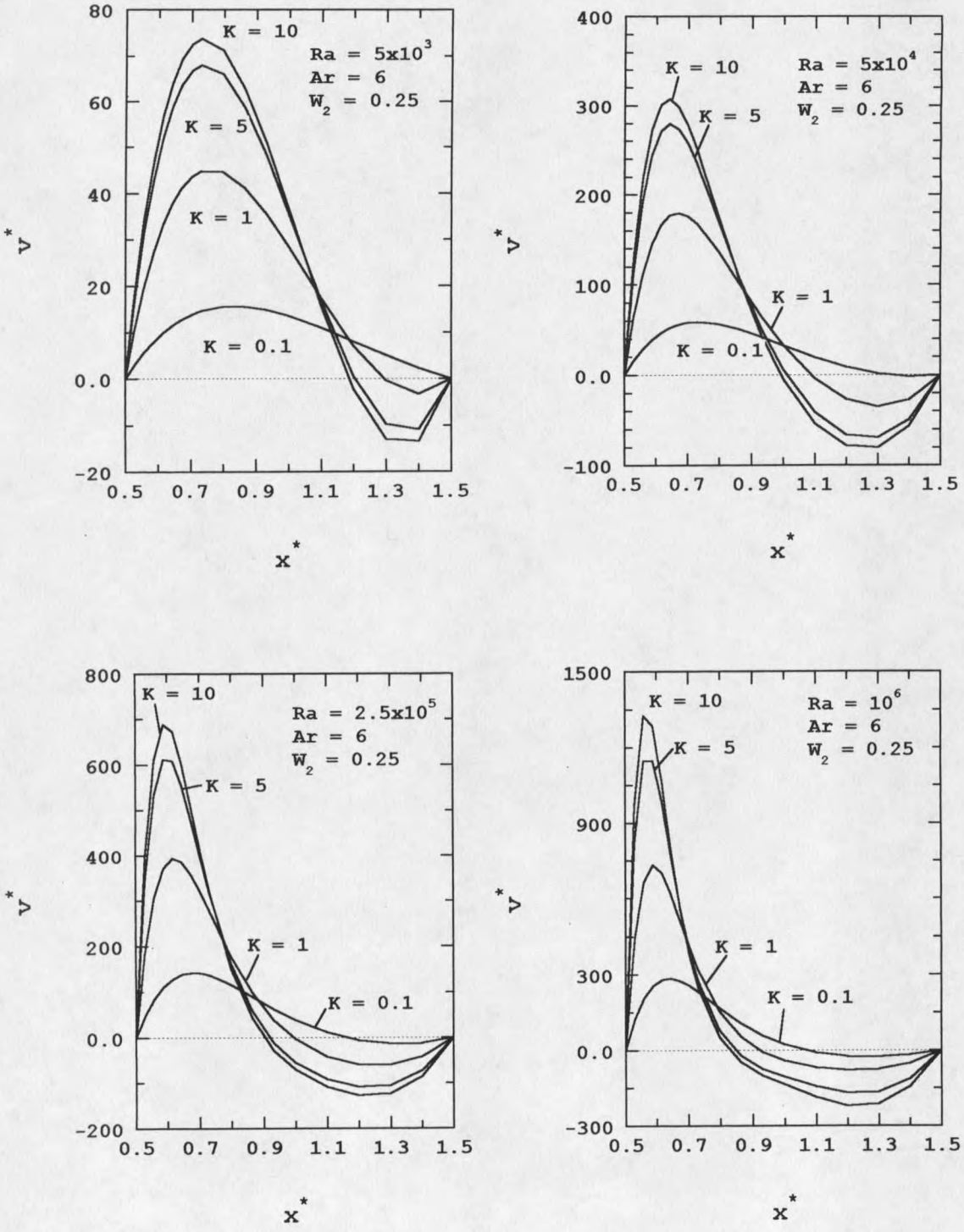


Figure 19. Vertical velocity distribution across outlet with parameters K and Ra.

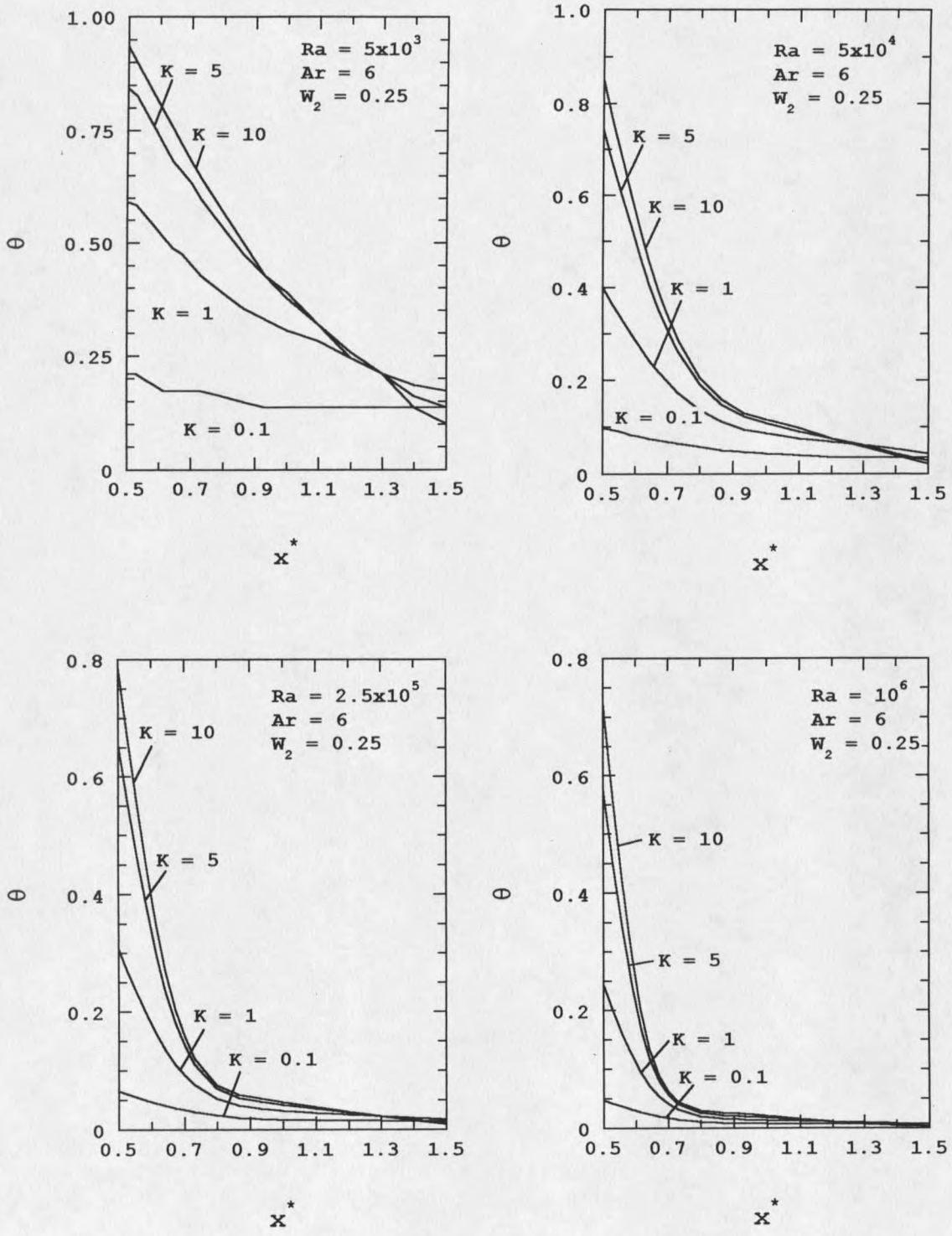


Figure 20. Temperature distribution across outlet with parameters K and Ra.

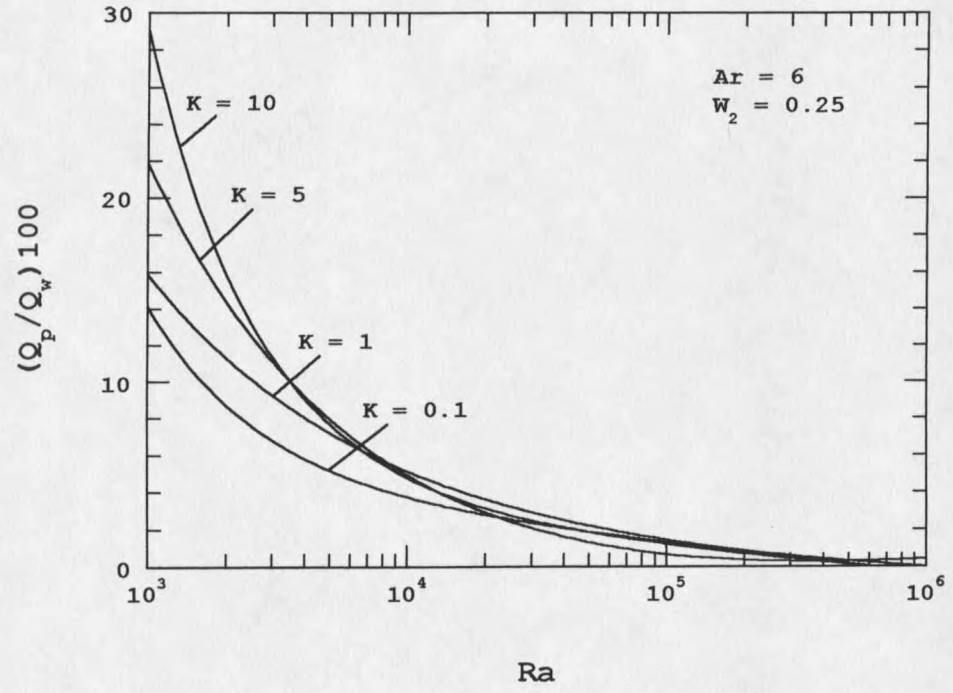


Figure 21. Heat transfer to upper inlet as a percent of total heat transfer ($(Q_p/Q_w)100$) vs. Ra.

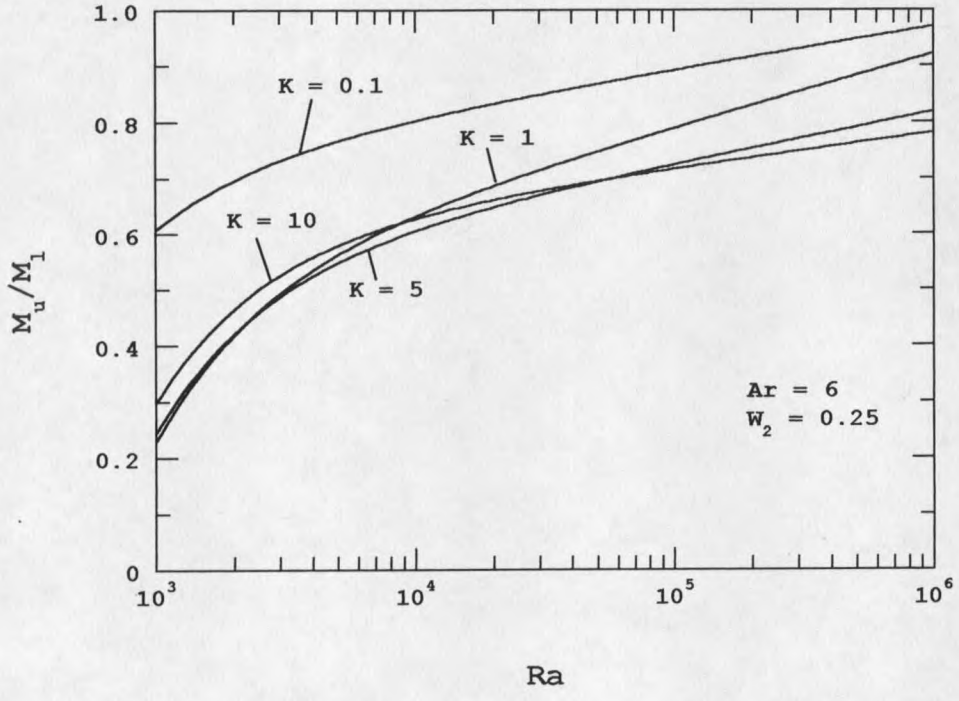


Figure 22. Ratio of upper inlet to lower inlet mass flow rate (M_u/M_l) vs. Ra.

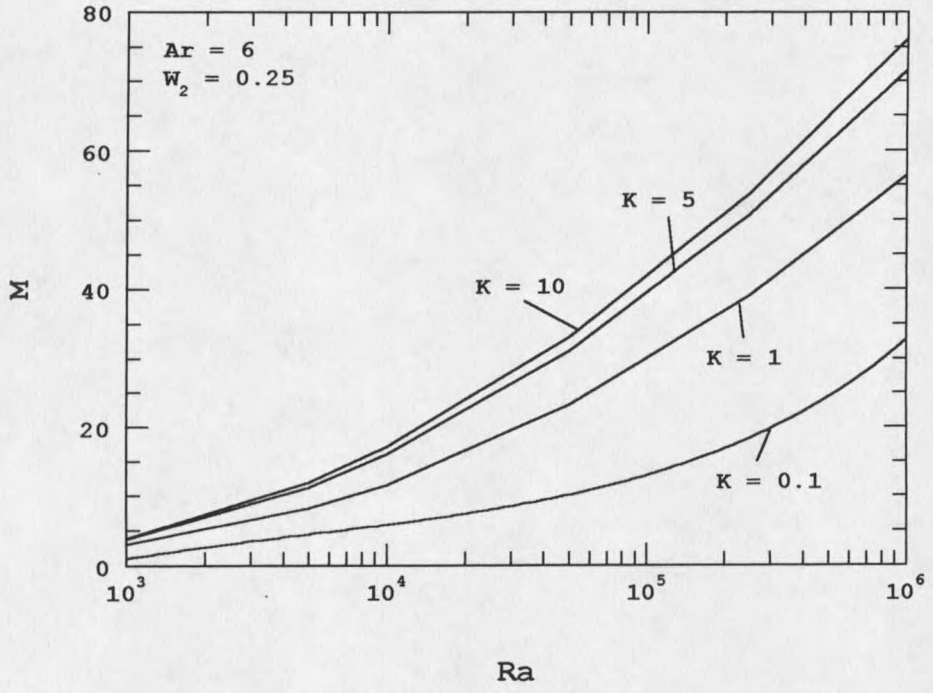


Figure 23. Total mass inflow rate from all sources vs. Ra

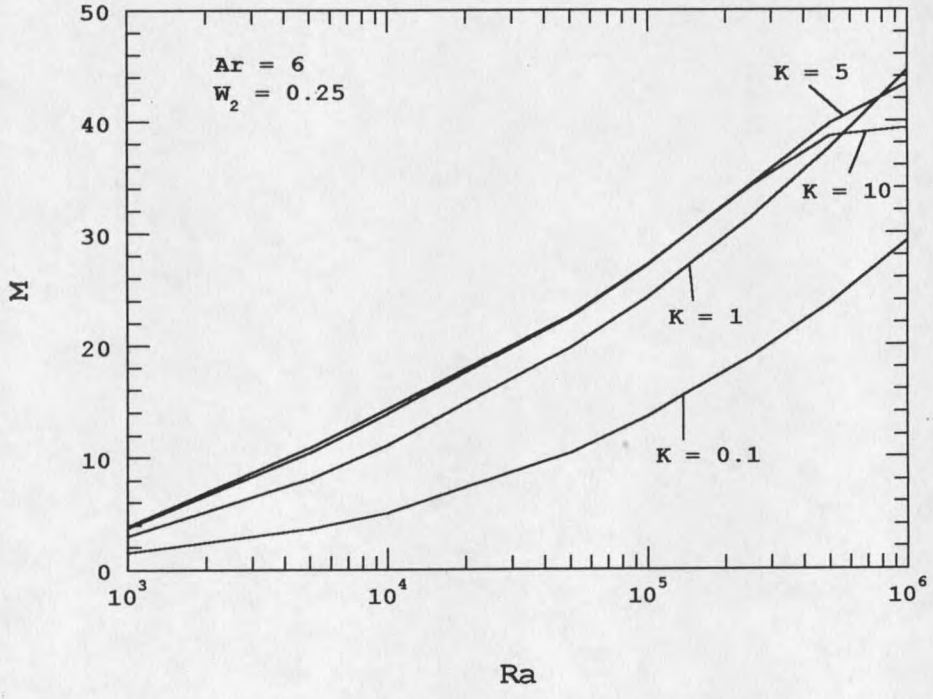


Figure 24. Total mass inflow rate from lower and upper inlets vs. Ra.

Average Nusselt Number Dependencies

Figures 25 and 26 show the average Nusselt number dependence on the parameters Ra, W_2, and K. It can be seen from the fixed K plots of Figure 25 that Nu increases with increasing Ra and W_2. However, for sufficiently large Rayleigh numbers ($>10^5$), Nu becomes nearly independent of W_2.

At lower Rayleigh numbers Nu depends on both W_2 and K. For values less than 0.5, W_2 strongly affects Nu. Increasing W_2 beyond 0.5 has little impact on Nu (<2%). It is evident that the effects of W_2 tend to diminish with larger K.

Examination of Figure 26 reveals that Nu tends to increase dramatically (up to 3000%) with K. The heat transfer enhancement due to the effects of K appears stronger at higher values of Rayleigh number. It is evident that Nu depends on K over the full range of Rayleigh numbers investigated. In all the cases investigated in this research, improved heat transfer is achieved with increasing K and/or W_2.

A few comments regarding the parameters K and W_2 will aid interpretation of the trends described above. Note that for cases with fixed aspect ratio, Ar, and fixed K (Figure 25), flow restrictions and Ra possess the only potential for affecting Nu. The partition wall and other boundaries cause flow restrictions that are not adequately represented by W_2. These flow restrictions essentially limit the physical access of the cool reservoir fluid to the heated wall and are

inherent in the thermosyphon geometry. The importance of these flow restrictions will be discussed later.

As noted previously, for Rayleigh numbers greater than 10^5, Nu is almost independent of W_2. With respect to Figure 26, this indicates that at large ($> 10^5$) Rayleigh numbers any change in Nu is due to changes in the parameters K, Ra, and any flow restrictions not represented by W_2.

Keeping in mind the points discussed above, the trends of Figures 25 and 26 are next examined to determine causes for the observed behavior.

In the previous section which studied effects due to W_2, it was found the temperature field became independent of W_2 at large Ra. As expected, Figure 25 indicates Nu follows the same trend with respect to W_2. The reason for this behavior is restated concisely as follows. As the thermal boundary layer approaches the heated wall with increasing Ra, cool reservoir fluid finds sufficient access at the outlet to compensate for the inlet configuration.

Figure 25 also indicates that restrictive W_2 decreases the average Nusselt number (Nu) at low Ra. This effect is less with increase in K or Ra. For low Ra, it is shown that one effect of increasing Ra is to reduce buoyancy effects opposing the upper inlet channel inflow. This reduces flow restriction and thus increases Nu.

In the previous section where the effects of K are studied, it is found that larger K tends to increase

recirculation. This is due to the greater thermal buoyancy force imparted to the fluid as K is increased and the subsequent decreased thermal boundary layer thickness. This recirculation flow also increases Nu as it compensates for restrictive W_2.

Figure 26 shows large changes in Nu for increased thermal conductivity ratio K. It is evident from Figure 26 that K affects Nu more strongly at larger Ra. The thermal conductivity ratio K affects Nu because it controls the temperature drop across the heated wall. Convection at the wall surface also plays a role.

Larger values of K increase the convection coefficient and also decrease the wall temperature drop. Either of these two effects will increase the average Nusselt number. The relative importance of each mechanism is not clear. This question will be discussed more later.

So far it is seen that besides Ra, flow restrictions and wall thermal conductivity (represented by W_2 and K) are the primary parameters affecting Nu. Let us now consider an optimized case for the present configuration. An "L" shaped wall resembles the present geometry if the partition wall and right adiabatic wall are removed. In this case flow is not restricted from the top and side, as in the present problem. This minimizes the flow restrictions. If the vertical leg of the "L" is made isothermal with large thermal conductivity, then the thermal conductivity parameter (K) is optimized.

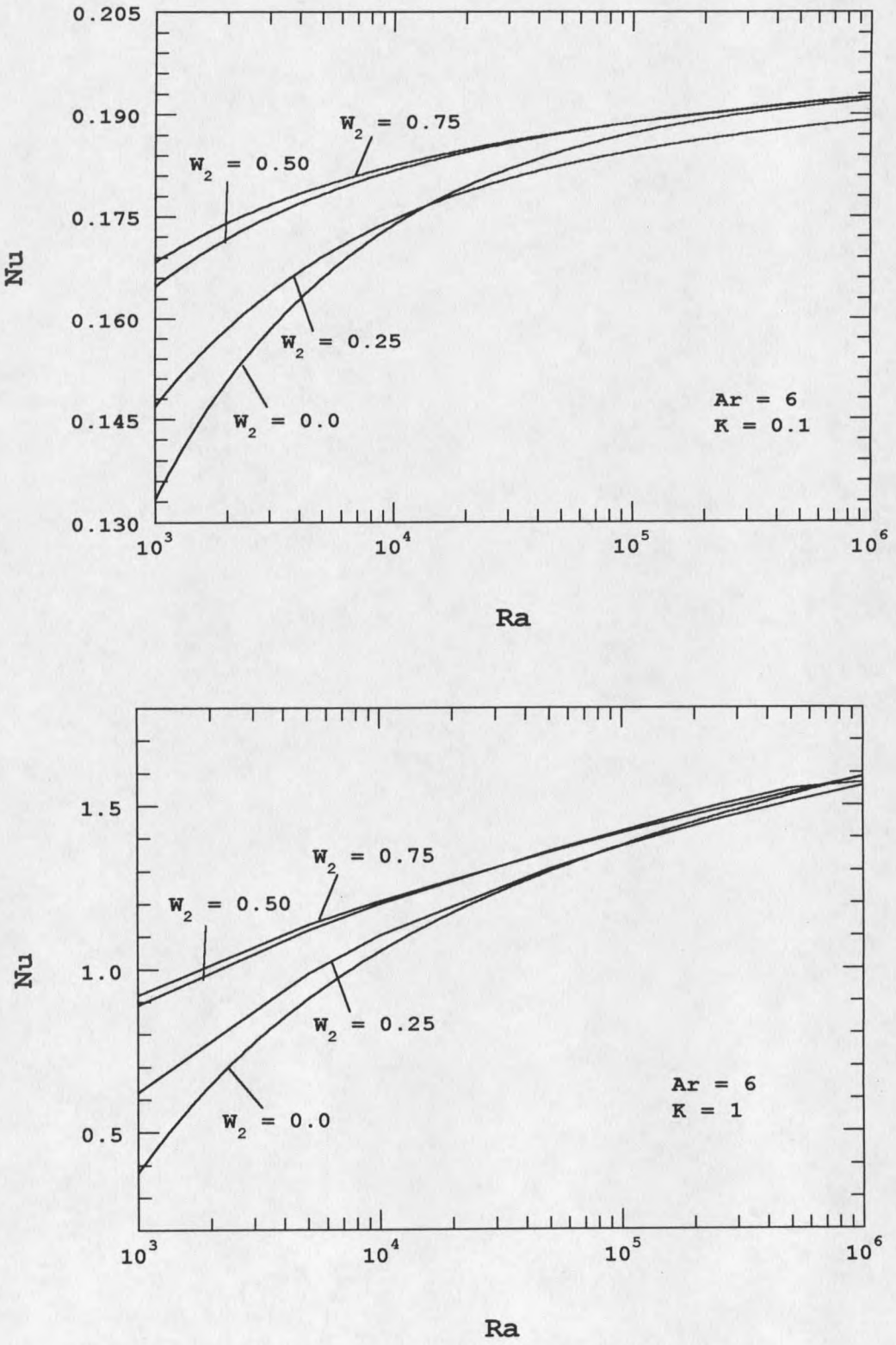
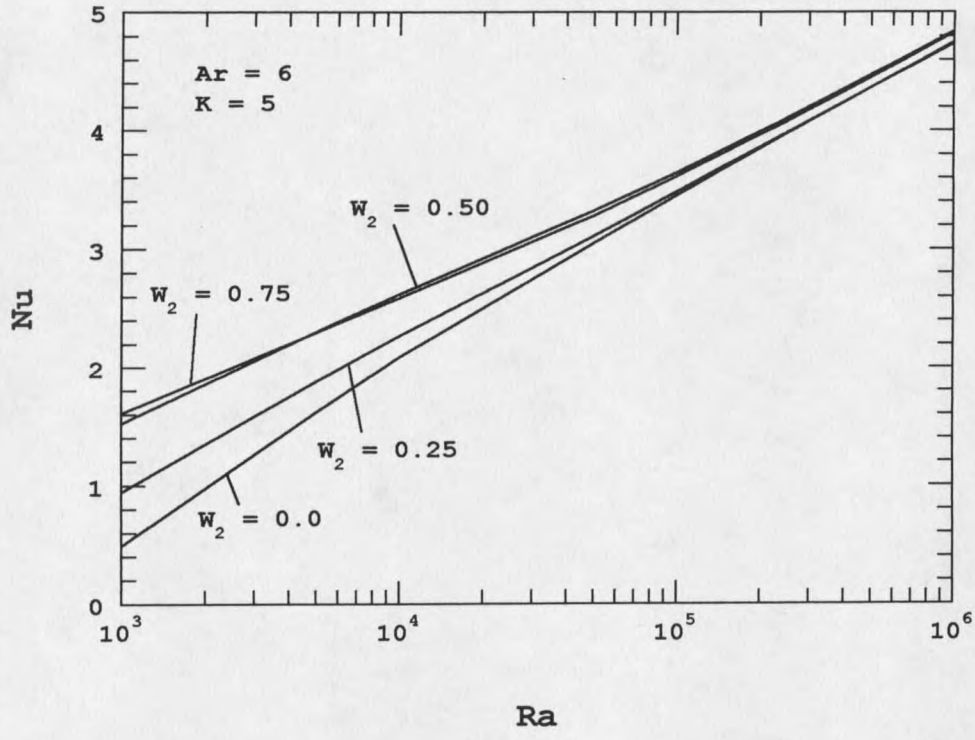


Figure 25. Average Nusselt number vs. Rayleigh number with parameters W_2 and K.



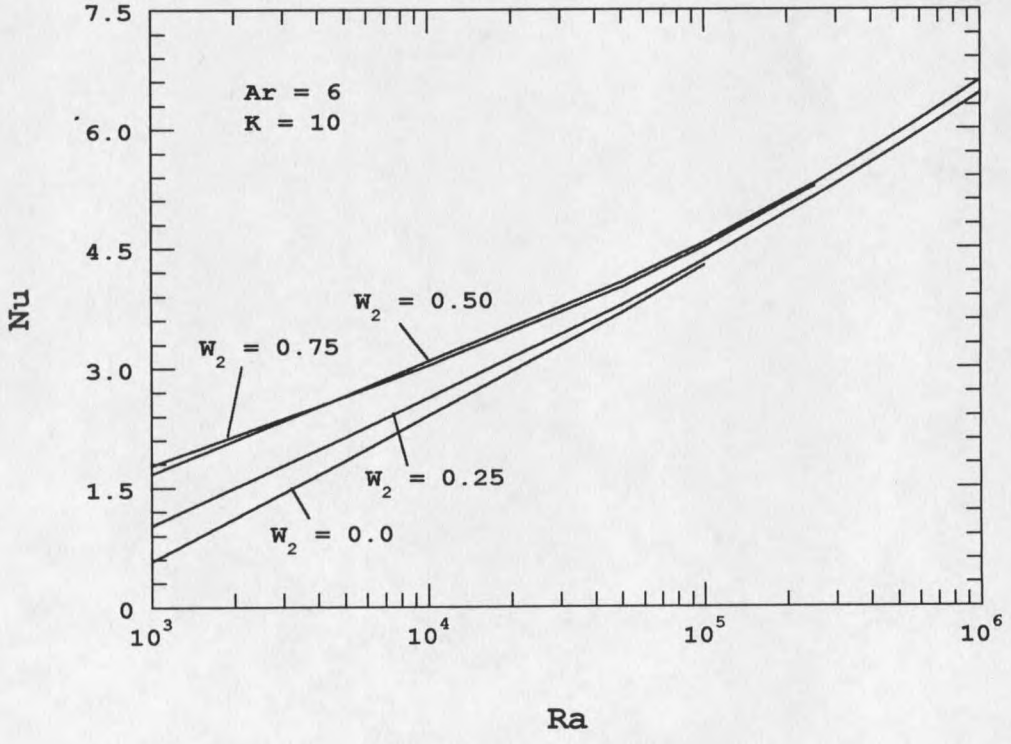


Figure 25.--continued

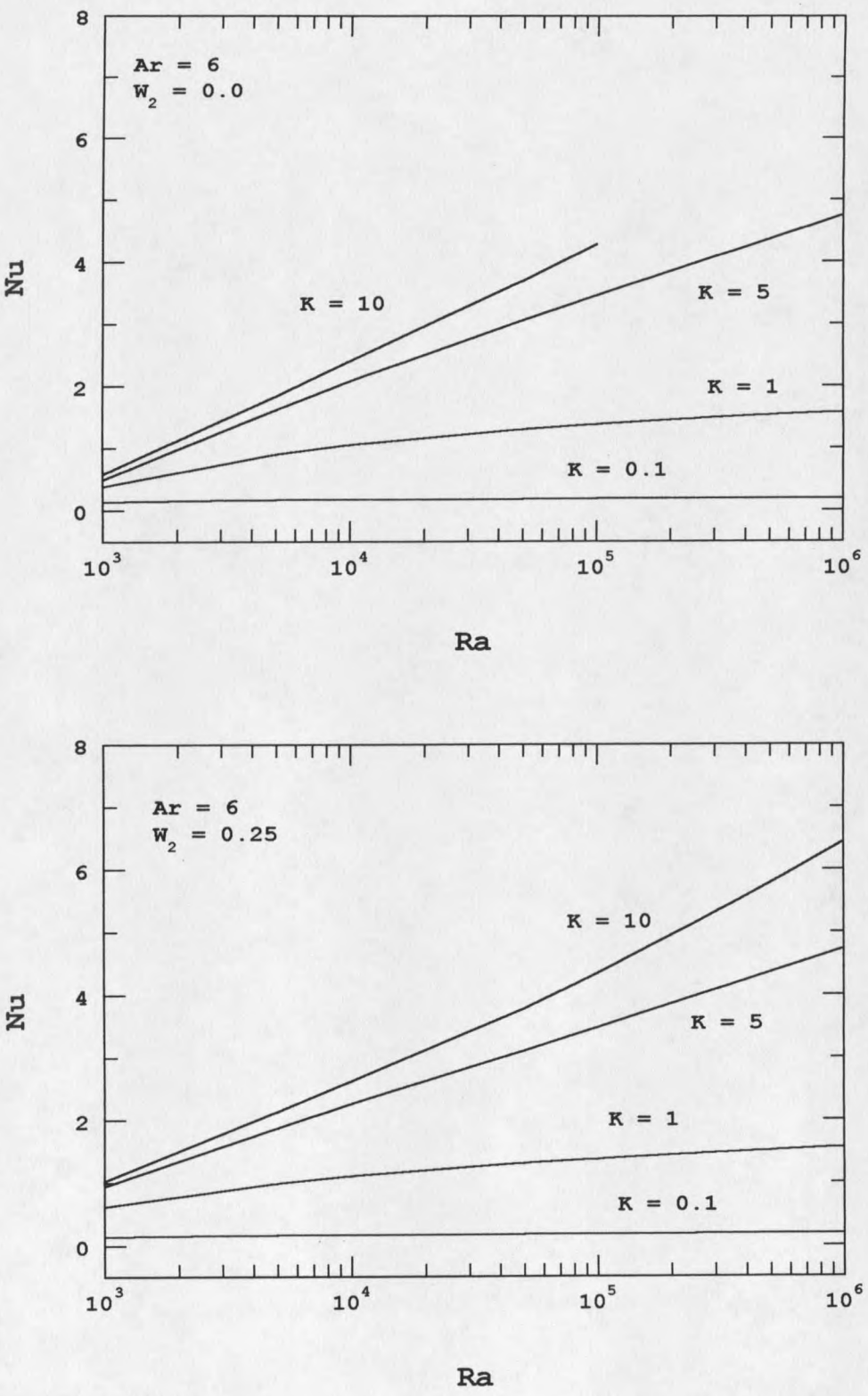
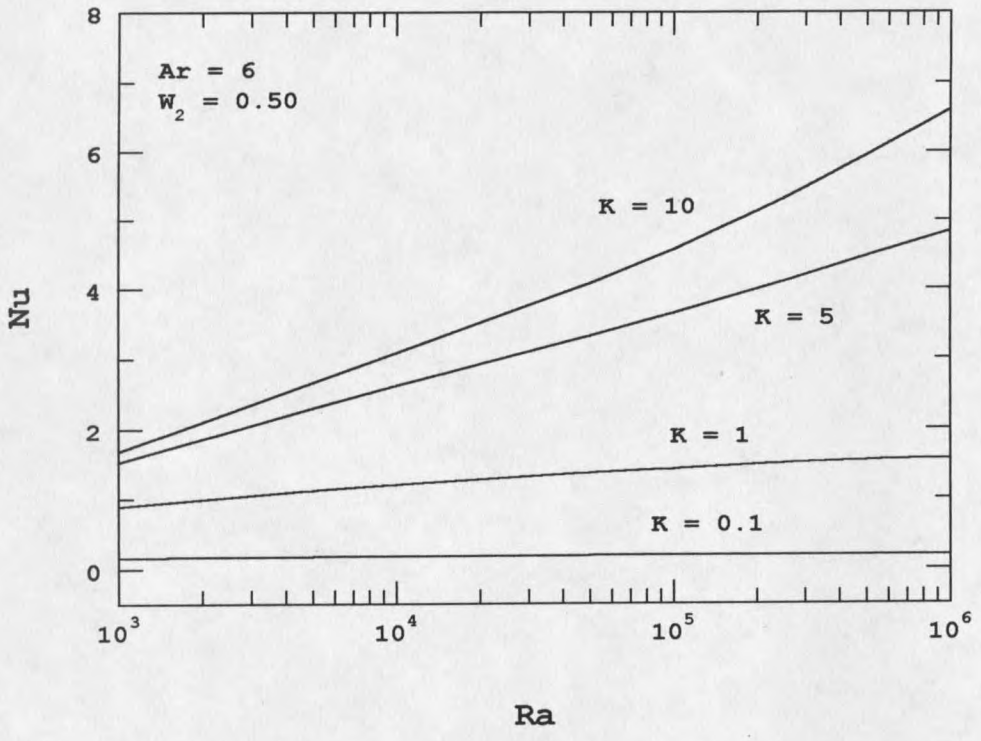


Figure 26. Average Nusselt number vs. Rayleigh number with parameters K and W_2.



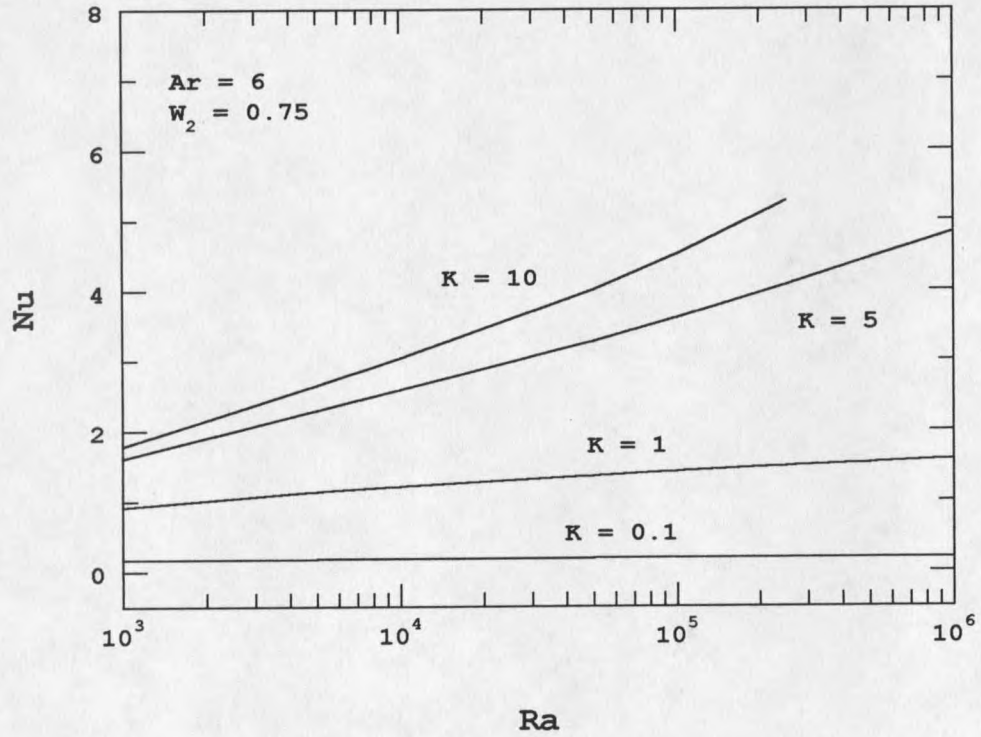


Figure 26.--continued

Heat transfer results for this geometry have been published [Rodighiero and de Socio (1983)]. The authors experimentally examined natural convection near a "L" shaped body with the vertical side isothermal and the horizontal side adiabatic. The vertical wall material was of high thermal conductivity so that wall conduction was not a parameter. The horizontal side is very long compared to the vertical side. The published experimental heat transfer correlation is given below.

$$Nu_l = 0.465\, Ra_l^{0.253} \qquad (52)$$

The author's Nusselt number (Nu_l) and Rayleigh number (Ra_l) above are based on the vertical wall length. Modifications to reflect the Nu and Ra definitions used in the present study are made with the result shown below.

$$Nu = 0.302\, Ra^{0.253} \qquad (53)$$

This correlation is valid in the laminar range from Ra = 4630 to Ra = 8.3×10^5. Instability was experimentally first observed at the largest Rayleigh number.

For comparison purposes, equation (53) is plotted in Figure 27 along with computed Nu (equation 48) results of this study. The difference in Nu values at low K values clearly shows the effect of low wall conductivity. However, for K=10 and in the range up to Ra=5×10^4 the maximum difference in Nu is only 15%. For larger Rayleigh numbers the wall thermal conductivity becomes much more important.

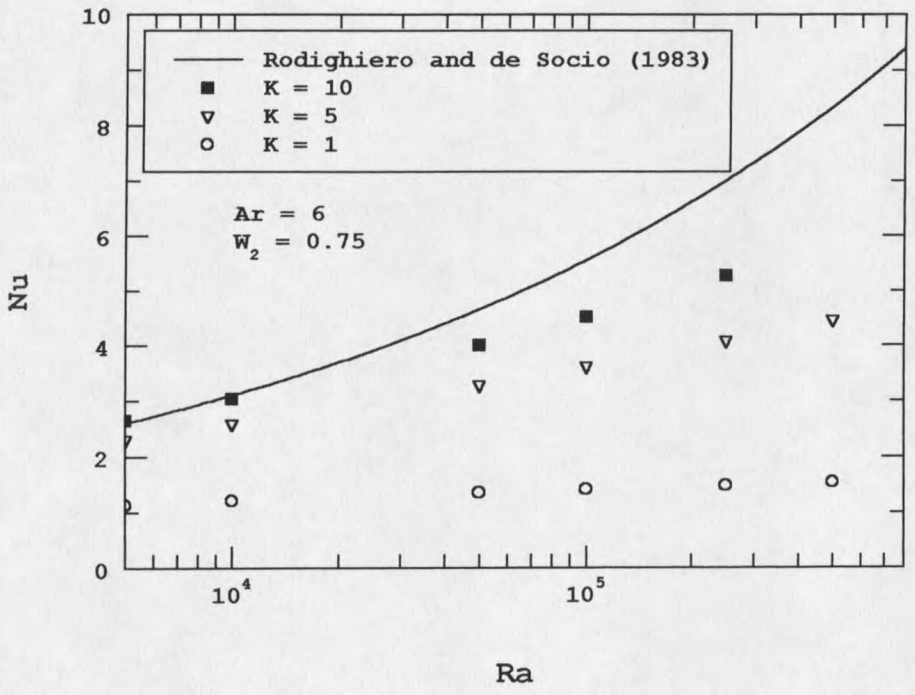


Figure 27. Published heat transfer results compared with Nu for present problem.

This comparison shows that heat transfer with the thermosyphon configuration is efficient for sufficiently large K and low Ra. As Ra is increased the thermosyphon does not perform as well as the optimized case. Figure 27 indicates that increased K will improve the thermosyphon performance. However, increasing K yields diminishing results with respect to Nu at large Ra. Recall that Nu is independent of W_2 at large Ra.

It appears that at large Ra another parameter other than W_2 and K becomes important in this comparison. This parameter can only be the presence of the partition and right adiabatic wall. The effects of these physically obstruct fluid flow from approaching the wall. This indicates that while the

average Nusselt number is independent of W_2 at large Ra, other flow restrictions remain.

Figure 28 shows the same comparison, but the Nusselt number (Nu_i) for the present study is computed along the heated wall internal surface. Here the local interface temperature and normal temperature gradient are used. This is shown in equation (54) below.

$$Nu_i = \frac{k_w}{k_a}\frac{b}{l_1}\int_0^{l_1}\frac{\partial T}{\partial x}\frac{1}{(T_i - T_\infty)}dy \qquad (54)$$

The internal Nusselt number (Nu_i) represents the normalized average convection coefficient along the heated wall internal surface. Nu_i also represents the normalized average heat flux, but based on the difference ($T_i - T_\infty$). This is in contrast to Nu, which as discussed earlier, represents the normalized average heat flux based on the temperature difference ($T_w - T_\infty$). Note that T_i varies with y^*, so Nu_i is not useful for correlating the overall heat transfer results. However, it does characterize very well the convection along the heated wall.

In the case of large wall thermal conductivity ($T_i=T_w$), Nu and Nu_i are equivalent. They quantify the average heat flux and the average convection coefficient. This is the case for the published correlation. Thus, the published correlation is used as a basis for comparison for Nu and Nu_i.

Figures 28 compares the normalized convection coefficient (Nu_i) to the published experimental results. It shows that

the Nu_i compares favorably to the published correlation. Increasing K affects Nu_i, but in a very limited way in comparison to the effect on Nu as is evident in Figure 27.

A question posed earlier concerns the effect of K to increase Nu through less wall conduction resistance and increased convection. It is not clear which effect is more important. Figure 27 shows dramatic increases in Nu for larger K which is due to both effects: reduced conduction resistance and increased convection. Figure 28 isolates the effect of K on the convection coefficient. It shows relatively modest increases with increased K. This indicates that the dramatic increases in Nu seen in Figure 27 for larger K are due primarily to reduced conduction resistance.

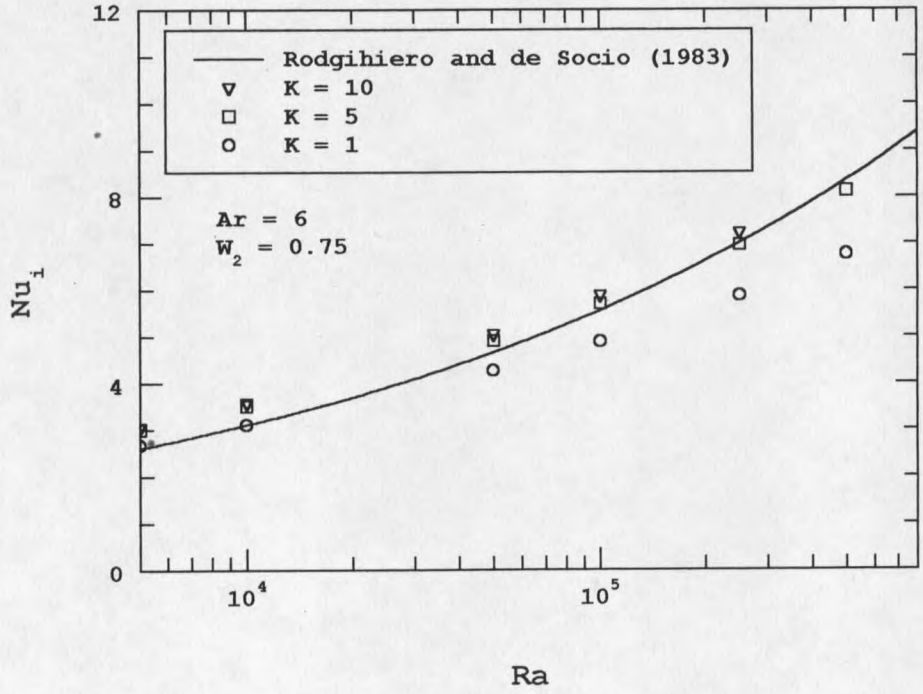


Figure 28. Published results compared with internal Nu_i for the present problem.

Wall Conductivity Parameter

There is some indication that the wall conductivity parameter ($K_r=k_w l_1/k_a h_1$) is an independent parameter. This is apparent in the problem formulation (equation 44) and in the literature reviewed by Kaminski and Prakash (1986).

To study the effects of K_r, the average Nusselt number (Nu) is compared for cases where K_r is a constant, but the wall geometry and thermal conductivity vary. The table below shows the cases considered. Note that the cases are chosen purposely so that there are minimal partition wall conduction effects on the average Nusselt number. This isolates thermal conductivity effects to the heated wall.

Table 6. Heated wall conductivity study parameters.

Case number	l_1/h_1	$K = k_w/k_a$	K_r
1	60	1	60
2	12	5	60
3	24	5	120
4	12	10	120

Average Nusselt number results for the cases above are given in Table 7. It is clear that for constant K_r, Nu changes only slightly even though wall geometry and thermal conductivity are dramatically different. Thus, K_r appears to be an independent parameter in this study. This is very much in agreement with the results presented by Kaminski and Prakash (1986).

Table 7. Overall Nusselt number results for K_r study.

	Overall Nusselt number (Nu)			
Ra	Case 1 K_r=60	Case 2 K_r=60	Case 3 K_r=120	Case 4 K_r=120
10^3	1.531	1.524	1.681	1.676
$5x10^3$	2.297	2.299	2.662	2.658
10^4	2.617	2.622	3.089	3.087
$5x10^4$	3.322	3.319	4.075	4.070
10^5	3.647	3.640	4.571	4.565
$2.5x10^5$	4.109	4.100	5.319	5.312
$5x10^5$	4.475	4.468	5.947	5.943
10^6	4.846	4.840	6.615	6.610

The parameter K_r correlates the overall heat transfer well. However, it is expected that the temperature field will vary locally for cases with constant K_r. Consider cases 1 and 2 of table 6; increasing the wall conductivity (K) should tend to make the solid-to-fluid interface temperature distribution more uniform. Larger K facilitates conduction in the vertical direction which tends to equalize local temperature fluctuations.

Figure 29 plots the solid-to-fluid interface temperature distribution (θ_i) along the heated wall for cases 1 and 2. It shows that increased K does affect local temperature variations as described above. Figure 30 shows the effect of K on the local convection coefficient $Nu_i(y^*)$. Again, local variation in $Nu_i(y^*)$ between cases 1 and 2 is apparent.

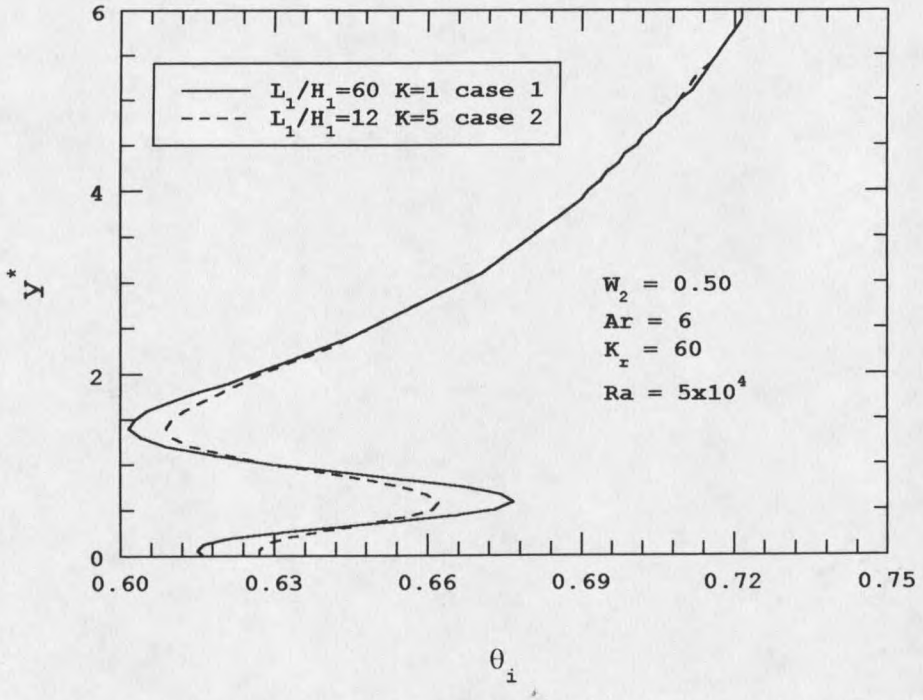


Figure 29. Constant K_r solid/fluid interface temperature distribution comparison cases 1 and 2.

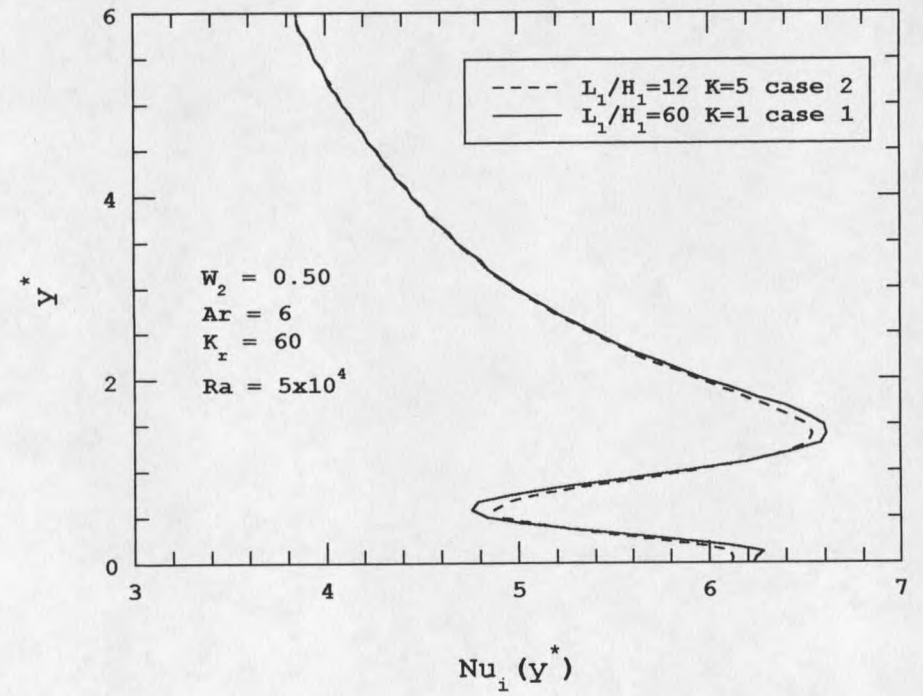


Figure 30. Constant K_r solid/fluid local convection coefficient comparison cases 1 and 2.

Aspect Ratio Parameter

The aspect ratio (Ar) of the inner channel is another parameter of interest. Extensive computations to evaluate the Nusselt number dependency on Ar were not carried out. It is important however, to show that Nu is dependent on Ar.

For many problems concerning vertical channels it has been shown that the modified Rayleigh (Ra/Ar) number is an independent parameter [Miyatake (1973)]. The problem formulation indicates that this is not the case here as Ar appears separately from Ra in the normalized governing equations (28 through 31). The objective here is to verify this indication. Table 8 below details the cases considered.

Table 8. Aspect ratio study parameters.

Case number	Ar	K_r
1	3	60
2	6	60

Overall Nusselt number results, as a function of the modified Rayleigh number, for the two cases above are shown in Figure 31. This figure shows that Ra/Ar is not an independent parameter and therefore Nu is also seperately dependent on Ar.

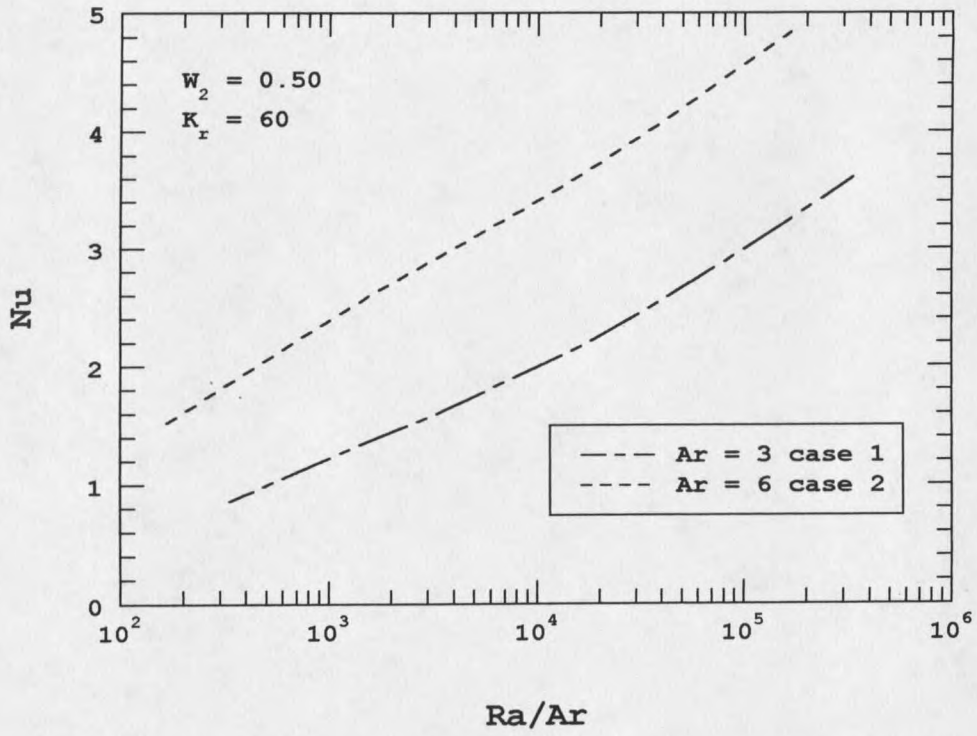


Figure 31. Correlation of Nu results vs. the modified Rayleigh number with constant K_r.

CONCLUSIONS AND RECOMMENDATIONS

Based on the numerical analysis presented here, and the previous discussions, several conclusions and recommendations are made. First, these are with respect to the average heat transfer, and second concerning points of interest that have not been fully addressed here.

Conclusions regarding the average heat transfer are as follows:

(1) The thermal conductivity ratio K is a very important parameter. Values of K less than 5 severely retard the heat transfer capabilities of the thermosyphon. This is primarily due to conduction resistance at the heated wall and is more pronounced as the Rayleigh number is increased. Conversely, larger values of K increase the heat transfer, but this effect gradually decreases.

(2) The lower inlet width parameter W_2 strongly affects the overall heat transfer at low Ra. For Ra less than 10^4, the heat transfer is reduced as much as 68% for the more restrictive W_2 values. As the Rayleigh number is increased, the effects of W_2 tend to diminish due to fluid recirculation at the outlet. Increasing W_2 beyond 0.5 for any Ra value only slightly increases the heat transfer. For Ra greater than 10^5 a completely closed lower inlet ($W_2 = 0$) decreases heat transfer by only 7 percent or less.

(3) The wall conductivity parameter K_r, is shown to be an independent parameter. The heat transfer rate for this problem cannot be fully correlated using K_r as the lone thermal conductivity parameter. Thermal resistance of the heated wall only is characterized by K_r. The partition wall has the same thermal conductivity ratio (K) as the heated wall, and at low Ra the partition wall conductivity affects the overall heat transfer. This is because of the opposing buoyancy effects near the upper inlet. Thus, to characterize the wall conductivity effects one could use K_r and K or K and l_1/h_1. For this problem the number of parameters is not reduced by use of K_r as a parameter.

(4) The Rayleigh number is also a very important parameter. The effectiveness of the other parameters depend on the magnitude of Ra. Essentially, Ra is an indication of the strength of the buoyancy force and resulting flow. Increasing the Rayleigh number increases the average heat transfer in all cases.

(5) Comparison to published experimental results shows that the modified "U" type thermosyphon examined here is not as effective for heat transfer as the open "L" wall configuration. However, for K greater than 10 and for relatively low Raleigh numbers ($5x10^4$), the thermosyphon compares well. For larger Rayleigh numbers the thermosyphon configuration restricts fluid flow to the

heated wall. Thus, less heat transfer occurs relative to the more open "L" configuration.

(6) The inner channel aspect ratio Ar is shown to affect the overall heat transfer.

Recommendations for points of interest that require further study are discussed below:

(1) Outlet boundary conditions need to be examined to ensure they are not affecting the results. Addition of an outlet plenum area would be useful to understand how the boundary conditions used affect recirculation at the outlet.

(2) Effects of the inner channel aspect ratio (Ar) on the overall heat transfer requires further investigation.

(3) Evaluation of a uniform heat flux boundary condition at the heated wall may of interest.

REFERENCES

REFERENCES

Abib, A. H. and Jaluria, Y., "Numerical Simulation of the Buoyancy-induced Flow in a Partially Open Enclosure," *Numerical Heat Transfer,* vol. 14, pp. 235-254, 1988.

Bau, H. H. and Torrance, K. E., "Transient and Steady Behavior of an Open Symmetrically-Heated Free Convection Loop," *Int. J. Heat Mass Transfer*, vol. 24, pp. 597-609, 1981.

Bejan, A., *Convection Heat Transfer,* John-Wiley and Sons, Inc., New York, 1984.

Burnette, D. S., *Finite Element Analysis,* Addison-Wesley Publishing Co., 1988.

Burch, T., Rhodes, T., Acharya, S., "Laminar Natural Convection Between Finitely Conducting Vertical Plates," *Int. J. Heat Mass Transfer,* vol.28, no. 6, pp. 1173-1186, 1985.

Chung, T. J., *Finite Element Analysis in Fluid Dynamics,* McGraw-Hill Book Co., New York, 1978.

Clarksean, R., "Experimental Analysis of Natural Convection Within a Thermosyphon," presented at the Third World Conference on Experimental Heat Transfer, Fluid Mechanics, and Thermodynamics, Honolulu, Hawaii, Oct., 1993.

COSMOS/M Users Manual, Seventh Edition, Version 1.67 Structural Research and Analysis Corporation, Santa Monica, California, April 1993.

De Vahl Davis, G., and Jones, I. P., "Natural Convection in a Square Cavity: a Comparison Exercise," *International Journal of Numerical Methods in Fluids,* vol. 3, pp. 227-248, 1983.

Elenbass, W., "Heat Dissipation of Parallel Plates by Free Convection," *Physica,* vol. 9, no. 1, pp. 1-23, 1942.

Gebhart, B., Jaluria, Y., Mahajan, R. L., Sammakia, B., *Buoyancy-Induced Flows and Transport,* Hemisphere Publishing Corp., New York, 1988.

Gray D. D., and Giorgini, A., "The Validity of the Boussinesq Approximation for Liquids and Gases," *International Journal of Heat and Mass Transfer,* vol. 19, pp. 545-551, 1976.

REFERENCES-continued

Huebner, K. H., and Thornton, E. A., *The Finite Element Method for Engineers,* John Wiley and Sons, 1982.

Jaluria, Y., "Natural Convective Cooling of Electronic Equipment," in *Natural Convection Fundamentals and Applications,* edited by Kakac, C., Aung, W., and Viskanta, R., Hemisphere Publishing Corporation, Washington, 1985.

Japikse, D., "Advances in Thermosyphon Technology," in *Advances in Heat Transfer,* edited by Irvine, T. F. Jr., and Hartnett, J. P., Academic Press, vol. 9, 1973.

Kaminski, D. A., and Prakash, C., "Conjugate Natural Convection in a Square Enclosure: Effect of Conduction in One of the Vertical Walls," *Int. J. Heat Mass Transfer,* vol. 29, no. 12, pp. 1979-1988, 1986.

Kays, W. M., and Crawford, M. E., *Convective Heat and Mass Transfer,* second edition, McGraw-Hill Book Co., 1980.

Kim, D. M., and Viskanta, R., "Effect of Wall Heat Conduction on Natural Convection Heat Transfer in a Square Enclosure," *Journal of Heat Transfer,* vol. 107, pp. 139-146, 1985.

Kim, w., Anand, N. K., and Aung, W., "Effect of Wall Conduction on Free Convection Between Asymmetrically Heated Vertical Plates: Uniform Wall Heat Flux," *Int. J. Heat Mass Transfer,* pp. 1013-1022, 1990.

Krieth, F., and Anderson, R., "Natural Convection in Solar Systems," in *Natural Convection Fundamentals and Applications,* edited by Kakac, C., Aung, W., and Viskanta, R., Hemisphere Publishing Corporation, Washington, 1985.

Kwant, W., and Boardman, C. E., "PRISM-Liquid Metal Cooled Reactor Plant Design and Performance," *Nuclear Engineering and Design,* vol. 136, pp. 135-141, 1992.

Lapin, Y. D., "Heat Transfer in Communicating Channels Under Conditions of Free Convection," *Thermal Engineering,* vol. 16, pp. 94-97, 1969.

Mallinson, G. D., "The Effects of Side-Wall Conduction on Natural Convection in a Slot," *Journal of Heat Transfer,* vol. 109, pp. 419-426, 1987.

REFERENCES-continued

Mertol, A. and Greif, R., "A Review of Natural Circulation Loops," in *Natural Convection Fundamentals and Applications*, edited by Kakac, C., Aung, W., and Viskanta, R., Hemisphere Pub. Corp., Washington, 1985.

Miyatake, O., Fujii, T., Fujii, M., and Tanaka, H., "Natural Convective Heat Transfer Between Vertical Parallel Plates-One Plate With a Uniform Heat Flux and the Other Thermally Insulated," *Heat Transfer-Japanese Research*, vol. 4, pp. 25-33, 1973.

Pantakar, S. V., *Numerical Heat Transfer and Fluid Flow*, Hemisphere Publishing Corporation, New York, 1980.

Papanicolaou, E., and Jaluria, Y., "Mixed Convection From a Localized Heat Source in a Cavity with Conducting Walls: a Numerical Study," *Numerical Heat Transfer*, Part A, vol. 23, pp. 463-484, 1993.

Sparrow, E. M., and Gregg, J. L., "The Variable Fluid Property Problem in Free Convection," *Transactions of The ASME*, pp. 879-886, 1958.

Torrance, K. E., "Open Loop Thermosyphons with Geological Applications," *Journal of Heat Transfer*, vol. 101, pp. 677-683, 1979.

Torrance, K. E., and Chan, V. W. C., "Heat Transfer by a Free Convection Loop Embedded in a Heat-Conducting Solid," *Int. J. Heat Mass Transfer*, vol. 23, pp. 1091-1097, 1980.

Zhong, Z. Y., Yang, K. T., and Lloyd, J. R., "Variable Property Effects in Laminar Natural Convection in a Square Enclosure," *ASME Journal of Heat Transfer*, vol. 107, pp. 133-138, 1985.

Zinnes, A. E., "The Coupling of Conduction With Laminar Natural Convection From a Vertical Flat Plate With Arbitrary Surface Heating," *Journal of Heat Transfer*, vol. 92, pp. 528-535, 1970.

APPENDICES

APPENDIX A

COSMOS/M FINITE ELEMENT PROGRAM

COSMOS/M FINITE ELEMENT PROGRAM

The fluid flow and heat transfer module of the COSMOS/M finite element analysis package is called FLOWSTAR. FLOWSTAR is capable of solving a wide variety of problems. This includes steady state and transient problems, internal or external flows, 2 and 3 dimensional problems, and problems coupling solid region conduction with fluid regions. Fluids considered may be Newtonian or non-Newtonian; fluid properties may be specified as functions of temperature. More specifically the types of flow analyses possible using FLOSWTAR are as follows:

(1) incompressible laminar flow (non-isothermal or isothermal) for 2 and 3 dimensional problems

(2) incompressible turbulent flow for internal, isothermal, steady, 2 dimensional problems

(3) supersonic compressible flow for internal, inviscid, steady, 2 dimensional problems

Each type of flow listed above is governed by the conservation laws for mass, momentum, and energy. Of interest for the present problem is the mathematical formulation of these laws for non-isothermal, incompressible, laminar flows. The governing equations as used by FLOWSTAR are given below. The Boussinesq approximation for natural convection flows is included.

Continuity equation:

$$\frac{\partial u}{\partial x} + \frac{\partial v}{\partial y} + \frac{\partial w}{\partial z} = 0$$

Momentum equations:

$$\rho \left(\frac{\partial u}{\partial t} + u \frac{\partial u}{\partial x} + v \frac{\partial u}{\partial y} + w \frac{\partial u}{\partial z} \right) = \frac{\partial \sigma_{xx}}{\partial x} + \frac{\partial \sigma_{xy}}{\partial y} + \frac{\partial \sigma_{xz}}{\partial z} - \rho g_x \beta (T - T_0)$$

$$\rho \left(\frac{\partial v}{\partial t} + u \frac{\partial v}{\partial x} + v \frac{\partial v}{\partial y} + w \frac{\partial v}{\partial z} \right) = \frac{\partial \sigma_{xy}}{\partial x} + \frac{\partial \sigma_{yy}}{\partial y} + \frac{\partial \sigma_{yz}}{\partial z} - \rho g_y \beta (T - T_0)$$

$$\rho \left(\frac{\partial w}{\partial t} + u \frac{\partial w}{\partial x} + v \frac{\partial w}{\partial y} + w \frac{\partial w}{\partial z} \right) = \frac{\partial \sigma_{xz}}{\partial x} + \frac{\partial \sigma_{yz}}{\partial y} + \frac{\partial \sigma_{zz}}{\partial z} - \rho g_z \beta (T - T_0)$$

Energy equation:

$$\rho C_p \left(\frac{\partial T}{\partial t} + u \frac{\partial T}{\partial x} + v \frac{\partial T}{\partial y} + w \frac{\partial T}{\partial z} \right) = \frac{\partial}{\partial x} \left(k \frac{\partial T}{\partial x} \right) + \frac{\partial}{\partial y} \left(k \frac{\partial T}{\partial y} \right) + \frac{\partial}{\partial z} \left(k \frac{\partial T}{\partial z} \right) + Q + \mu \Phi$$

The stress tensor σ_{ij} and other terms are defined below:

$$\sigma_{ij} = -p \delta_{ij} + \mu \left(\frac{\partial u_i}{\partial x_j} + \frac{\partial u_j}{\partial x_i} \right)$$

ρ = density

μ = dynamic viscosity

C_p = specific heat

k = thermal conductivity

β = coefficient of volumetric expansion

u,v,w = velocity components in x,y,z directions

T = temperature

t = time

p = motion pressure

g_x, g_y, g_z = gravity acceleration components

T_o = reference temperature at which buoyancy forces are zero

Q = volumetric heat generation rate

Φ = viscous dissipation function

δ_{ij} = Kronecker delta function

The penalty function formulation of the governing equations is used which eliminates the pressure variable (p) and the need to solve the continuity equation. The penalty function is given below:

$$\frac{\partial u}{\partial x} + \frac{\partial v}{\partial y} + \frac{\partial w}{\partial z} = -\frac{1}{\lambda} p$$

where λ is a large number called the penalty parameter. This is substituted into the momentum equations and effectively eliminates both the pressure variable and the continuity equation from the system of equations. This reduces the size of the equation system significantly.

Galerkin's method of weighted residuals (MWR) is used to transform the governing equations into a system of algebraic equations. A general description in one dimension which gives the basic concepts of this method follows.

Let a differential equation be represented by L(y(x))=0, where L is the differential operator, y is the dependent variable and x is the independent variable. Next, assume an approximate solution $\bar{y}(x)$ so that $L(\bar{y}(x)) = R$. The method of weighted residuals seeks to make the residual (R) small, so

that the error due to the assumed approximate solution is small. This is accomplished in a weighted sense by integration of R over the domain of interest as follows:

$$\int R W dx = \int L(\bar{y}(x)) W dx = 0 \qquad \text{(A1)}$$

where W is the weighting function.

Derivation of the finite element (algebraic) equations is done by carrying out this integration over a single finite element. First, the weighting function and form of the approximate solution are chosen and then the indicated operations are performed. The approximate solution is defined over a finite element containing several nodes. Its form is a linear combination of terms as follows.

$$\bar{y} = \sum_{i=1}^{n} \bar{y}_i N_i$$

Here n is the number of nodes, $\bar{y}_i$ is the value (unknown) of $\bar{y}$ at the node (i), and N_i is the shape function which depends on the known position (x_i) of each node. In the Galerkin method of weighted residuals the weighting functions are chosen to be the same as the shape functions. Since the approximate solution is a linear combination of terms the integrand (equation A1) results in a linear combination. Each term of this combination may be integrated separately and each resulting integral is separately equal to zero. Thus, one constraint equation is produced for each unknown ($\bar{y}_i$).

The constraint equations are coupled to those in adjacent finite elements because they share nodes along common boundaries. Thus, the finite element equations can be assembled into one large system of algebraic equations encompassing the entire problem domain. Values for the dependent variable along domain boundaries must be specified as boundary conditions. The assembled equation system is then solved, which results in values for the dependent variable at each node in the domain.

The finite element equations used by FLOWSTAR and derived by the Galerkin method are much more complicated than one dimensional example above. However, the same basic concepts apply. The finite element equations and description of terms are given below:

$$[M]\{\dot{V}\} + [[K_c(V)] + [K_d] + [K_p]]\{V\} + [K_b]\{T\} = \{f_v\} \quad \text{(A2)}$$

$$[C]\{\dot{V}\} + [[T_a(V)] + [T_d] + [T_c]]\{T\} = \{f_t\} \quad \text{(A3)}$$

where

$[M]$ = mass matrix

$[K_c]$ = momentum convection matrix

$[K_d]$ = momentum diffusion matrix

$[K_p]$ = penalty matrix

$[K_b]$ = buoyancy matrix

$[C]$ = thermal capacitance matrix

$[T_a]$ = thermal advection matrix

$[T_c]$ = thermal convection matrix

$[T_d]$ = thermal diffusion matrix

$\{T\}$ = temperature vector

$\{f_v\}, \{f_t\}$ = load vectors

$$\{v\} = \begin{Bmatrix} \{u\} \\ \{v\} \\ \{w\} \end{Bmatrix} = \text{velocity vector}$$

The dependent variables are given below.

$$u = \sum_{i=1}^{n} u_i N_i \ , \ v = \sum_{i=1}^{n} v_i N_i \ , \ w = \sum_{i=1}^{n} w_i N_i \ , \ T = \sum_{i=1}^{n} T_i N_i$$

The equations (A2) and (A3) are a system of ordinary nonlinear differential equations with respect to time. To reduce these equations to a system of algebraic equations a time integration method is used. The resulting algebraic equations are assembled and then solved utilizing the Newton-Raphson or Picard iteration methods.

APPENDIX B

FORTRAN PROGRAMS

Figure 32. Program to compute internal average Nusselt number.

```
C     THIS PROGRAM COMPUTES THE AVERAGE NUSSELT NUMBER AT THE LEFT
C     WALL INTERNAL SURFACE USING THE LOCAL TEMPERATURE.  THIS CODE
C     IS APPLICABLE ONLY FOR AN ODD NUMBER OF NODES.

      CHARACTER*17 KEYWORD,TESTWORD
      INTEGER J,I,NODESB,NODE
      REAL Y(100),X(100),Z,GRX(100),GRY,GRZ,RAT,GRN,H1(100),H2(100),
     ? AP,WIDTH,LENGTH,U,V,W,VR,P,T(100),TINF

C     OPEN DATA FILES CONTAINING FLOWSTAR NODAL DATA
C     XYEXT.LIS CONTAINS LEFT WALL INTERNAL SURFACE NODE COORDINATES
C     NUYINT.LIS CONTAINS TEMPERATURE GRADIENT DATA
C     TEMPYINT.LIS CONTAINS TEMPERATURE DATA

      OPEN(UNIT=5,FILE='XYEXT.LIS',STATUS='OLD')
      OPEN(UNIT=4,FILE='NUYINT.LIS',STATUS='OLD')
      OPEN(UNIT=3,FILE='TEMPYINT.LIS',STATUS='OLD')

C     READ INNER CHANNEL VERTICAL LENGTH, HORIZONTAL WIDTH, RESERVOIR
C     TEMPERATURE (TINF), AND THERMAL CONDUCTIVITY RATIO (RAT).

        WRITE(*,*) 'INPUT LENGTH, WIDTH, TINF, AND THERMAL CONDUCTIVITY RATIO'

      READ(*,*) LENGTH,WIDTH,TINF,RAT

      KEYWORD = 'X-Coordinate      '
      WRITE(*,*) 'COMPUTING AVERAGE NUSSELT NUMBER'

C     INITIALIZE ARRAYS

      DO 5 N = 1,100
        Y(N) = 0
        X(N) = 0
        GRX(N) = 0
        T(N) = 0
        H1(N) = 0
        H2(N) = 0
 5    CONTINUE

C     OPEN XYEXT.LIS AND FIND BEGINNING OF NUMERICAL DATA

      DO 10 J = 1,100

         READ(5,11) TESTWORD
 11      FORMAT(18X,A)
         IF(TESTWORD.EQ.KEYWORD) THEN
         GO TO 15
         ENDIF
 10   CONTINUE

 15   NODESB = 0

C     READ XYEXT.LIS AND STORE CONTENTS IN ARRAYS

      DO 20 I = 1,100
      NODESB = NODESB + 1
      READ(5,*,END=21) NODE,X(I),Y(I),Z
 20   CONTINUE
```

Figure 32.--continued

```
C     OPEN NUYINT.LIS AND FIND BEGINNING OF NUMERICAL DATA

 21   KEYWORD = 'GRAD_X      GRAD_'

      DO 25 J = 1,500

         READ(4,26) TESTWORD
 26      FORMAT(10X,A)
         IF(TESTWORD.EQ.KEYWORD) THEN
         GO TO 30
         ENDIF
 25   CONTINUE

 C     READ NUYINT.LIS AND STORE CONTENTS IN ARRAYS

 30   DO 35 I = 1,100
      READ(4,*,END=36) NODE,GRX(I),GRY,GRZ,GRN
 35   CONTINUE

C     OPEN TEMPYINT.LIS AND FIND BEGINNING OF NUMERICAL DATA

 36   KEYWORD = 'Node'

      DO 37 KK = 1,100
      READ(3,*) TESTWORD
         IF(TESTWORD.EQ.KEYWORD) THEN
         GO TO 4
         ENDIF
 37   CONTINUE

C     READ TEMPYINT.LIS AND STORE CONTENTS IN ARRAYS

  4   DO 38 JJ = 1,100
      READ(3,*,END=39) NODE,U,V,W,VR,P,T(JJ)
 38   CONTINUE

C     COMPUTE AND STORE Y INTERVALS

 39   JJ = 0

      DO 40 K = 1,NODESB-2,2
         JJ = JJ + 1
         H1(JJ) = Y(K+1) - Y(K)
         H2(JJ) = Y(K+2) - Y(K+1)
  40  CONTINUE

C     PERFORM SIMPSON'S RULE INTEGRATION

      SUM = 0.0
      I = 0

      DO 45 J = 1,NODESB-2,2
      I = I + 1
      AP = (1.0/6.0)*(H2(I)+H1(I))/(H1(I)*H2(I))*((2*H1(I)*H2(I)-
     ? H2(I)**2)*(GRX(J)/(T(J)-TINF))+(H1(I)+H2(I))**2*(GRX(J+1)/
     ? (T(J+1)-TINF))+(2*H1(I)*H2(I)-H1(I)**2)*(GRX(J+2)/
     ? (T(J+2)-TINF)))
```

Figure 32.--continued

```
      SUM = SUM + AP

   45 CONTINUE

C     COMPUTE AVERAGE INTERNAL NUSSELT NUMBER

      AP = -1*SUM
      AVNUS = RAT*AP*WIDTH/LENGTH

C     OUTPUT RESULTS

      WRITE(*,*) 'AVERAGE NUSSELT NUMBER = ',AVNUS

      END
```

Figure 33. Program to compute external average Nusselt number.

```
C     THIS PROGRAM COMPUTES THE AVERAGE NUSSELT NUMBER ON THE LEFT WALL
C     EXTERNAL SURFACE.  SIMPSON'S RULE INTEGRATION FOR IRREGULAR
C     INTERVALS IS USED.  THIS CODE IS APPLICABLE ONLY FOR AN ODD NUMBER
C     OF NODES (EVEN NUMBER OF ELEMENTS).

      CHARACTER*17 KEYWORD,TESTWORD
      INTEGER J,I,NODESB,NODE
      REAL Y(200),X(200),Z,GRX(200),GRY,GRZ,K,
     ? GRN,H1(100),H2(100),AP,DT,WIDTH,LENGTH

C     OPEN DATA FILES CONTAINING FLOWSTAR NODAL DATA
C     XYEXT.LIS CONTAINS NODE COORDINATES ALONG LEFT WALL EXTERNAL SURFACE
C     NUYEXT.LIS CONTAINS NODE TEMPERATURE AND TEMPERATURE GRADIENT DATA

      OPEN(UNIT=5,FILE='XYEXT.LIS',STATUS='OLD')
      OPEN(UNIT=4,FILE='NUYEXT.LIS',STATUS='OLD')

      KEYWORD = 'X-Coordinate      '
      WRITE(*,*) 'COMPUTING AVERAGE NUSSELT NUMBER'

C     INITIALIZE ARRAYS TO ZERO

      DO 5 N = 1,200
        Y(N) = 0
        X(N) = 0
        GRX(N) = 0
 5    CONTINUE

      DO 6 NN = 1,100
         H1(NN) = 0
         H2(NN) = 0
 6    CONTINUE

C     OPEN XYEXT.LIS AND FIND BEGINNING OF NUMERICAL DATA

      DO 10 J = 1,1000

         READ(5,11) TESTWORD
 11      FORMAT(18X,A)
         IF(TESTWORD.EQ.KEYWORD) THEN
         GO TO 15
         ENDIF
 10   CONTINUE

 15   NODESB = 0

C     READ XYEXT.LIS AND STORE CONTENTS IN ARRAYS

      DO 20 I = 1,100
      NODESB = NODESB + 1
      READ(5,*,END=21) NODE,X(I),Y(I),Z
 20   CONTINUE

C     OPEN NUYEXT.LIS AND FIND BEGINNING OF NUMERICAL DATA

 21   KEYWORD = 'GRAD_X       GRAD_'
```

Figure 33.--continued

```
      DO 25 J = 1,500

         READ(4,26) TESTWORD
 26      FORMAT(10X,A)
         IF(TESTWORD.EQ.KEYWORD) THEN
         GO TO 30
         ENDIF
 25    CONTINUE

C     READ NUYEXT.LIS AND STORE CONTENTS IN ARRAYS

 30    DO 35 I = 1,100
       READ(4,*,END=36) NODE,GRX(I),GRY,GRZ,GRN
 35    CONTINUE

 36    JJ = 0

C     COMPUTE AND STORE Y INTERVALS

      DO 40 K = 1,NODESB-2,2
         JJ = JJ + 1
         H1(JJ) = Y(K+1) - Y(K)
         H2(JJ) = Y(K+2) - Y(K+1)
  40  CONTINUE

      SUM = 0.0
      I = 0

C     PERFORM SIMPSON'S RULE INTERATION

      DO 45 J = 1,NODESB-2,2
      I = I + 1
      AP = (1.0/6.0)*(H2(I)+H1(I))/(H1(I)*H2(I))*((2*H1(I)*H2(I)-
     ? H2(I)**2)*GRX(J)+(H1(I)+H2(I))**2*GRX(J+1)+(2*H1(I)*H2(I)-
     ? H1(I)**2)*GRX(J+2))

      SUM = SUM + AP

  45  CONTINUE

C     OUTPUT RESULTS

      AP = -1*SUM
      READ(*,*) WIDTH,LENGTH,DT,K
      AVNUS = AP*WIDTH*K/(LENGTH*DT)
      WRITE(*,*) 'AVERAGE NUSSELT NUMBER = ',AVNUS


      END
```

Figure 34. Program for combining COSMOS/M output files.

```
C     THIS PROGRAM READS NODE X,Y COORDINATE DATA FROM COSMOSM OUTPUT
C     FILE (XYEXT.LIS). IT ALSO READS NODE TEMPERATURES (TEMPYINT.LIS)
C     AND NODE TEMPERATURE GRADIENTS (NUYINT.LIS).  THESE ARE COMBINED
C     TO FORM A FILE TEMPYINT.DAT, USED IN MAKING WALL TEMPERATURE AND
C     HEAT FLUX PROFILE PLOTS

      CHARACTER KEYWORD*17,TESTWORD*17,KEYWORD1*4,TESTWORD1*4
      INTEGER I,K,J
      REAL X,Y,NODES,U,V,W,P,T,ST,VR,GRXINT,GRXEXT

      OPEN(UNIT=7,FILE='TEMPYINT.LIS',STATUS='OLD')
      OPEN(UNIT=5,FILE='XYEXT.LIS',STATUS='OLD')
      OPEN(UNIT=6,FILE='TEMPYINT.DAT',STATUS='NEW')
      OPEN(UNIT=8,FILE='NUYINT.LIS',STATUS='OLD')
      OPEN(UNIT=9,FILE='NUYEXT.LIS',STATUS='OLD')

      KEYWORD = 'X-Coordinate      '
      KEYWORD1 = 'Node'
      WRITE(*,*) 'STANDBY, FORMING INPUT FILE'

      DO 1 I = 1,60

      READ(7,*) TESTWORD1
         IF(TESTWORD1.EQ.KEYWORD1) THEN
         GO TO 3
         ENDIF
 1    CONTINUE

 3    DO 10 K = 1,60

         READ(5,11) TESTWORD
11       FORMAT(18X,A)
         IF(TESTWORD.EQ.KEYWORD) THEN
         GO TO 16
         ENDIF
10    CONTINUE

16    DO 17 J = 1,60
         READ(8,*) TESTWORD1
         IF(TESTWORD1.EQ.KEYWORD1) THEN
         GO TO 18
         ENDIF
17    CONTINUE

18    DO 22 JK = 1,60
         READ(9,*) TESTWORD1
         IF(TESTWORD1.EQ.KEYWORD1) THEN
         GO TO 21
         ENDIF
22    CONTINUE

21    DO 19 JJ = 1,100
      READ(5,*,END=20) NODES,X,Y
      READ(7,*) NODES,U,V,W,VR,P,T
      READ(8,*) NODES,GRXINT
      READ(9,*) NODES,GRXEXT
      WRITE(6,*) Y,T,GRXINT,GRXEXT
 19   CONTINUE
20    WRITE(*,*) 'FILE CREATION COMPLETE'
      END
```

MONTANA STATE UNIVERSITY LIBRARIES
3 1762 10217119 4

HOUCHEN
BINDERY LTD
UTICA/OMAHA
NE.